



Dynamic organization of chromosomes in the mammalian cell nucleus

Lothar Schermelleh

Dissertation der Fakultät für Biologie
der Ludwig-Maximilians-Universität München
eingerichtet am 12. Mai 2003

Dynamic organization of chromosomes in the mammalian cell nucleus

Dissertation der Fakultät für Biologie
der Ludwig Maximilians Universität München (LMU)

vorgelegt von
Dipl. Biol. Lothar Schermelleh
aus München

Gutachter:
Prof. Dr. Thomas Cremer
Prof. Dr. Heinrich Leonhardt

Tag der mündlichen Prüfung: 15.Juli 2003

*"Zerstreutheit ist ein Zeichen von Klugheit und Güte.
Dumme und boshaft Menschen sind immer geistesgegenwärtig."*

Charles Joseph von Ligne
(*1735, †1814, österreichischer Feldmarschall und Diplomat)

Vorwort

Die Erforschung des Genoms, d.h. der Gesamtheit der Gene eines Organismus, stellt eine der zentralen Frage der Biologie dar. Die Entdeckung der DNA-Doppelhelix-Struktur durch Watson & Crick vor fast genau 50 Jahren hat den Blick geöffnet auf die Eleganz und Einfachheit mit der die Erbinformation in einer Abfolge von Nukleotidbasen (Adenin, Thymin, Guanin und Cytosin), den vier Buchstaben des genetischen Codes, verschlüsselt wird. Fast ein halbes Jahrhundert später konnte im Jahr 2000 dank einer enormen gemeinschaftlichen Anstrengung die Rohfassung der menschlichen Genomssequenz durch das *Human Genome Project* (HGP) sowie das Celera-Konsortium präsentiert werden. Die damit einhergehenden Verheißungen im Hinblick auf das Verständnis und die Heilung komplexer Erkrankungen, etwa durch Gentherapie oder die gezielte Herstellung von Geweben aus Stammzellen haben hier zu einem enormen Schub in der öffentlichen Wahrnehmung geführt.

Trotz der Kenntnis der Genom-Sequenz ist die Wissenschaft heute noch immer weit davon entfernt etwa Krebs in seinen vielen Formen zu bekämpfen oder eine sichere Gentherapie anzubieten. Spätestens hier offenbart sich wie weit der Weg ist zu einem umfassenden Verständnis jener komplexen Vorgänge, die für die Umsetzung des genetischen Codes nötig sind. Denn auch wenn das Wissen über die Funktionsweise und die Regulation von Genen auf der linearen Ebene der DNA-Sequenz (*in vitro*) heute weit fortgeschritten ist, bleibt es bislang wenig verstanden wie die Expression des genetischen Programms in der Zelle selbst (*in vivo*) reguliert wird und wie die Vielzahl der Gene derart aufeinander abgestimmt werden, dass komplexe vielzellige Organismen wie etwa der Mensch mit Billionen von Zellen und hunderten verschiedener Zelltypen entstehen können.

Fast der gesamte Teil der Erbinformation befindet sich im Zellkern. Ein typischer Zellkern einer menschlichen Zelle hat einen Durchmesser von etwa 10 µm und enthält einen diploiden Chromosomensatz von 46 Chromosomen (22 Autosomenpaare + 2 Geschlechtschromosomen). Die einfache Genom-Sequenz des Menschen umfasst mehr als 3,2 Milliarden Basenpaare mit einer Gesamtlänge von 1 m und enthält etwa 30.000 Protein-codierende Gene. Weniger als 2% der DNA sind codierend (Exons), ein weiterer Teil beinhaltet regulierende Sequenzen und Introns. Der weitaus größte Teil des Genoms hat jedoch keine offensichtliche Funktion („*Junk-DNA*“). Der DNA Faden bildet mit Proteinen, darunter die Histone, eine komplexe, funktionell bedeutsame Struktur, das Chromatin. Wie die DNA um ein tausendfaches auf den Raum eines Zellkerns kompaktiert und darüber hinaus funktionell organisiert ist, stellt dabei ein noch immer weitgehend ungelöstes Problem dar. Möglicherweise liefert aber gerade die Art der Kompaktierung, wie auch die Lokalisation von spezifischen Sequenzabschnitten den Schlüssel zum Verständnis dafür, dass von den ~30.000 Genen in jeder Zelle nur ein kleiner Teil von wenigen Tausend entwicklungs- bzw. zelltypspezifisch in jeder individuellen Zelle abgelesen werden.

Heute erst beginnt man zu verstehen dass es verschiedene zusammenwirkende hierarchische Ebenen der Genregulation gibt, die über die

Sequenzinformation hinausgehen. Zu diesen epigenetischen Mechanismen gehören Modifikationen der DNA durch Methylgruppen, wie auch verschiedene Modifikationen der DNA verpackenden Proteine („*Histone-Code*“). Die spezifische Anheftung funktioneller Gruppen an kritischen Stellen beeinflusst (entweder durch Änderung der Ladung oder durch die Rekrutierung bestimmter strukturmodifizierender Proteine) den Kompaktierungsgrad und damit die Zugänglichkeit der DNA für bestimmte Transkriptionskomplexe in einem Vorgang, der als „*chromatin remodelling*“ bezeichnet wird. Neue Studien haben überraschenderweise zeigen können, dass auch kurze komplementäre RNA Sequenzen durch Interferenz (RNAi) die Ausbildung von transkriptionsinaktiven Heterochromatin maßgeblich mit beeinflussen. Über diese lokale Ebene hinaus scheint die Positionierung von aktiven und inaktiven Genen im dreidimensionalen Kontext eines „kompartimentalisierten“ Zellkerns von funktioneller Bedeutung zu sein, eine Vorstellung die sich in dem Chromosomen Territorien / Interchromatin-Compartment (CT-IC) Modell der funktionellen Zellenarchitektur wiederfindet.

Nicht zuletzt die Vielzahl neuer Erkenntnisse zu den epigenetischen Einflüssen auf die Genregulation und der Bedeutung einer funktionellen Zellkernarchitektur offenbaren hier ein sehr viel komplexeres Wirkungsgefüge für die Ausbildung eines zelltypspezifischen Genexpressionsmusters, als es frühere mechanistisch geprägte Vorstellungen nahe legten. Die Erfassung und Beschreibung dynamischer Änderungen der Zellkernarchitektur ist daher ein wichtiger Beitrag auf dem Weg zu einem umfassenden Verständnis der Vorgänge im Zellkern.

Zur vorliegenden Dissertation:

Im Gegensatz zu vielen vorangegangenen Studien zur funktionellen Zellkernarchitektur an fixierten Zellen, legt die vorliegende Arbeit einen Schwerpunkt auf die Untersuchung von dynamischen Vorgängen in der lebenden Zelle. Die Einführung von GFP (*green fluorescent protein*) vor wenigen Jahren als universeller Lebendzellmarker für nahezu jedes gewünschte Zielprotein hat hier einen enormen Trend in die Wege geleitet. Dies macht sich auch diese Arbeit zunutze, indem u.a. eine Zelllinie verwendet wurde, die ein Gen für ein Histon-GFP Fusionsprotein (H2B-GFP) exprimiert, wodurch das Chromatin in den Zellkernen jener Zellen bei Anregung mit geeignetem Licht grün fluoresziert.

Die hier vorgestellte Dissertation behandelt im weitesten Sinne die dynamische Architektur des Zellkerns. Ein Teil der Arbeit befasst sich mit der Frage einer suprachromosomalen Ordnung, die bereits Theodor Boveri im frühen 20. Jahrhundert zu einer wegweisenden Hypothese zur chromosomalen Anordnung während des Zellzyklus bewegt hat. Hier konnte durch die Anwendung verschiedener sich ergänzender Methoden (Langzeitbeobachtung fluoreszenzmarkierter Chromosomen, *Photobleaching* von Histon-GFP, 3D-FISH) gezeigt werden, dass die Anordnung der Chromosomen in den Zellkernen von Säugerzellen über den größten Teil der Interphase nahezu unverändert bleibt, während sich die Nachbarschaften von Chromosomen im Zuge der Mitose beträchtlich ändern können. Zudem konnte eine erhöhte Chromosomenbewegung in der frühen G1 Phase gezeigt werden, in einem Zeitraum der in vieler Hinsicht kritisch für die Ausbildung einer funktionellen Topologie zu sein scheint.

Darüber sollte in der vorliegenden Arbeit das dynamische Verhalten von funktionell distinktem, früh und mittel-bis-spät replizierendem Chromatin

untersucht werden, wobei ein besonderer Schwerpunkt auf die Interaktion mit der Zellkernhülle in lebenden und fixierten Zellen gelegt wurde. Die hierzu durchgeführten Versuche sind zwar nicht als abschließend zu bewerten, geben aber einen deutlichen Hinweis auf den Einfluss der Zellkernhülle als Faktor für die Determinierung und Aufrechterhaltung einer funktionellen Topologie.

Als Voraussetzung für die Beantwortung dieser biologischen Fragestellungen wurde im Zuge dieser Arbeit eine „*in vivo* Replikationsmarkierung“ methodisch weiterentwickelt, die es erlaubt funktionell distinkte „Chromatin-Kompartimente“ oder auch einzelne Chromosomen in lebenden Zellen zu markieren und zu verfolgen. Daneben war die Entwicklung eines geeigneten Beobachtungssystems für eine Lebendzellmikroskopie über vergleichsweise lange Zeiträume (z.B. die Länge eines Zellzyklus) erforderlich. Diese beiden methodischen Entwicklungen werden daher ausführlich im Methoden-Teil (Kapitel 3.9 und 3.12) beschrieben und am Ende des Methodenteils zusammenfassend kritisch diskutiert (Kapitel 3.16).

CD-Rom:

Der Arbeit ist eine CD-Rom beigelegt, die neben der vorliegenden Arbeit im pdf-Format, eine Reihe von Filmsequenzen von Lebendzellaufnahmen (im Quicktime™-Format oder QuicktimeVR™-Format) beinhaltet. Außerdem befindet sich darauf (im Ordner „Literature“) ein Grossteil der zitierten Veröffentlichungen, sofern diese über das Internet verfügbar waren.

Danksagung:

An erster Stelle danke ich meinem Doktorvater Thomas Cremer, der mir mit seiner ungemeinen Begeisterung für die Architektur des Zellkerns meine Arbeit mehr als nur vorantrieb und der, im Gegensatz zu mir selber, nie Zweifel an meinen Fähigkeiten hat auftreten lassen.

Ein bedeutender Teil der Arbeit, im speziellen die Entwicklung des Lebendzell-Beobachtungssystems sowie die *Photobleaching*-Experimente, sind in enger Zusammenarbeit mit Joachim Walter entstanden. Bei ihm möchte ich mich daher für das perfekte Teamwork bedanken, speziell auch dafür, dass er für fast jedes physikalische, mikroskopie- oder computer-technische Problem eine Lösung parat hatte.

Besonderen Dank aussprechen möchte ich:

- ◆ Marion Cremer für die kritische Durchsicht des vorliegenden Textes, sowie für die Durchführung der 3D-FISH an HeLa Zellklonen und vor allem für ihre Eigenschaft jederzeit mit Rat und Tat zur Seite zu gestanden zu haben.
- ◆ Irina Solovei für ihre fortwährende Unterstützung, ohne deren unermüdlichen Einsatz als Labor-Organisatorin die experimentelle Arbeit um vieles erschwert gewesen wäre.
- ◆ Stefan Müller, für seine Hilfestellung bei allen cytogenetischen Problemen, insbesondere der Karyotypisierung der SH-EP Zelllinie.
- ◆ Christine Fauth für die Durchführung der m-FISH.
- ◆ Christane Horn für die Durchsicht und Korrektur des englischen Textes.
- ◆ Prof. Dr. Heinrich Leonhardt für wertvolle Tipps und die Übernahme des Zweitgutachtens.
- ◆ PD Dr. Daniele Zink für die Einführung in die Lebendzellforschung.

- ◆ Dr. Robert D. Goldman für die Ermöglichung eines 2-monatigen Forschungsaufenthaltes an der Northwestern University, Chicago.
- ◆ Allen Mitgliedern der Arbeitsgruppe, die meine Arbeit über die letzten Jahre begleiteten und entweder durch die wissenschaftlichen Diskussionen förderten oder einfach durch die Bereitstellung eines perfekten „Betriebsklimas“ erst ermöglichten.
- ◆ Meiner Familie für die Liebe und Unterstützung und meiner Freundin Andrea für ihre Geduld und die Fähigkeit mich zum Lachen zu bringen.

Contents

Vorwort.....	V
Contents.....	IX
List of figures.....	XI
Abbreviations.....	XII
1. Summary.....	1
2. Introduction.....	3
2.1 Transcriptional regulation on the chromatin level	3
2.2 Motifs of a higher order functional nuclear topology	6
2.3 Chromosome order and chromosome dynamics during cell cycle	12
2.4 The role of the nuclear lamina on chromatin organization	14
2.5 Goals of the present work.....	15
3. Methods and Protocols.....	17
3.1 Cell culture	17
3.2 Freezing and thawing of cells	19
3.3 Slide preparation.....	20
3.4 Seeding cells on coverslips	20
3.5 Fixation of cells grown on coverslips	21
3.6 Post-fixation treatments and immunostaining.....	22
3.7 Metaphase preparation.....	24
3.7.1 Fixation of mitotic cells in methanol/acetic acid.....	24
3.7.2 Preparing metaphase spreads.....	25
3.8 Replication labeling with BrdU.....	27
3.9 In vivo replication labeling.....	29
3.9.1 Scratch replication labeling (SRL)	30
3.9.2 Two-color scratch replication labeling	33
3.9.3 Microinjection of fluorescent nucleotides	34
3.9.4 Direct pulse labeling after permeabilization with digitonin	35
3.10 Characterization of the cell cycle stages	36
3.10.1 Doubling time / Cell cycle length	36
3.10.2 Determination of cell cycle stages	37
3.10.3 Cell cycle parameter under live cell imaging conditions.....	38
3.11 Synchronisation at G1/S transition.....	39
3.12 Microscopy of living and fixed cells.....	43
3.12.1 Confocal laser scanning microscopy of fixed specimen.....	43
3.12.2 Long-term confocal time-lapse microscopy of living cells.....	43
3.12.3 Short-term microscopy of living cells	51
3.13 3D-FISH of HeLa cell clones	52
3.14 Image processing and 3D-reconstruction	52
3.15 Quantitative evaluation of nuclear volumes and CT movements	52
3.16 Methodological limitations.....	53

4. Results	57
4.1 In vivo replication labeling.....	57
4.2 Dynamic behavior of chromosomes through the cell cycle	64
4.3 Mid-to-late replicating chromatin associates to the nuclear lamina.....	73
4.4 Cell cycle dependent redistribution of centromeres	84
5. Discussion.....	87
5.1 Chromosome dynamics in interphase nuclei.....	87
5.2 Changes of CT order from one cell cycle to the next.....	89
5.3 Nuclear lamina and heterochromatin: an intimate relationship.....	93
5.4 Concluding remarks	97
6. References.....	99
7. Appendix.....	109
7.1 Supplementary material	109
7.2 Materials and technical equipment	112
7.2.1 Cells	112
7.2.2 Chemicals, enzymes and reagents	113
7.2.3 Media, buffers and solutions.....	115
7.2.4 Equipment and Instrumentation.....	117
Publikationen	120
Lebenslauf	121

List of figures

Figure 1.	CT-IC model of a functional nuclear architecture.	8
Figure 2.	Characteristic replication pattern in mammalian cell nuclei.....	10
Figure 3.	Chromosome arrangements in blastomere nuclei of <i>Parascaris equorum</i> drawn by Theodor Boveri (Boveri 1909).....	12
Figure 4.	Scratch replication labeling procedure.	31
Figure 5.	Short-term permeabilization induced by scratching.	31
Figure 6.	Simultaneous immunodetection of pKi-67 and BrdU in SH-EP N14 cells.....	37
Figure 7.	Time-series of two-step synchronized SH-EP cells.....	41
Figure 8.	Quantitative evaluation of proliferation parameters.....	42
Figure 9.	Experimental setup (A) and scheme (B) for long term live cell confocal microscopy.	44
Figure 10.	Live cell observation set-up does not impair cell growth.	44
Figure 11.	Macro for live cell microscopy at the LSM 410.....	48
Figure 12.	Scratch replication labeling (SRL) of SH-EP N14 cells.	57
Figure 13.	Karyogram of the SH-EP N14 cell line revealed by m-FISH.	58
Figure 14.	Confocal images of double-labeled nuclei of synchronized SH-EP N14 cells.	59
Figure 15.	Replication banding pattern of metaphase chromosomes after two-color <i>in vivo</i> replication labeling.	60
Figure 16.	Second mitosis after two-color SRL.	63
Figure 17.	Stability of large-scale chromosome territory arrangements studied in nuclei with Cy3-labeled CTs.	66
Figure 18.	Stability of chromosome territory neighborhood during interphase of living HeLa cells.	69
Figure 19.	Large-scale chromosome territory arrangements in HeLa cell nuclei change from one cell cycle to the next.	71
Figure 20.	CT #7 and #10 arrangements in nuclei of 2-cell clones.	72
Figure 21.	CT #7 and #10 arrangements in a 4-cell clone.	72
Figure 22.	Overview of mitotic stages in SH-EP cells.	74
Figure 23.	Centrosome location in prophase cells.	75
Figure 24.	Different mitotic figures of SH-EP cell nuclei.	76
Figure 25.	Lamin B and nuclear pore complex (NPC) in mitotic cells.	78
Figure 26.	Association of mid-to-late replicating chromatin domains with the nuclear lamina.	79
Figure 27.	Synchronous movements of lamin invagination and associated mid-to-late replicating chromatin domain.	80
Figure 28.	Dramatic changes of nuclear morphology accompany disruption of the lamina.	82
Figure 29.	Detailed view of disrupted replication labeled BHK cell nuclei.	83
Figure 30.	Centromere distribution in SH-EP N14 cells during cell cycle.	85
Figure 31.	Changes or maintenance of relative chromosomal positions during mitosis?	92

Abbreviations

Ab	antibody
bp	base pair
BrdU	5-bromo-2'-deoxyuridine
BSA	bovine serum albumin
BHK	baby hamster kidney fibroblast cells
CCD	charge-coupled device
CHO	chinese hamster ovary
CLSM	confocal laser scanning microscope
CN	center of nucleus
CT	chromosome territory
DAPI	4',6-diamidino-2-phenylindole
d H₂O	de-ionized water
dd H₂O	ultrapure (or double-distilled) water
DMEM	Dulbecco's modified Eagle medium
DNA	deoxyribo-nucleic acid
DNase	deoxyribo-nuclease
dUTP	deoxyuridine-triphosphate
EDTA	ethylenediamintetraacetat = Titriplex III
FBS	fetal bovine serum
FISH	fluorescence <i>in situ</i> hybridization
FITC	fluorescein-isothiocyanat
G-band	Giemsa dark chromosome band
HEPES	N-2-hydroxyethylpiperazin-N'-2-ethanesulfonic acid
HP-1	heterochromatin protein 1
kb	kilobase
LBR	lamin B receptor
Mb	megabase
m-FISH	multicolor-FISH
NOR	nucleolar-organizer region
NPC	nuclear pore complex
PBS	phosphate-buffered saline
PI	propidium iodide
R-band	reverse (Giemsa light) chromosome band
RNA	ribonucleic acid
RNase	ribonuclease
RPMI	cell culture medium (Roswell Park Memorial Institute)
rpm	rotations per minute
Tris	tris(hydroxymethyl)aminomethane
Triton X-100	octylphenoldecaethylenglycolether
Trolox®	(±)6-hydroxy-2,5,7,8-tetramethylchroman-2-carboxylic acid
Tween® 20	polyoxyethylensorbitanmonolaurat

1. Summary

Uncovering the motifs of a higher order nuclear architecture and its implications on nuclear function has raised increasing interest in the past decade. The nucleus of higher eukaryotes is considered to display a highly dynamic interaction of DNA and protein factors. There is an emerging view that there are hierarchical levels of gene regulation, reaching from epigenetic modifications at the DNA- and histone level to a higher order functional nuclear topology, in the context of which gene-activating and -repressing processes influence the gene expression profile of an individual cell beyond the sequence information of the DNA.

The present work focuses on the analysis of the dynamic aspects of higher order nuclear architecture in living cells. As a prerequisite, an *in vivo* replication labeling strategy was developed, that enabled the simultaneous visualization of early and mid-to-late replicating chromatin as well as single chromosome territories on the basis of a labeling/segregation approach. The presented scratch replication labeling protocol combines a high labeling efficiency with reduced “damaging” effects and can be successfully applied to a number of adherently growing cell lines, including primary human fibroblasts. In addition, a live cell observation system was developed that facilitates time-lapse confocal (4D) microscopy over elongated time periods which made it possible to follow a complete cell cycle or more.

To address possible long-range movements of chromosome territories (CTs) during an entire interphase, fluorescence labeling of a small number of CTs was performed in living HeLa cells stably expressing histone H2B-GFP. This was achieved by *in vivo* scratch replication labeling with fluorescent nucleotides. Labeled cells were cultivated for several cell cycles until labeled chromatids had segregated. Such cells were followed by time-lapse confocal microscopy over time-scales of up to 20 hours covering major parts of the complete cell cycle. Positional changes of the intensity gravity centers of labeled CTs in the order of several μm were observed in early G1, thereafter, the positions remained within a range of $\sim 1 \mu\text{m}$ till the end of G2. In conclusion, CT arrangements were highly constrained from mid G1 to late G2 / early prophase, whereas major changes of CT neighborhoods occurred from one cell cycle to the next. More extended movements observed in early G1 might play a role when CTs “home in” to establish a non-random radial CT arrangement.

To analyze possible changes of chromosome arrangements from one cell cycle to the next, nuclei were photobleached in G2 maintaining a contiguous zone of unbleached chromatin at one nuclear pole. This zone was stably preserved until the onset of prophase whereas unbleached chromosome segments were often observed to become located at distant sites in the metaphase plates. Accordingly, chromatin patterns observed in daughter nuclei differed significantly from the mother cell nucleus, indicating that CT neighborhoods were not preserved during mitosis. The variability of CT neighborhoods during clonal growth was further confirmed by 3D-FISH experiments.

A series of experiments of a more preliminary character looked at the influence of the nuclear lamina in constraining and determining a higher order nuclear architecture by selectively interacting with mid-to-late replicating chromatin. Simultaneous immunodetection of lamin B on two-color replication labeled neuroblastoma cell nuclei revealed specific attachment of the mid-to-late replicating chromatin compartment not only along the periphery but also inside the nucleus along invaginations of the lamina. 4D-live cell observation of lamin C-GFP expressing CHO cells with mid-to-late replicating chromatin labeled simultaneously revealed concomitant movements of replication foci attached to lamin invaginations. Moreover, a functional essay was employed which uses injection of a dominant negative lamin A mutant protein (Δ NLA) to cause a reversible disruption of the nuclear lamina. Initial results point to concomitant distortion of the mid-to-late replication pattern and a preferential attachment of the respective chromatin sites to partially disrupted lamin B (as compared to lamin A and nuclear pore complex).

Finally, a model is presented on the chromosome positioning in mammalian nuclei depending on cell cycle and nuclear shape.

2. Introduction

The cell nucleus attracts particular interest as it contains the genetic information and performs vital functions, such as the replication of the DNA, the transcription and processing of genes and the assembly of ribosomes. In the past decade a view of the nucleus has emerged as a highly compartmentalized organelle that combines a remarkable degree of order in fundamental substructures with a surprising dynamic of many protein components (Lamond and Earnshaw, 1998; Cremer and Cremer, 2001; Dundr and Misteli, 2001; Misteli, 2001).

Much of the knowledge on the nuclear structure has been obtained on fixed specimen by immunocytochemical detection of nuclear proteins or by visualizing specific DNA sequences with fluorescence *in situ* hybridization (FISH) techniques. Enhanced 3D-microscopy, digital image analysis and 3D visualization have contributed to gain insight into spatial relationships of nuclear substructures. Recent developments in live cell microscopy nowadays have made it possible to address the dynamic nature of diverse nuclear structures in space and time. This has been especially promoted by the introduction of green-fluorescent protein (GFP) techniques. GFP gene sequence can be fused by recombinant DNA techniques to virtually any desired target gene to be expressed and visualized in living cells (Chalfie *et al.*, 1994). The introduction of fluorescently labeled nucleotides into cells provides another approach for visualizing chromatin and interphase chromosomes in living cells (Zink and Cremer, 1998). Moreover, specific chromosomal sites down to the single gene level can be tagged by inserting repeats of a bacterial operator sequence, which is bound by a corresponding repressor protein fused to GFP (Tsukamoto *et al.*, 2000; Belmont, 2001).

2.1 Transcriptional regulation on the chromatin level

Over the past decades detailed knowledge has accumulated on the molecular switches at the level of the linear DNA sequence. The function of regulatory sequences like promoters or enhancers has been studied in detail and is now basic part of every textbook (Alberts *et al.*, 2002). Despite the wealth of DNA sequence information collected by now, it becomes more and more clear that the realization of a differentiation- and development-specific gene program requires superordinate levels of regulation. These levels involve epigenetic modifications of chromatin as well as higher order chromatin structures within the context of the nuclear topology (Baltimore, 2001; Cremer and Cremer, 2001).

Packaging the genome: heterochromatin versus euchromatin

Within the nucleus of eukaryotic cells the genetic information is embedded in the chromatin, a protein-DNA complex that serves not only the compaction but also the regulation of gene expression. The fundamental packaging unit of chromatin is the nucleosome, which consists of a histone octamere (2 of each core histones H2A, H2B, H3, H4) around which the DNA double helix is wrapped in 1.7 superhelical turns spanning 146 bp (Luger *et al.*, 1997). Nucleosomes in addition with linker DNA of variable size (10-80 bp) give rise to the 10-nm fiber ("beads on

a string" conformation). Stabilized by linker histones (H1), nucleosomes then array into the 30-nm fiber. Additional levels of higher order chromatin structure are less well defined and may involve a chromonema fiber of ~100 nm diameter (Belmont *et al.*, 1999; Tumbar *et al.*, 1999) or the organization into loops of some 100 kb size that may be attached by a central transcription factory (Cook, 2002). Specific histone variants may be exclusive components of nucleosomes in specialized chromatin structures, e.g CENP-A, a histone 3 variant required for kinetochor formation at centromeres (Sullivan *et al.*, 1994).

Different degrees of chromatin compaction in interphase nuclei hallmark the distinction into euchromatin and heterochromatin (Dillon and Festenstein, 2002). Decondensed euchromatin is sensitive to nuclease digestion and mainly early replicating in S-phase. Genes located within euchromatin are commonly expressed. Conversely, condensed heterochromatin (originally defining densely stained regions in interphase nuclei) is characterized by a regular nucleosome array, inaccessibility to nucleases and later replication. It is further subdivided into constitutive and facultative heterochromatin. Constitutive heterochromatin is often located in pericentromeric regions with stretches of satellite repeat sequences as underlying DNA sequence (e.g. 171-bp α -satellite repeat in human). Genes translocated within or in close neighborhood may become silenced in a variegating manner, which accounts e.g. for position effect variegation (PEV) in *Drosophila* (Csink and Henikoff, 1996; Dernburg *et al.*, 1996). In contrast, facultative heterochromatin denotes developmentally regulated heterochromatin that preferentially harbors tissue-specific genes and is capable of converting into euchromatic state. The inactivated X chromosome (X_i) in female mammalian cells represents the most prominent example of this class of chromatin.

Epigenetic mechanism regulating gene expression

The degree of compaction essentially influences gene silencing or activation by either permitting or restricting the accessibility of the DNA to transcription factors (Horn and Peterson, 2002). Recent studies have identified a complex interdependent network of covalent modifications of the DNA and of histones as well as associations with non-histone proteins as the underlying mechanism of chromatin compaction. The three best-characterized epigenetic marks are acetylation of histone H3 and H4, methylation of H3 and methylation of cytosine residues (5mC) of DNA (Richards and Elgin, 2002). The epigenetic information for a certain chromatin conformation is maintained during replication and stably transmitted over several cell cycles.

N-terminal tails of histones, extending from each nucleosome can be subject to various post-translational modifications including phosphorylation, acetylation, methylation and ubiquitination. Patterns of different modifications are thought to modulate chromatin properties either by changing the charge and/or creating recognition sites for specific remodeling complexes, thus representing a specific "histone code" (Strahl and Allis, 2000; Jenuwein and Allis, 2001).

A well-known epigenetic marker for transcriptionally active euchromatin is hyperacetylation of histones H3 and H4, which is mediated by histone acetyl transferases (HATs) (Struhl, 1998). Conversely, hypoacetylation accompanies heterochromatin formation and gene silencing, and is mediated by histone deacetylases (HDACs). HATs and HDACs are themselves recruited by various sets of transcriptional activators or repressors. Hence, acetylation is considered

to be a rather late step in a complex chain of events causing remodeling of chromatin (see below).

Special interest has been recently attracted to the methylation of lysine at position 4 and 9 in the histone H3 amino terminus (H3-K4 and H3-K9) that has been allocated a central role in the framework of epigenetic modifications (Lachner and Jenuwein, 2002). H3-K9 methylation is mediated by a specific histone methyl transferase (HMTase) termed Suv39h*. It provides a high-affinity binding site for heterochromatin protein 1 (HP1). Bound HP1 is able to dimerize and thus promotes heterochromatin formation and gene silencing (Lachner *et al.*, 2001; Peters *et al.*, 2001). Furthermore, HP1 again forms a complex with Suv39h HMTase, which creates a self-reinforcing loop, that adds to the spreading of heterochromatin.

Suv39h1/HP1 mediated repression in mammals is associated mainly with pericentric (constitutive) heterochromatin but may also be involved in gene repression at euchromatic targets (Nielsen *et al.*, 2001). Moreover H3-K9 methylation (in a Suv39h/HP1-independent pathway) has been linked to direct DNA methylation (see below) and may act as an epigenetic imprint for developmentally regulated, facultative heterochromatin as well as X chromosome inactivation in female mammals (Boggs *et al.*, 2002; Peters *et al.*, 2002).

Conversely, methylation of lysine at position 4 (methH3-K4) by specific HMTs (SET-9/SET-7) appears to render chromatin permissive for transcription. This modification may either recruit factors necessary for further chromatin opening, like SWI/SNF remodeling complex and HATs or prevent the association of the negatively acting complexes. Hence it acts antagonistic to negative chromatin modifier Suv39h in mammalian cells (Lachner and Jenuwein, 2002).

At the DNA level methylation of cytosine (5mC) is another important epigenetic marker in higher eukaryotes, which is mediating gene silencing in a heritable fashion (reviewed in Leonhardt and Cardoso, 2000; Jones and Takai, 2001). DNA methylation predominantly occurs at CpG sites with both cytosines on each strand bearing a methyl-residue. CpG sites are often enriched within control regions of genes. Methylation at these sites prevents transcriptional initiation causing the silencing of the according gene. Methylation is mediated by DNA methyltransferases (DNMTs). The ubiquitous Dnmt1 is essential for the maintenance of a given methylation pattern as it preferentially binds hemimethylated cytosine and has been shown to be associated with the replication machinery. In contrast, the tissue specific Dnmt3a and Dnmt3b were connected to *de novo* methylation. DNA methylation is directly linked to histone modification as it recruits HDACs via methylated CpG binding proteins like MeCP2 (Jones *et al.*, 1998). In addition, Dnmt1 may also directly bind to HDAC2 (Rountree *et al.*, 2000). Recent studies on *N.crassa* and *Arabidopsis* demonstrated that cytosine methylation itself can be directed by H3-methyl K9 (see above) (Tamaru and Selker, 2001; Jackson *et al.*, 2002). Finally, recent studies have identified short noncoding interfering RNAs (RNAi) to establish centromeric heterochromatin formation, which adds another surprising key player in the increasingly complex network of gene silencing (Dernburg and Karpen, 2002).

Taken together these findings show a complex interconnected network of repressing factors that are stabilizing and propagating silent heterochromatin by

* mammalian homologues of *Drosophila* suppressor of variegation Su(var)3-9

reinforcing feed back loops. These repressing factors may be counteracted by a number of activating factors (see also Table 1). This system may allow the genome to remain competent for differentiation- and development-specific switching of the transcriptional program and therefore provides some degree of "genome plasticity". This view is further supported by recent findings that binding of HP1 to form transcriptionally repressed heterochromatin is not static but rather dynamic thus providing accessibility for regulating factors (Cheutin *et al.*, 2003; Festenstein *et al.*, 2003).

Boundaries and Insulators

The spreading of heterochromatin to regions of actively transcribed genes (and vice versa) is prevented by specific DNA sequences, termed boundary or insulator elements, which have been characterized in yeast, *Drosophila* and vertebrates. Boundary/insulator elements act as recognition sequence for specific protein complexes that have DNA binding properties as well as the ability to dimerize. Hence insulator elements might establish independent domains of co-regulated gene expression characterized by globally differing chromatin states (Gerasimova and Corces, 2001; Labrador and Corces, 2002). This view is consistent with recent findings that show significant clustering of co-expressed genes within the human genome (Caron *et al.*, 2001). Insulators elements may be related to physical chromatin domains and have been connected with a physical attachment to the nuclear lamina (Gerasimova *et al.*, 2000).

2.2 Motifs of a higher order functional nuclear topology

Beyond the impact of local changes in the chromatin structure on the gene activity, there is now growing evidence that regulation of gene expression is influenced in a superordinate way by nuclear architecture and, moreover, that changes in nuclear organization may be directly correlated with changes of the transcriptional program during development and cell differentiation.

The CT-IC model

Cytological studies over the past two decades have led to the formulation of a topological model of gene expression, the chromosome territory - interchromatin compartment (CT-IC) model (Cremer 1993, Cremer 2001). The underlying idea is that chromatin forms higher order structures within the interphase nucleus represented by focal chromatin aggregates of variable density, called subchromosomal domains (see Figure 1). Chromatin of a chromosome organizes into a discrete chromosome territory (CT), which has a strongly convoluted three-dimensional internal structure. Starting from the nuclear pores, a space devoid of chromatin, termed interchromatin compartment (IC), extends between territories of neighboring CT and further, inside the territory, surrounding chromatin dense focal aggregates inside the CT. Within the IC, factors necessary for transcription, splicing, DNA replication and repair can freely roam. Focal chromatin aggregates may physically exclude large factor complexes. Consequently, the interface between chromatin domains creates a reaction site facilitating e.g. the transcription and processing of active genes. Further the IC also serves the transport of transcripts to the nuclear pores. Conversely, inactive or silenced genes may become located inside a compacted chromatin domain and are thus

excluded from the transcription machinery. The IC furthermore harbors various non-chromatin domains, such as nucleoli, splicing factor compartments (SFCs or speckles), Cajal bodies (CB) and PML bodies that may serve either as storage or as functional sites (reviewed in Dundr and Misteli, 2001). Bleaching studies revealed that these nuclear compartments, although overall stable, are characterized by a highly dynamic exchange of its constituting protein components. This is consistent with a role of self-organization of the nuclear architecture (Misteli, 2001).

Evidences for the CT-IC model and its impact on gene regulation

Evidence for the organization of chromosomes into discrete territories came from early UV microirradiation experiments. Unscheduled DNA synthesis induced by microirradiation of discrete sites in interphase nuclei of CHO cells was detected in subsequent metaphases and was found to be restricted to a few chromosomes (Cremer *et al.*, 1982). The territorial organization was later established by FISH experiments with whole chromosome painting probes (Manuelidis, 1985; Lichter *et al.*, 1988), thereby confirming an early hypothesis of Theodor Bovery (see below). FISH experiments could also demonstrate that chromosome arms as well as chromosome bands and centromeres, themselves form discrete domains within the CT. (Dietzel *et al.*, 1998). In FISH experiments with gene specific probes the 3D-position of genes within a territory could be assessed depending on their activity. Several papers correlated the transcriptional activity of genes to the position in their respective CT or to their proximity to pericentric heterochromatin. Large chromatin segments containing the major histocompatibility (MHC) gene cluster were frequently found to loop out of the chromosome 6 territory upon transcriptional activation (Volpi *et al.*, 2000). Similar observations were made for the epidermal differentiation complex (EDC) on chromosome 1 in keratinocytes (Williams *et al.*, 2002). Transcriptionally active α and β globin genes in erythroblasts were localized remote from constitutive heterochromatin, whereas in lymphocytes, which do not express globin genes, the inactive β globin locus (but not α globin) was found closely associated with pericentric heterochromatin (Brown *et al.*, 2001). Diezel *et al.* (1999) found ANT3, a gene that is transcribed from both X_a and X_i on the surface of both CTs, whereas ANT2, which is transcribed only from X_a is located in the interior of X_i . However, a recent study by Mahy *et al.* (2002) found local gene density rather than activity of individual genes influencing CT organization, arguing against a strict correlation of internal or peripheral positioning of genes with their transcriptional activity.

Evidence for the IC was provided by microinjection experiments with (*Xenopus*) vimentin fused to GFP and a nuclear localization sequence (NLS). The construct aggregates to filaments at 28°C, which were found exclusively outside of CTs (Bridger *et al.*, 1998a; Reichenzeller *et al.*, 2000). In another study, poly(A)-RNA was visualized and tracked in living cells. RNA was found to be restricted to the chromatin free space, where it was moving in a diffusive manner (Politz *et al.*, 1999).

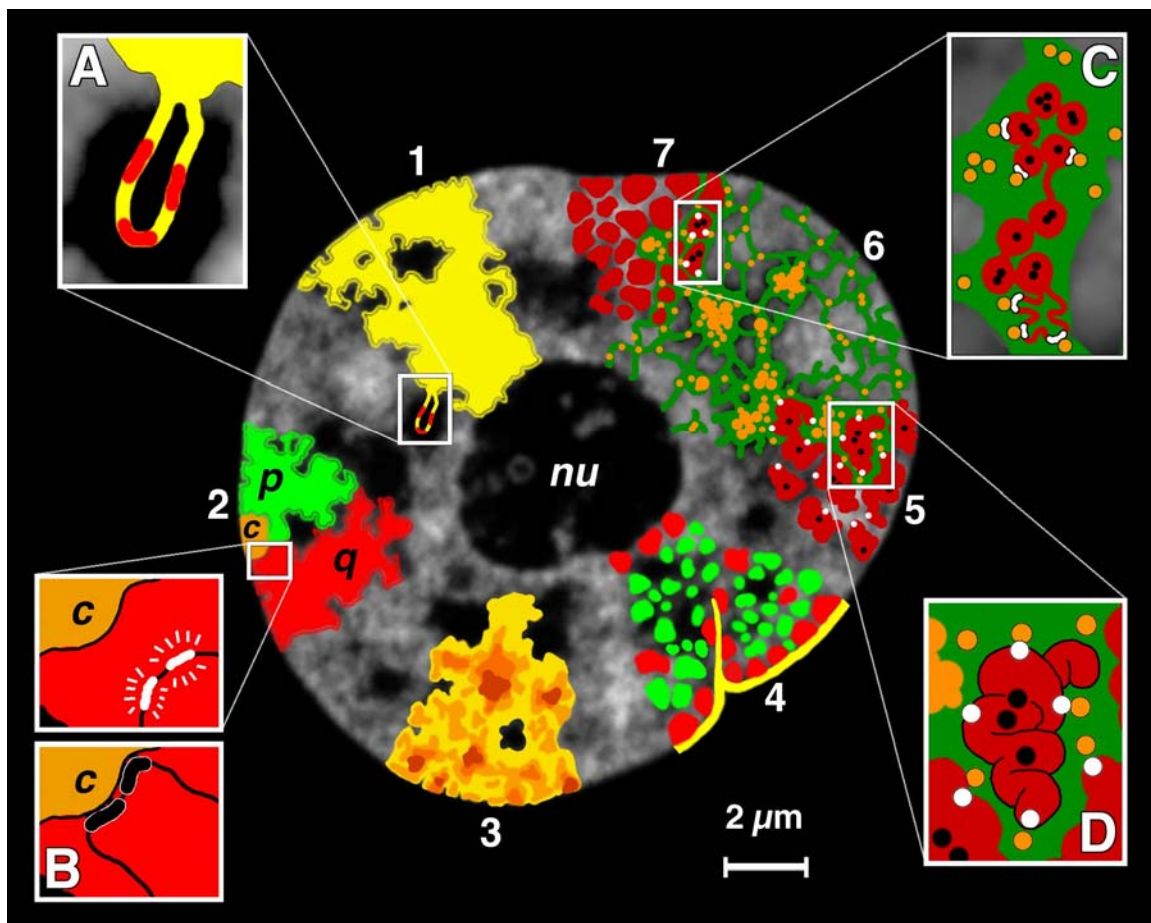


Figure 1. CT-IC model of a functional nuclear architecture. Structural features are drawn roughly to scale on an optical section from a nucleus of a HeLa histone H2B-GFP expressing cell. Insets each show a topological model of gene regulation based on recent studies, in the context of the indicated structure. (1) CTs have complex folded surfaces. Inset A: a giant loop with active gene cluster expands into the IC space (Volpi *et al.*, 2000; Williams *et al.*, 2002) (2) CTs contain separate arm domains for the short (p) and long chromosome arms (q), and a centromeric domain (c). Inset B: Top, actively transcribed genes (white) are located on a chromatin loop that is remote from centromeric heterochromatin. Bottom, recruitment of the same genes (black) to the centromeric heterochromatin leads to their silencing (Dernburg *et al.*, 1996; Brown *et al.*, 1997; Brown *et al.*, 1999). (3) CTs have a variable chromatin density. Loose chromatin expands into the IC, whereas the condensed chromatin is remote from the IC. (4) CT showing early replicating chromatin domains (green) and mid-to-late replicating chromatin domains (red). Each domain comprises ~1 Mb. Gene-poor chromatin (red), is preferentially located at the nuclear periphery and in close contact with the nuclear lamina (yellow) and around the nucleolus (nu). Gene-rich chromatin (green) is located between the gene-poor compartments. (5) Higher-order chromatin structures built up from a hierarchy of chromatin fibers (Belmont and Bruce, 1994). Inset D: active genes (white dots) may be at the surface of convoluted chromatin fibers. Silenced genes (black dots) may be located towards the interior of the chromatin structure. (6) The CT-IC model predicts that the IC (green) contains complexes (orange dots) and larger non-chromatin domains (aggregations of orange dots) for transcription, splicing, DNA replication and repair. (7) CT with ~1-Mb chromatin domains (red) and IC (green) expanding between these domains. Inset C: the topological relationships between the IC, and active and inactive genes. The finest branches of the IC end between ~100-kb chromatin domains. Top: active genes (white dots) are located at the surface of these domains, whereas silenced genes (black dots) are located in the interior. Bottom: alternatively, closed ~100-kb chromatin domains with silenced genes are transformed into an open configuration before transcriptional activation. (Scheme taken from Cremer and Cremer, 2001.)

DNA replication and focal chromatin organization

Compelling evidence for the suborganization of CTs in focal chromatin aggregate is provided by pulse labeling of replicating DNA with halogenated thymidine analogues (Gratzner, 1982). Likewise, transcription and RNA processing (Wansink *et al.*, 1993; Wei *et al.*, 1998) as well as DNA-repair (Tashiro *et al.*, 1996) occur at discrete sites.

Generally, DNA replication in higher eukaryotes takes place in a well-defined spatial and temporal manner. Large numbers of replication sites are simultaneously active creating characteristic replication patterns during progression through S-phase (Nakamura *et al.*, 1986; Nakayasu and Berezney, 1989; O'Keefe *et al.*, 1992; Dimitrova and Berezney, 2002) (see Figure 2 for details). Each replication site is typically active for ~45 min forming a replication focus of some 100 kb up to several Mb in size, consisting of a cluster of 1-10 simultaneously firing replicons (Jackson and Pombo, 1998; Ma *et al.*, 1998; Berezney *et al.*, 2000). As could be demonstrated by *in vivo* analysis of the DNA polymerase clamp PCNA tagged with GFP, the replication foci are stably anchored in the nucleus and show no directional movement. After having replicated one replication site adjacent origin clusters are activated in a domino-like fashion (Leonhardt *et al.*, 2000; Sporbert *et al.*, 2002). The higher order chromatin structures revealed by focal replication labeling persist through all stages of the cell cycle and are therefore thought to represent fundamental subunits of chromatin organization. To account for this fact these structures were also termed subchromosomal foci or ~1Mb chromatin domains (Cremer and Cremer, 2001).

Compartmentalization of the genome

Importantly, characteristic spatial patterns of replication foci are correlated with the time when the chromatin was replicated during S-phase. Moreover, replication timing also reflects important qualitative chromatin features (Ferreira *et al.*, 1997; Sadoni *et al.*, 1999): Housekeeping gene rich, transcriptionally active euchromatin predominantly replicates during the first half of S-phase. The corresponding "early" replication pattern (I) displays several hundred discrete foci dispersed in the nuclear interior excluding the nuclear periphery and the space around nucleoli (perinucleolar space), thus defining a specific compartment (Figure 2). Conversely, gene poor heterochromatic sequences, harboring mainly tissue specific genes replicate within the second half of S-phase. The corresponding "mid" replication pattern (II) becomes most prominent at two-thirds of S-phase. The according chromatin is therefore referred to as mid-to-late replicating chromatin compartment. The characteristic pattern shows somewhat more densely packed foci that are preferentially located at the nuclear periphery and around nucleoli. Constitutive heterochromatin containing highly repetitive sequences (α -satellite) is nearly devoid of genes and replicates, at the very end of S-phase (reviewed in Goren and Cedar, 2003). The late replication pattern (III) shows few larger sized foci at the periphery as well as in the nuclear interior. Consequently, each CT consists of distinctly localized early and later replicating chromatin compartments. With the onset of mitosis this three-dimensional distribution condenses to a linear succession of chromosome bands. In the metaphase chromosome, early replicating chromatin constitutes Giemsa light R-bands, and later replicating chromatin constitutes Giemsa dark G-bands,

comprising the subset of mainly contromere-located C-bands, which are latest replicating. The staining of R- and G- bands basically reflects their difference in AT- and GC-content (Craig and Bickmore, 1993). The genome has been shown to be a mosaic of five subfamilies of isochores, long DNA segments (>300 bp) with homogeneous GC/AT content (Bernardi, 1995). R bands contain mainly GC-rich isochore families (H1, H2, H3) The GC-richest isochore H3 is preferentially enriched in T-Bands, a subset of R-bands located mainly at subtelomeric regions, which are characterized by very early replication and very high gene density (Federico *et al.*, 1998). In contrast G-bands contain mainly GC-poor families L1 and L2 (see also Table 1).

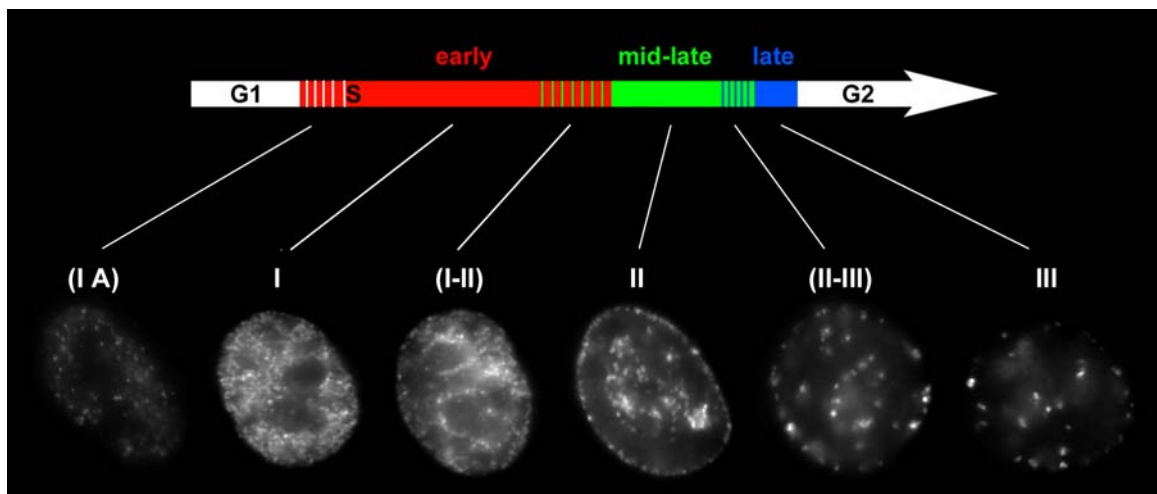


Figure 2. Characteristic replication pattern in mammalian cell nuclei. Epifluorescence images of HeLa cell nuclei after 30 min pulse labeled with BrdU (see chapter 3.8) and fixation with formaldehyde. Nuclei of cells traversing S-phase (typical length in mammalian cells 6-8 hrs) incorporate BrdU into the DNA. The replication sites were detected with specific antibodies. Replication foci in S-phase nuclei display distinct patterns, dependent on the time when the pulse was applied in S-phase. Early replication pattern (pattern I) is observed during the first half of S-phase. Mid replication pattern (II) shows chromatin domains replicating later in the second half of S-phase. (C) The late replication pattern (III) highlights chromatin replicating during the last hour of S-phase. Intermediate patterns (I-II and II-III) are present as well and have been defined as distinct pattern in some publications (O'Keefe *et al.*, 1992). A recent study by Dimitrova (2002) further defined a pattern (I A) with relatively low number of small discrete sites that are visible during the first ~30 min of S-phase (visible with shorter pulse length) indicating an initial phase until early replication pattern (I) is fully established. Importantly, though each replication focus may be static for 45 min or longer, the overall DNA replication is a contiguous process with constant assembly and disassembly of replication foci. Hence the patterns defined here have to be considered as snapshots of a continuous and dynamic process (Sporbert *et al.*, 2002).

Table 1. Summary of genome compartmentalization

	Euchromatin	Facultative heterochromatin	Constitutive heterochromatin
<i>State</i>	dispersed	condensed ↔	highly condensed
<i>Nucleosome array</i>	irregular	regular	regular
<i>Nuclease sensitive (HS) sites</i>	+	- (+)	-
<i>Replication timing</i>	early (first half of S phase)	mid-to-late	very late
<i>Replication pattern (interphase)</i>	early (I) ↔ (?)	mid (II)	late (III)
<i>Banding pattern (metaphase)</i>	R	G	C (subset of G)
<i>Base content</i>	GC rich	relatively AT rich	mostly AT rich
<i>Isochores</i>	T-bands: H3 (H2, H1) R'-bands: H1, L (H2, H3)		L (H1)
<i>Genes</i>	gene dense most housekeeping genes, tissue specific genes	gene poor preferentially tissue specific genes	(nearly) devoid of genes
<i>Characteristic sequences</i>	single copy, <i>SINES</i>	<i>LINES</i>	repetitive sequences (satellite-DNA), transposons
<i>CpG islands</i>	frequent	infrequent	absent
<i>Important epigenetic marks</i>	H3/4 hyperacetylation H3-m Lys4 hypomethylated DNA	(variable)	H3/4 hypoacetylation H3-m Lys9 / HP-1 methylated DNA RNAi

Note: The table displays a simplified summary: Intermediate states are possible as well, e.g. some constitutive heterochromatin may also contribute to the mid replication pattern. Particularly sequences belonging to facultative heterochromatin may adopt characteristics of euchromatic when tissue specific genes or gene cluster become activated (indicated by bidirectional arrows)

2.3 Chromosome order and chromosome dynamics during cell cycle

A controversially discussed question in the context of a functional higher order nuclear topology concerns the extent to which chromosomes exhibit an ordered positioning and whether there are fixed or preferential neighborhoods of CTs that are maintained during interphase and cell division. Early attempts to study higher order interphase chromosome arrangements were undertaken in the 19th century by Carl Rabl (1885) who proposed a centromere-telomere orientation of chromosomes in Salamander nuclei, later referred to as the “Rabl-orientation”. In 1909, based on studies of blastomere nuclei in the nematode *Parascaris equorum*, Theodor Boveri developed a hypothesis on the nature of chromosomes (Figure 3) (Boveri, 1909): (1) Chromosomes occupy distinct chromosome territories (CTs) in the cell nucleus. (2) CT order is stably maintained during the “silent stage” (in modern terms from early G1 to late G2). (3) Changes of chromosome neighborhoods occur during mitosis. Accordingly, CT order during interphase can profoundly vary from one cell cycle to the next. (4) Chromosomal neighborhoods established in the metaphase plate are maintained during anaphase and telophase resulting in a rather symmetrical CT arrangement in the two daughter nuclei. As a consequence of (3), however, different pairs of daughter nuclei often show distinctly different arrangements.

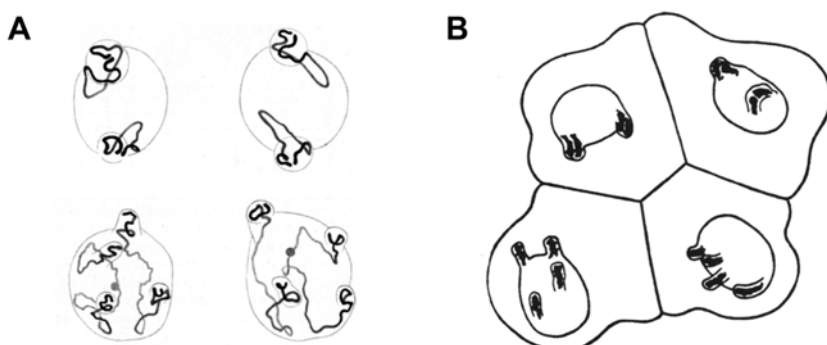


Figure 3. Chromosome arrangements in blastomere nuclei of *Parascaris equorum* ($2n = 2$) drawn by Theodor Boveri (Boveri 1909). (A) The two nuclei above and below each represent a pair of daughter nuclei from blastomeres studied at prophase of the two-cell stage. Chromosome ends are fixed within evaginations of the nuclear envelope. Note that chromosome arrangements and the positions of the evaginations are similar in each pair, while different pairs show striking differences. (B) Interphase blastomere cells from an embryo drawn at the four-cell stage. Chromosome arrangements within the nucleus are invisible except for nuclear evaginations that indicate telomere positions. Each pair of daughter nuclei shows symmetrical positions of the evaginations, while a comparison of the two pairs reveals striking differences.

Since Boveri's early paper, conclusive evidence has been obtained for the existence of chromosome territories in animal and plant cell nuclei (Cremer *et al.*, 1993; Leitch, 2000). With regard to Boveri's second assumption the evidence is less clear. A number of reports describe a high degree of stability of large scale chromatin arrangements in mammalian cell nuclei (Shelby *et al.*, 1996; Abney *et al.*, 1997; Zink and Cremer, 1998; Bornfleth *et al.*, 1999; Chubb *et al.*, 2002; Lucas and Cervantes, 2002), but considerable movements of chromosomal subregions, such as centromeres, were observed during the cell cycle or terminal differentiation (Martou and De Boni, 2000; Cremer *et al.*, 2003 (in press)). Major changes of heterochromatin positioning were also reported in somatic cell nuclei of *Drosophila* (Csink and Henikoff, 1998). Moreover, extensive and rapid movements of individual GFP-tagged chromatin sites were observed in live cell experiments with nuclei of budding yeast and *Drosophila* (Marshall *et al.*, 1997; Heun *et al.*, 2001).

Rather conflicting results have been also reported on the degree of chromosomal order: A number of studies described variable neighborhoods of both mitotic chromosomes and CTs (Lesko *et al.*, 1995; Allison and Nestor, 1999; Cremer *et al.*, 2001; Habermann *et al.*, 2001; Bolzer, 2002; Cornforth *et al.*, 2002), thus supporting Boveri's third assumption. In contrast, a recent study presented evidence for a clustering of a subset of chromosomes in different mouse cells (Parada *et al.*, 2002). Other investigators noted a precise spatial positioning of chromosomes in prometaphase chromosome rosettes from human fibroblasts and HeLa cells and suggested stable associations among adjacent chromosomes due to hypothetical centromere interconnections (Nagele *et al.*, 1995). Such connections could also provide a mechanism for ordered arrangements of CTs during interphase (Koss, 1998; Nagele *et al.*, 1999).

For Boveri's fourth assumption anecdotal evidence has been reported, but a quantitative, high-resolution analysis has not yet been provided. Early studies indicated rather symmetrical locations of nucleoli as well as chromocenters in daughter nuclei from a variety of plant species (Heitz, 1932). FISH-experiments suggested a considerable degree of symmetry in the arrangement of centromeres and whole CTs in daughter nuclei (Sun and Yokota, 1999; Habermann *et al.*, 2001).

Non-random chromosome positioning

In contrast to the apparently variable side-by-side neighborhoods there is convincing evidence of a non-random radial arrangement of CTs. A size-correlated distribution of chromosomes, with smaller chromosomes located more centrally, has been described for human fibroblast nuclei and amniotic fluid cells (Sun *et al.*, 2000; Cremer *et al.*, 2001) and for chicken fibroblast nuclei (Habermann *et al.*, 2001). However, in a majority of cells analyzed so far, the key determinant for the location of a given CT seems to be the gene density: gene dense chromosomes rather tend to be positioned in the nuclear interior while gene poor chromosomes are preferentially located at the periphery (Croft *et al.*, 1999; Boyle *et al.*, 2001; Cremer *et al.*, 2001). The most striking example has been provided by the differential location of CTs #18 and #19 in a number of human cell lines. Both chromosomes are very similar in size (85 and 67 Mb) but CT #18 is rather gene poor (with an estimated gene density of ~8 genes/Mb^{*}),

* reference: <http://www.ncbi.nlm.nih.gov/genome/guide/human>

whereas CT #19 is the gene densest human chromosome (~28 genes/Mb^{*}). The significance of this finding has been firmly corroborated by a study on lymphoblastoid nuclei of higher primate species (Tanabe *et al.*, 2002). Chromosome segments homologous to *Homo sapiens* (HSA) chromosome 18 were found to be located towards the nuclear periphery, whereas HSA 19 homologous segments were preferentially found in the nuclear interior irrespective of major chromosomal rearrangements that occurred in different phylogenetic lineages. This finding points to a conservation of segment specific nuclear location over 30 million years of evolution.

2.4 The role of the nuclear lamina on chromatin organization

Three major determinants of the nuclear architecture have been discussed since decades: the nuclear matrix, the nucleolus and the nuclear lamina. While the functional implication or even the existence of a nuclear matrix is still heavily debated (Pederson, 2000), the nucleolus has an obvious implication in determining the position and orientation of a subset of chromosomes bearing nucleolus-organizing regions (NORs). In human cells approximately 250 copies of rDNA are distributed in the NORs of five pairs of acrocentric chromosomes. These sequences constitute one or more nucleoli in a self-organizing manner due to the function of rRNA synthesis as well as processing and assembly of ribosomal subunits (Dundr and Misteli, 2001). Thus, nucleoli likely create a physical constraint for the neighboring centromeric heterochromatin and the movement of the respective CTs.

The nuclear lamina is a filamentous meshwork underlying the inner membrane of the nuclear envelope, interconnecting nuclear pore complexes (NPCs). The main components of the peripheral lamina in metazoans are lamins, which belong to the class of intermediate filaments (IF). Besides, a number of integral proteins of the inner nuclear membrane have been characterized that interact with lamin, as e.g. emerin, lamin associated protein 2 (LAP2), lamin B receptor (LBR) and others. In mammals, three lamin genes encoding seven alternatively spliced isoforms have been identified that were classified to A-type and B-type lamins. B-type lamins are expressed in all cells and are essential for cell viability, whereas A-type lamins (lamin A, AΔ10, and C) are developmentally regulated and primarily expressed in differentiated cells. Importantly, a number of diseases are linked to mutations in A-type lamins, e.g. Emery-Dreifuss Muscular Dystrophy (EDMD) (for reviews see Burke and Ellenberg, 2002; Goldman *et al.*, 2002; Hutchison, 2002).

A major function of the peripheral lamina is to maintain the nuclear shape by providing mechanical stability and elasticity. In addition to the peripheral location lamins are also dispersed in the nuclear interior. As could be shown by fluorescence recovery after photobleaching (FRAP) of GFP-tagged lamins, this nucleoplasmic veil, like the peripheral staining, is a rather stable structure and not caused by freely diffusing lamins (Moir *et al.*, 2000b). Nucleoplasmic lamins were proposed as having a function in DNA replication (Moir *et al.*, 1994; Spann *et al.*, 1997) and RNA polymerase II dependent transcription (Spann *et al.*, 2002). As peripheral heterochromatin is closely associated to the nuclear lamina, lamins have been suggested to interact with chromatin and thus influence nuclear architecture (Paddy *et al.*, 1990). In fact, lamins have been shown to bind to

chromatin *in vitro* (Taniura *et al.*, 1995) as well as to matrix attachment DNA sequences (MARs) (Luderus *et al.*, 1992). Perhaps even more important for chromatin attachment are lamin associated inner nuclear membran proteins (Wilson, 2000). For example, some isoforms of LAP2 can bind DNA directly (*in vitro*) or via a specific DNA binding protein (BAF) (Furukawa, 1999; Cai *et al.*, 2001) and LBR has been shown to bind *in vitro* DNA and moreover interact with HP-1, suggesting a major docking function for peripheral heterochromatin (Pyrpasopoulou *et al.*, 1996; Ye and Worman, 1996).

Apart from the obvious peripheral location of the lamina, nuclear lamins as well as associate proteins also often display cell type specific internal structures like foci, invaginations and tube like structures that do sometimes branch or even cross the nucleus (Bridger *et al.*, 1993; Moir *et al.*, 1994; Ellenberg *et al.*, 1997; Fricker *et al.*, 1997). Moreover, live cell observation of GFP-tagged lamina-proteins revealed a considerable dynamic nature of the nuclear lamina, forming indentations and foldings (Broers *et al.*, 1999; Moir *et al.*, 2000a; Daigle *et al.*, 2001). Despite the evidence of interaction of the nuclear lamina and chromatin it is not yet clear to which extent it is involved in the spatial nuclear organization.

2.5 Goals of the present work

The present work focuses on the fluorescent labeling of distinct chromatin sites in living cells and their long-term observation in order to study chromatin dynamics over one or more cell cycles and potentially during terminal differentiation. A particular aim was to assess methods to follow the fate of early and mid-to-late replicating chromatin sites and/or entire chromosome territories.

To achieve these goals an optimized *in vivo* replication labeling protocol, termed scratch replication labeling (SRL, described in detail in chapter 3.9.1) as well as a system for long-term 4D-microscopy (chapter 3.12.2) were established. These developments helped to investigate dynamic properties of CTs and chromatin domains in relation to other nuclear structures labeled by GFP, such as the nuclear chromatin labeled by histone H2b-GFP and the nuclear lamina labeled by lamin C-GFP (see below).

Chromosomal order during cell cycle

To investigate whether major changes of CT positions in interphase nuclei may occur during more extended time periods, scratch replication labeling with Cy3-dUTP was performed on a HeLa cell line stably expressing GFP-tagged histone H2B (Kanda *et al.*, 1998). During the second and subsequent post-labeling mitoses Cy3-labeled and unlabeled chromatids segregate resulting in nuclei with a steadily decreasing number of labeled CTs. By using this labeling/segregation approach with HeLa H2B-GFP cells, it was possible to follow relative movements of ~1Mb domains and chromosome territories in the context of overall nuclear movements. A setup for long-term confocal microscopy was developed to extend observations to cover a complete cell cycle. The mobility of CTs during different cell cycle stages was assessed by measuring 3D distances of fluorescence intensity centers of CTs and the nucleus at different time points.

A photo-bleaching approach was employed to analyze possible changes of chromosome arrangements during mitosis. As histone H2B-GFP shows only slow recovery after photobleaching in non S-phase cells (Kimura and Cook, 2001),

nuclear chromatin could be partially bleached in mother cell nuclei during G2. The unbleached chromatin was then followed from mother nuclei to their daughter nuclei. In case where chromosome positions were globally inherited through mitosis, faithful restoration of the nuclear topology of GFP labeled chromatin would be expected.

In complementing 3D FISH experiments with chromosome paint probes performed on HeLa cell clones at the 2- and 4-cell stage, the potential symmetry in daughter cell nuclei, as well as the possibility of major differences of chromosome arrangements at the 4-cell stage should be assessed.

Interaction of chromatin with the nuclear lamina

To address the interaction of the nuclear lamina and mid-to-late replicating chromatin, preliminary experiments were performed employing *in vivo* replication labeling at defined time points to label functionally distinct chromatin compartments in combination with immunostaining of the lamina in fixed cells to investigate spatial relationships. Furthermore labeling/segregation experiments were performed with living CHO cells expressing lamin C-GFP (Broers *et al.*, 1999) to gain insight into the dynamic association of the nuclear lamina and chromatin.

In addition, initial experiments shall be presented to assess the functional interconnection between specific chromatin compartments and the nuclear lamina. These experiments employ a dominant negative mutant lamin A protein, Δ NLA, which is lacking the amino terminal nonhelical domain of human lamin A (developed in the Lab of R.D.Goldman, NWU Chicago). The mutant protein prevents normal assembly of the lamina and thereby causes disruption of the lamin organization as well as a reduction of DNA replication (Spann *et al.*, 1997).

3. Methods and Protocols

3.1 Cell culture

Cells are routinely cultivated in 25 cm² tissue culture flasks in RPMI 1640 medium or *Dulbeccos modified Eagle* medium (DMEM)* supplemented with 10% fetal bovine serum (FBS) and antibiotics at 37°C and 5% CO₂ in a humidified incubator. When cells reach confluence (*i.e.* cells form a dense monolayer on the bottom of the culture flask), they are trypsinized and resuspended in fresh medium. A fraction of cells (1/3 to 1/12, depending on proliferation rate and splitting frequency; see Table 2 for recommendations) are transferred into a new tissue culture flask for further cultivation. The remaining cells are either discarded or seeded onto coverslips for further experiments.

Table 2. Cell lines used in the present work.

cell line	medium	split ratio	split frequency
HeLa H2B-GFP	RPMI 1640 + 10% FBS + 100 U/100 µg/ml Penicillin/Streptomycin	1:4 - 1:8	every 2-3 days
SH-EP N14	RPMI 1640 + 10% FBS + 100µg/ml Gentamycin	1:8 - 1:12	every 2-3 days
CHO Lamin C-GFP	DMEM+ 10% FBS + 100 U/100 µg/ml Penicillin/Streptomycin	1:8 - 1:12	every 2-3 days
BHK-21	DMEM+ 10% FBS + 100 U/100 µg/ml Penicillin/Streptomycin	1:8 - 1:12	every 2-3 days
Primary human fibroblasts	DMEM+ 10% FBS + 100 U/100 µg/ml Penicillin/Streptomycin	1:3 -1-6	every 3-4 days

* DMEM and RPMI 1640 media generally contained stable glutamine. In live cell experiments (see 3.12), media containing 15 mM or 25 mM HEPES buffer were used.

Equipment and solutions:

- Serological pipettes (5 ml / 10 ml / 25ml)
- Autoclaved Pasteur pipettes (optional)
- 25 cm² tissue culture flasks
- PBS (calcium and magnesium free)
- Trypsin-EDTA: 0.05% (w/v) trypsin and 0.02% (w/v) EDTA in PBS.
- Appropriate culture medium (see above; prewarmed to 37°C)
- Trypsin-EDTA solution (0,05%/0,02% in PBS)

Method:

All steps are performed in a sterile laminar flow cabinet equipped with a Bunsen burner, an automatic pipette aid and a waste container.

1. Decant medium to a waste medium container or aspirate medium with the aid of a Pasteur pipette connected to vacuum pump. Then wash 1× with PBS.
2. Add 1 ml Trypsin/EDTA-solution. After a few seconds decant or aspirate supernatant Trypsin.
3. Incubate 2 to 4 min at 37°C in the CO₂ incubator.
4. Tap the flask a few times gently against the palm of the hand until all cells have detached from the flask bottom. Control this process under a phase contrast microscope.
5. Resuspend cells in 3-12 ml appropriate culture medium, depending on the desired split ratio. Transfer 1 ml of the suspension to a fresh 25 cm² tissue culture flask which has previously been filled with 9 ml fresh medium. Mix the suspension by pipetting up and down. (Remaining cells can be used for further experiments, otherwise discard.)
6. Incubate at 37°C and 5% CO₂ in a humidified incubator.

3.2 Freezing and thawing of cells

Equipment and solutions:

- Cryotubes
- Ice in bucket
- 50 ml FALCON tube
- PBS
- Trypsin-EDTA solution (0,05%/0,02% in PBS)
- Appropriate culture medium (see above; prewarmed to 37°C)
- Freezing medium (RPMI 1640 or DMEM / 20% FBS / 10% DMSO), on ice

Method:

Freezing (Cryopreservation):

1. Grow cells in a 75 cm² tissue culture flask.
2. Use cells in the logarithmic phase of growth (50%-80% confluency). After washing and trypsinizing (see protocol 3.1) resuspend cells in 20 ml full medium and transfer them to a 50 ml FALCON tube.
3. Centrifuge for 10 min at 200 g. Aspirate supernatant with a Pasteur pipette and resuspend pellet in 20 ml freezing medium.
4. Aliquot cell suspension into 2 ml cryotubes, and immediately place them onto ice. Cool down cryotubes at -20°C on ice for a few hours. Subsequently keep them at -80°C over night. Thereafter the cells can be stored in liquid nitrogen.

Thawing:

1. Remove cells from liquid nitrogen tank, loosen the cap of the cryotube and quickly place it into a 37°C water bath.
2. Immediately after cell suspension has melted transfer it to a 25 cm² tissue culture flask filled with 8 ml prewarmed culture medium.
3. When cells attached to the bottom (after ~30 min) exchange medium.

3.3 Slide preparation

Coverslips (15×15 mm / 20×20 mm square or 40 mm Ø round) are washed thoroughly with d H₂O to remove dust and then stored in 80% ethanol. Before use, each coverslip is flamed and then transferred to a 35/10 mm or 60/15 mm tissue culture dish.

3.4 Seeding cells on coverslips

Equipment and solutions:

- Fine forceps
- Coverslips (stored in 80% ethanol)
- 35/10 mm or 60/15 mm tissue culture dishes
- FALCON tube
- Appropriate cell culture medium
- PBS (37°C)
- Trypsin-EDTA solution (0,05%/0,02% in PBS)

Method:

1. Trypsinize cells from a confluent grown culture flask under routine conditions (see 3.1) and resuspend in 10 ml medium.
2. Calculate volume of cell suspension (V_c) needed for n dishes and transfer it to a FALCON tube; add appropriate amount of fresh medium (V_d) given by:

$$V_c = n \times r_{split} \times 10 \text{ ml} \times \frac{A_{dish}}{A_{flask}}$$
$$V_d = (n \times V_{dish}) - V_c$$

where r_{split} denotes the splitting ratio, A_{dish} the dish area = 28.3 cm² (60/15 mm) or 9.6 cm² (35/10 mm), A_{flask} the flask area (25 cm² or 75 cm²) and V_{dish} the final volume in one dish = 5 ml (60/15 mm) or 2 ml (35/10 mm).

3. Mix well and distribute onto dishes with coverslips.
4. Incubate in CO₂ incubator over night or longer until the cells reached the desired density.

3.5 Fixation of cells grown on coverslips

Equipment and solutions:

- Fine forceps
- Coverslips (stored in 80% ethanol)
- 60/15 mm tissue culture dishes
- PBS (37°C)
- Fixative (4% paraformaldehyde in 1×PBS or 3,7% formalin 1:10 in 1×PBS)
- PBST washing buffer (0,02% Tween 20 / 1×PBS (0.04% Na-Azid)

Method:

1. Wash coverslip with cells briefly in PBS, then transfer quickly to the fixative (5 ml in a 60/15 mm dish) with aid of a fine forceps.
2. Incubate 10 min in fixative at room temperature.
3. Exchange fixative with PBST by adding a few ml PBST, then decant approximately half of the amount and fill up again with PBST.
4. Wash 2 × briefly with PBST (at this point a complete exchange of solutions is possible without a risk of drying).
5. If required the specimen can be stored at this point for a few days at 4°C, otherwise proceed to protocol 3.6.

Notes:

- Cells grown on coverslips are very sensitive to drying. Therefore all steps involving transfer of the coverslip or exchange of buffers should be performed as quickly as possible. The addition of a small amount of detergent (0.02% Tween 20) to the washing buffer facilitates the moistening of the cells and helps to prevent drying artifacts.
- All washing buffers contain Na-azid to prevent growth of microorganism. Skin contact should be avoided.

3.6 Post-fixation treatments and immunostaining

Equipment and solutions:

- Light proof humidified chamber for incubation with antibodies
- Fine forceps
- Microscopic slides
- Nail polish (transparent)
- PBS (37°C)
- Fixiative (4% paraformaldehyde / 1×PBS or 3,7% Formalin 1:10 / 1×PBS)
- PBST washing buffer (0,02% Tween 20 / 1×PBS (0.04% Na-Azid))
- Permeabilization buffer (0,2% Triton X-100 / 1×PBS)
- Blocking solution (2% BSA in PBST)
- Primary antibodies (against the epitope to be detected) diluted in appropriate concentration in blocking solution.
- Fluorochrome-conjugated secondary antibodies against primary antibodies, diluted in appropriate concentration in blocking solution.
- Counterstaining solution: DAPI-solution (0,02 µg/ml in PBST) or
PI-solution (1-10 µg/ml in PBST) or TO-PRO-3 solution (1-2 µM in PBST)
- Antifade mounting medium (Vectashield®)

Method:

1. Incubate 3 min in permeabilization buffer (0.2% Triton X-100/PBS).
2. Wash 2 × briefly with PBST.
(If no immunodetection is required proceed to 8)
3. Incubate 10 min in blocking solution (2% BSA in PBST).
4. Apply primary antibody solution: Add one drop (50-100 µl is sufficient for a 15 mm² coverslip) onto a piece of PARAFILM stretched on a (used) QuadriPERM™ cover (or any other appropriate device that fits inside the humidified chamber). Take the coverslip from the blocking solution with a forceps and place it cell-side down onto the drop. Incubate 30 min at 37°C or 1 h at RT in humidified chamber.
5. Wash 3 × 3 min with PBST while shaking.
6. Incubate 30 min at 37°C or 1 h at RT with secondary antibody solution.
7. Wash at least 5 × 3 min (or longer) with PBST while shaking.
8. Incubate 2 - 5 min with counterstaining solution, thereafter wash briefly with PBST.
9. Place a drop of mounting medium on a microscope slide and mount the coverslip with the cell side down.
10. Remove excess medium around the coverslip with soft paper and seal the coverslip with nail polish.

RNase treatment (optional):

Some counterstain dyes (e.g. PI and TO-PRO-3) also bind to RNA, which may lead to unwanted staining of the nucleoli and the cytoplasm. This can be avoided by additional 30 min incubation in 200 µg/ml RNase/PBST at 37°C, after fixation and washing.

Notes:

- In case of labeling with light sensitive fluorochromes all steps should be performed light protected.
- The tissue culture dish used for fixation can generally be used throughout the following washing procedures. When several coverslips are processed at the same time, it is recommendable to use a 6-well plate and to exchange buffers using disposable Pasteur pipettes.
- To avoid background problems with the fluorescing secondary antibodies the subsequent washing steps should be performed very thoroughly. More washing steps and/or longer washing periods will reduce background. It might also be helpful to switch to a new dish after the 2nd or 3rd washing step.

3.7 Metaphase preparation

3.7.1 Fixation of mitotic cells in methanol/acetic acid

Equipment and solutions:

- 37° water bath
- Appropriate cell culture medium (prewarmed to 37°C)
- Colcemid (10 µg/ml)
- Fixative (Methanol/acetic acid, 3:1, v/v), -20°C
- Hypotonic solution (75 mM KCl), prewarmed to 37 °C
- 15 ml FALCON tubes
- disposable Pasteur pipettes

Method:

Metaphase enrichment:

1. Grow cells in a 25cm² tissue culture dish to approx. 80% confluency. To obtain a higher rate of metaphases the cells may be synchronized (see protocol 3.11).
2. Add 100 µl colcemid, mix well and return flask to the incubator for another 20-40 min* (for 5-10 min in case of synchronized cells).
3. Trypsinize cells and resuspend in 10 ml fresh prewarmed medium (see protocol 3.1).

Hypotonic treatment:

4. Transfer to a 15 ml FALCON tube and centrifuge 10 min at 200 g.
5. Aspirate supernatant with a Pasteur pipette leaving a ~1 ml in the tube, resuspend cell pellet by tapping on the tube.
6. Add dropwise 5 ml of the hypotonic solution (prewarmed to 37°C) with a plastic pipette, while gently vortexing or tapping the tube, then fill up to 12 ml with KCl solution.
7. Incubate 10-15 min at 37°C in water bath.

Fixation:

8. Add approx. 20 drops freshly made, ice-cold fixative, mix by turning the tube upside down.
9. Centrifuge 7 min at 1100 rpm. Aspirate supernatant up to 2 ml and resuspend cell pellet by tapping on the tube.
10. Add dropwise 5 ml fixative while gently vortexing with lowest speed. Then add fixative to 12 ml.
11. Centrifuge 7 min at 1100 rpm. Aspirate supernatant up to 0.5 ml and resuspend cell pellet again, then add fixative to 12 ml.
12. Repeat this step at least 4 times.
13. The cell suspension may be stored at -20°C, otherwise proceed to 3.7.2.

* longer incubation periods will result in higher fraction of metaphases, however it is accompanied by a stronger condensation of the chromosomes.

3.7.2 Preparing metaphase spreads

The quality of metaphase chromosome spreads depends primarily on the humidity over the slide and ambient temperature during the drying of cell suspension on pre-cleaned slides. The method described here creates reproducible conditions and lead to consistently good quality of metaphase preparation as judged by metaphase area and chromosome overlap (Deng *et al.*, 2003). A water bath is used to create the suitable humidity and ambient temperature for cell drying.

Equipment and solutions:

- Disposable Pasteur pipette
- Cleaned microscopic slides: Place slides ~1 h in a coplin jar filled with Ethanol/Ether (1:1). Wipe dry with a clean towel and place into a coplin jar filled with d H₂O.
- 50°C water bath (Lauda T15: 30×30cm water surface, filled to a level of 3.7 cm from the water surface to the water bath cover)
- Metal tray (16×10cm)
- Cell suspension (on ice)
- Fixative (methanol/acetic acid, 3:1, v:v), freshly prepared (on ice)
- Coplin jar filled with 70% ethanol

Method:

1. Centrifuge 7 min at 1100 rpm, aspirate supernatant and resuspend cell pellet in 0.5 - 5 ml ice cold fixative depending on the size of the pellet and the desired nuclei/metaphase density.
2. Wipe the cleaned microscopic slide dry with a Kimwipe tissue and place it into the metal tray.
3. Drop 12 µl of the cell suspension from a height of 1 cm onto a horizontally placed dry slide.
4. Then quickly place the tray into the water bath and close the cover immediately.
5. After ~40 sec drying remove metal tray from the water bath, check the slides under a phase-contrast microscope.
6. Cool down the metal tray under tap water for the next use.
7. Place the slides in 70% ethanol (over night or for a few hours) to wash away acetic acid.
8. Age slide at least 2 days at room temperature.

Notes:

- In principle, any water bath and any size metal tray can be used, however, the ratio (R) of the net water surface area available for evaporation (*i.e.* the entire water surface minus the area occupied by the metal tray) to the air volume in the covered water bath is important. R should be in the range of ~0.22 (Deng *et al.*, 2003) and can be adjusted by changing the water level and therefore the air volume.
- Dropping height, slide angle, cooling or moistening of the slides before dropping, etc. have no apparent effects on the quality of chromosome spreads.

- For longer storage dehydrate slides by subsequent incubations in 70%, 90% and 100% ethanol (3 min each) and store at -20°C for several months in a slide box together with a desiccant.

8. Apply primary antibody solution: Add one drop (50-100 µl is sufficient for a 15 mm² coverslip) onto a piece of PARAFILM and place the coverslip cell-side down onto the drop. Incubate 30 min at 37°C in humidified chamber.
9. Wash 3 × 3 min with PBST while shaking.
10. Incubate 30 min at 37°C or 1 h at RT with secondary antibody solution:
sheep anti-mouse Cy3 (1:500 in blocking solution) or
goat anti-mouse Alexa488 (1:300 in blocking solution)
11. Wash at least 5 × 3 min (or longer) with PBST while shaking.
12. Counterstain and mount in antifade medium.

Notes:

BrdU pulse length can be varied. 5 min may already be sufficient to detect the typical replication pattern. However, extended incubation times will result in brighter signals as more BrdU is incorporated per replication focus. Since each replication focus is active for ~45 - 60 min the distinct pattern will gradually become more dispersed with pulse lengths exceeding one hour (although this may be intended in certain cases).

The success of the detection mainly depends on the denaturation step. As the activity of the DNase may vary from batch to batch it might be necessary to adjust either concentration or incubation time.

3.9 *In vivo* replication labeling

The detection of halogenated thymidine analogues requires chemical fixation of the cells (e.g. with paraformaldehyde), permeabilisation with detergents and denaturation of the DNA by endonucleases, HCl or heating in formamid, in order to make the epitopes accessible to the antibodies. All of these steps may raise concerns about possible artifacts and, moreover, are incompatible with *in vivo* analyses of chromatin dynamics. For the visualization of replication labeled DNA in living cells, DNA precursors have to be employed that are directly coupled to a fluorochrome. Several fluorochrome-coupled deoxy-nucleotides (dNTPs) are commercially available. Unlike BrdU, which is taken up by the cells from the surrounding medium and becomes phosphorylated and incorporated into DNA, these nucleotides are membrane impermeable due to the charged phosphate group as well as to the fluorophore residue. Hence, a procedure is required for dNTPs to pass the cell membrane barrier. A well-established and reliable method is microinjection of a nucleotide solution through a thin glass capillary directly into the cytoplasm or nuclei of adherently growing cells (Pepperkok and Ansorge, 1995). This method has been successfully applied to mark the DNA of individual chromosomes as well as specific chromatin compartments (Zink *et al.*, 1998). However, this procedure is tedious, requires costly equipment and allows only treatment of a rather small number (some 100) of cells in each experiment. In a considerable number of microinjected cells the cell cycle is arrested or delayed, even cell death was noted especially when applying two labeling pulses within one S-phase. Consequently, the success rate of surviving double-labeled cells is rather low. In addition, the generally limited number of labeled cells is disadvantageous for the *in vivo* observation of single CTs after segregation. Although it may be possible to microinject cells seeded at low density they will grow more or less confluent until they are showing sufficient segregation after some 5 to 6 cell divisions. A proper live cell observation thus requires subcultivation of labeled cells, which in the case of a microinjected culture will lead to a considerable small fraction of labeled cells within the bulk of unlabeled ones.

A short-term, transient permeabilization that allows the uptake of macromolecules from the surrounding medium can be achieved by a number of methods (reviewed in McNeil, 1989), yet not all of them are useful for *in vivo* replication labeling. Chemical detergents (e.g. Triton X-100, saponin or digitonin) permeabilize cells effectively, but have detrimental effects on cell viability. Application of more gentle, “non-invasive” methods like lipofection (Haukenes *et al.*, 1997), hypotonic shift loading (Koberna *et al.*, 1999) and osmotic lysis of pinosomes (Okada and Rechsteiner, 1982) resulted in labeling of cells with only low efficiency. More suitable with regard to loading efficiency and viability are methods creating slight mechanical damage to the cell membrane in the presence of nucleotides. Uptake of macromolecules to the cytoplasm can be achieved by a bead loading protocol involving the shaking of cultures in the presence of glass beads with 100 µm diameter (McNeil and Warder, 1987), by complete detachment of a cell layer with a cell scraper (McNeil *et al.*, 1984) or by applying scratches in a cell layer with a pointed instrument (Swanson and McNeil, 1987). With regard to replication labeling, the bead loading procedure allowed effective labeling of attached cells (Manders *et al.*, 1999). However, the efficiency of labeling and the viability of bead-loaded cells were difficult to reproduce. Scrape loading provided

efficient labeling of a large proportion of cells but was notably damaging and required additional time for the reattachment of cells.

The most consistent results in terms of labeling efficiency, reproducibility and amount of nucleotides needed, were obtained with an adapted scratch loading protocol, termed scratch replication labeling (SRL). This protocol is simple to perform and allows the labeling of large numbers of adherently growing cells with superior reproducibility. Most importantly, it does not impair the further cell growth of a large fraction of affected cells. (Schermelleh *et al.*, 2001). The SRL protocol is useful to obtain cells with labeled chromosome territories for analysis in live cell experiments and can be applied for a 2-color labeling at two distinct time points in S-phase (see chapter 3.9.1). Furthermore, this method can be used for the labeling of nascent RNA using BrUTP (5 mM) as an alternative to microinjection or run-on-transcription labeling (Wansink *et al.*, 1993)*.

3.9.1 Scratch replication labeling (SRL)

Equipment and solutions:

- Appropriate cell culture medium, prewarmed to 37°C
- Labeling solution: 20 µM Cy3-dUTP (1:50 diluted in medium)
or 50 µM FITC-dUTP (1:20) or 50 µM Cy5-dUTP (1:20)
- Hypodermic needle (e.g. Sterican 0,90 × 40 mm; Braun, Melsungen)
- Tissue culture dish (Ø 60 mm)
- Paper wipe (e.g. KIMWIPES lite precision wipes)
- Fine forceps

Method:

1. Seed cells on small coverslips (15×15 mm) and grow them until they reach near confluence
2. Take the coverslip with a fine forceps, drain excess medium, briefly dry the bottom side of the coverslip with a wipe and place it into the empty tissue culture dish. This will prevent sliding of the coverslip during the subsequent scratching procedure.
3. Add 8-10 µl of the labeling solution onto the coverslip and distribute it evenly over the cells by tilting the dish. Surface tension prevents the solution from running off the coverslip.
4. With the tip of a hypodermic needle apply parallel scratches into the cell layer. For a high fraction of labeled cells, scratches should be performed a few cell diameters apart from each other, then cover the complete coverslip (Figure 4). For an optimal coverage the procedure can be performed under a low magnification phase-contrast microscope (e.g. 5× objective lens). The procedure should not take longer than a few minutes to avoid drying of the cells.
5. Add 5 ml pre-warmed medium and incubate further. Exchange medium after 30-60 min to remove non-incorporated nucleotides.

* Scratch transcription labeling (STL) protocol has been already successfully applied in the diploma thesis of C. Ahrens (2002) and H. Albiez (2003).

6. To obtain nuclei with segregated labeled and unlabeled chromosome territories the cells can be harvested by trypsinization some hours later and be further cultivated for two or more cell cycles prior to live cell observation. The day before live cell observations are carried out cells are seeded on round coverslips fitting the live cell chamber (see protocol 3.12.2).

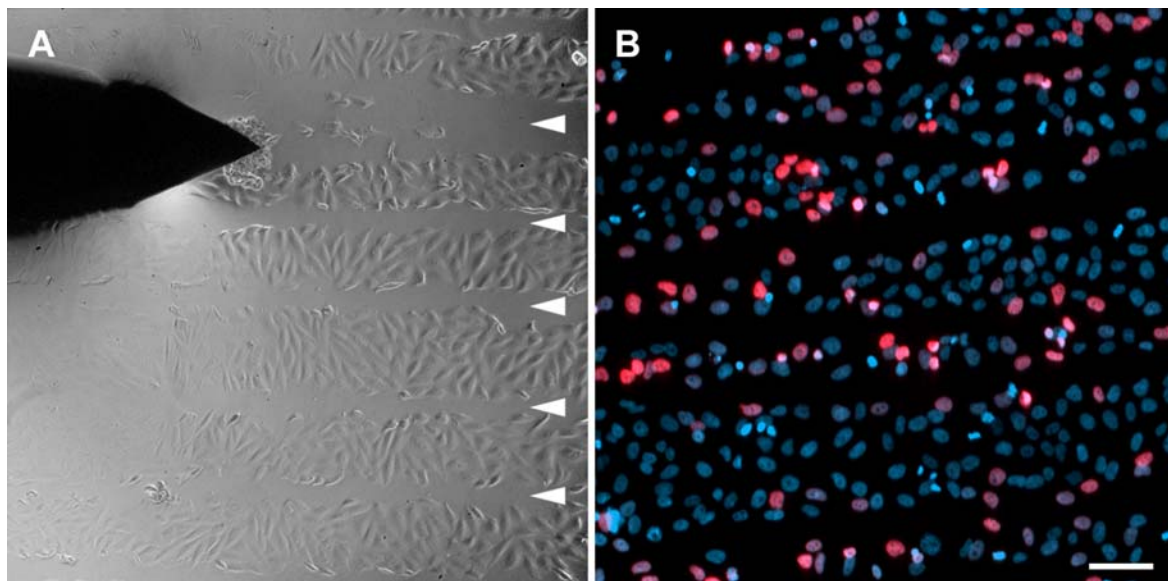


Figure 4. Scratch replication labeling procedure. (A) Arrowheads indicate scratches applied with the tip of a hypodermic needle (shadow) in the presence of Cy3-dUTP to a monolayer of SH-EP N14 neuroblastoma cells. (B) Cells were fixed with 4% formaldehyde two hours after scratching procedure and counterstained with DAPI (red). Numerous cells display Cy3-dUTP labeled nuclei (green) along the scratch lines. Bar: 100 μ m.

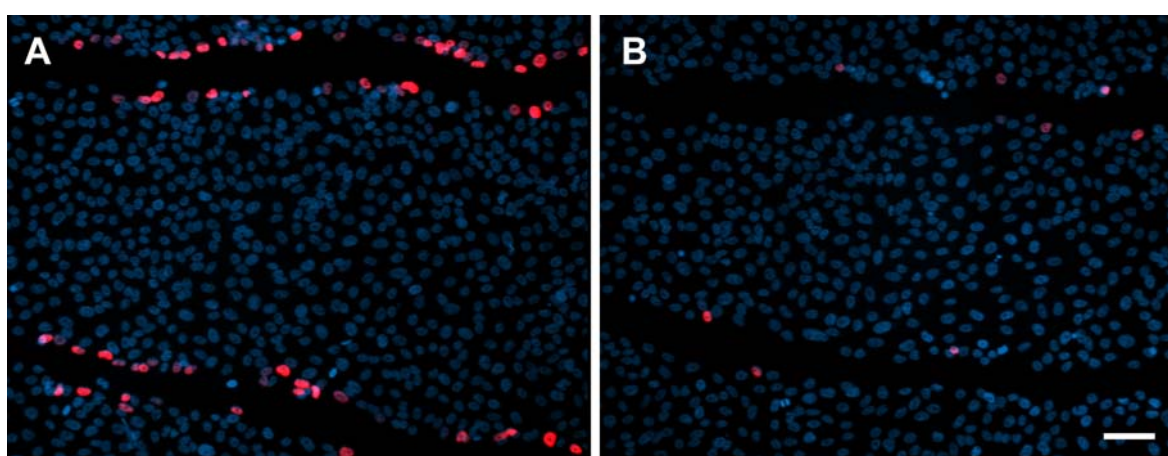


Figure 5. Short-term permeabilization induced by scratching. (A) Scratches were applied in a monolayer of synchronized SH-EP N14 cells in the presence of Cy3-dUTP (green). The scratchlines are outlined by numerous labeled nuclei. (B) The Cy3-dUTP solution was applied \sim 1 min after scratching. Only a limited number of cells incorporated the label indicating the transient permeabilization. Cells were fixed 2 hours after SRL with 4% formaldehyde and counterstained with DAPI (red). Bar: 100 μ m.

Notes:

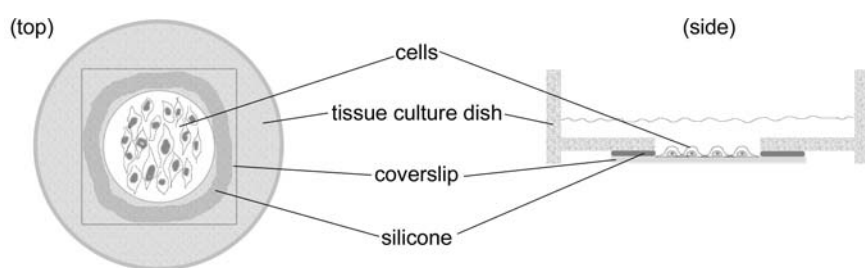
- The scratch procedure creates damage in the cell membrane that probably last only for a few seconds (“transient holes”). This allows the uptake of charged macromolecules (like fluorochrome coupled dUTPs) from the surrounding medium, for which cells would normally be impermeable (Figure 5). Accordingly, affected S-phase cells alongside the scratch line as well as cells that are lifted off the surface by the needle will incorporate the modified nucleotides.
- The fraction of replication labeled cells depends (1) on the density of scratches applied, *i.e.* how many cells are affected and (2) on the number of cells that are in S-phase. Synchronization of cells at G1/S transition (*e.g.* by aphidicolin, see protocol 3.11) is recommended to obtain a high yield of labeled cells.
- The mechanical treatment will notably have variable effects on individual cells depending on the degree of membrane damage. As with the microinjection approach, the staining intensities of each individual cell may vary depending on the amount of the nucleotide influx. The size of the initial cytoplasmic nucleotide pool may also influence the effective length of incorporation. Generally the initial pool constantly decreases during a period of 1.5 to 2.5 hours, probably mediated by active vesicular export processes. (Fauth and Zink, 2001). However, the resulting replication patterns rather correspond to BrdU labeling of no more than one hour pulse duration, indicating effective pulse duration of near one hour with *in vivo* labeling approaches.
- Similar to microinjection, the scratching procedure is likely to cause more severe damages to a fraction of cells, possibly leading to cell cycle arrest or cell death of a number of cells. However, the relative and absolute number of labeled cells obtained is far higher when the SRL protocol is applied. The majority of cells seem to pass the mitotic checkpoint, although some may show a delay possibly due to excision repair processes. Surviving cells that have passed the first mitosis show no obvious differences in further cell cycle kinetics in comparison to non-labeled cells.
- Cy3-dUTP is significantly brighter and more photostable than Cy5- and FITC-dUTP and is therefore best suited for *in vivo* observation. In case where especially high fluorescence intensities are desirable (*e.g.* for long term *in vivo* observations after segregation) a higher concentration of nucleotides (100 µM) is advantageous. No improvements of label intensities were noted when adding non-fluorescent dNTPs to the labeling solution or by using different labeling buffers (PBS or TBS instead of medium).

3.9.2 Two-color scratch replication labeling

Double labeling with different fluorochrome coupled dUTPs at two distinct time points in one S-phase requires a particularly high labeling efficiency. Therefore, the cells have to be synchronized effectively at G1/S transition prior to the first labeling (see chapter 3.11) and cell cycle parameters of the given cell line should be determined. In particular, S-phase length and the timing after release from the synchronization block at which the majority of cells display the early, mid or late replication pattern have to be determined first (see chapter 3.10).

Use of a self-made glass bottom tissue culture dish further enhanced labeling efficiency in double labeling experiments: A hole with a diameter of about 15 mm was made in a 30 mm Ø tissue culture dish. The drilling edge was trimmed with an abrasive paper; the dish was then thoroughly cleaned with d H₂O. The hole was covered on the bottom side with a 20×20 mm coverslip attached with silicone vacuum grease* (Bayer silicone, medium, Neolab) at the bottom surface of the culture dish (see diagram below). This assembly was subsequently UV irradiated for sterilization.

Cells were seeded on the glass coverslips attached at the bottom of the perforated tissue culture dish. Cells were then grown to subconfluence and synchronized as described in protocol 3.11. For the labeling, the medium was aspirated with a Pasteur pipette and 5 µl of labeling solution were added onto the coverslip. Scratches were applied as described above. Only a small amount (0.5 ml) of prewarmed CO₂-adapted medium was then added into the indentation formed by the dish and the attached coverslip. This procedure assures reattachment of the labeled cells that were completely detached by the scratching procedure, thus resulting in higher yields of labeled cells. After 30 min, this medium was replaced by 2 ml fresh culture medium to remove any non-incorporated nucleotides. The culture dish was then kept at 37°C in a humidified incubator with 5% CO₂ until second labeling.



* Silicone does not interfere with cell growth and allows the removal of the coverslip for a subsequent fixation. The described device may also be used for short-term observation of cells with an inverted epifluorescence microscope at high resolution.

3.9.3 Microinjection of fluorescent nucleotides

Equipment and solutions:

- coverslips for live cell chamber (FCS2: 40 mm Ø or CELLocate for EMBL chamber) in a 60/15 mm tissue culture dish
- Tungsten pen
- Borsilicate glass capillaries (\varnothing_i 0.94 mm, \varnothing_e 1.2 mm)
- Microloader tips
- Microinjection system
- Appropriate cell culture medium (with HEPES), prewarmed to 37°C
- Fluorescent nucleotides (1mM)
- PBS

Method:

1. Seed cells on coverslips fitting into live cell chamber. To relocate microinjected cells when using a 40 mm Ø coverslip seed cells only on a limited central area of a clean dry coverslip (see 3.12.2 A). Central area of the coverslip may be also labeled with a tungsten pen before seeding cells.
2. Dilute fluorescent nucleotides 1:10 in PBS (100 µM final concentration) and centrifuge 15 min at 13000 rpm before microinjection in order to pellet particles that might clog the capillary.
3. Load ~1-2 µl of the labeling solution into a freshly pulled capillary and attach the needle to the microinjection device.
4. Microinject cells (according to the manufactures instructions) during a maximum 30 min period, either into cytoplasm or directly into the nucleus.
5. Then replace the old medium with fresh CO₂ adapted medium and incubate further.

3.9.4 Direct pulse labeling after permeabilization with digitonin

Time consuming immunodetection of BrdU can be bypassed by direct labeling with flourochrome coupled dUTPs mediated by *in vivo* permeabilization with digitonin. This mild nonionic detergent was previously shown, unlike Triton X-100 and NP40, not to inhibit DNA replication (Dimitrova and Gilbert, 1998). Moreover, digitonin does not cause living cells to detach from the surface, which is the case with other permeabilizing agents, like Triton X-100 and saponin. The protocol presented here creates an even permeabilization of the treated cell culture without (or only slightly) affecting nuclear architecture (as judged on light microscopical level). Although digitonin treatment does not impair DNA replication it still has obvious detrimental effects leading to increasing cell death several hours after the treatment. Hence the method is restricted to short puls labeling (15-30 min incorporation) followed by cell-fixation. Thus, *in vivo* labeling using digitonin provides a quick and simple alternative to short-term replication labeling with BrdU and transcription labeling with BrUTP.

Equipment and solutions:

- Fine forceps
- Empty tissue culture dish
- Microscopic slides
- Nail polish (transparent)
- Appropriate cell culture medium
- Digitonin-labeling solution (40 µg/ml digitonin / 20µM Cy3-dUTP in medium)
- PBS (37°C)
- Fixiative (4% paraformaldehyhde / 1×PBS or 3,7% Formalin 1:10 / 1×PBS)
- PBST washing buffer (0,02% Tween 20 / 1×PBS (0.04% Na-Azid))
- Permeabilization buffer (0,2% Triton X-100 / 1×PBS)
- Counterstaining solution: DAPI-solution (0,02 µg/ml in PBST) or PI-solution (1-10 µg/ml in PBST) or TO-PRO-3 solution (1-2 µM in PBST)
- Antifade mounting medium (Vectashield)

Method:

1. Seed cells on small coverslips (15 ×15 mm) and grow them until they reach ~80% confluency.
2. Take the coverslip with a fine forceps, drain excess medium and place it into an empty tissue culture dish.
3. Add 10 µl of the digitonin-labeling solution onto the coverslip. Shake the dish a little, so that the solution distributes evenly over the cells. Due to the surface tension the solution should not run off the coverslip.
4. Incubate 5 min at room temperature.
5. Add a few ml prewarmed medium, wash briefly, aspirate and add another 5 ml medium and incubate another 15 min in the CO₂ incubator at 37°C.
6. Fix cells in 3,7% formaldehyde (as described in 2.4).
7. Incubate 3 min in permeabilization buffer (0.2% Triton X-100/PBS) and then wash in PBST. This step is will remove cytoplasmic Cy3-dUTP background.
8. Counterstain and mount on microscopic slides as described above.

Note:

The final concentration of digitonin has to be adapted for each cell line. Too low concentration does not provide permeabilization of all cells, whereas too high concentration causes immediate changes of the nuclear morphology within 15-30 min.

3.10 Characterization of the cell cycle stages

3.10.1 Doubling time / Cell cycle length

A simple way to calculate the cell cycle is to determine the density of proliferating cells at two different time points. Ideally the two chosen time points should fall into the logarithmic growth phase when cells reached more than ~30% confluence and do not exceed ~80% confluence. The cells have to regain the full proliferation rate after the trypsinization process (lag-phase). On the other hand, high cell density may slow down proliferation due to contact inhibition.

The cell density can be assessed in a cell counting chamber (e.g. Fuchs-Rosenthal, according to the manufacturers instructions) after trypsinising and resuspending cells in PBS-trypan blue (v/v 1:1). The number of living cells (non-stained by trypan-blue) is then counted for a defined volume.

Alternatively cells may be seeded with equal density on coverslips and fixed at different time points. After fixation the cells are permeabilized, DAPI stained and mounted on microscopic slides according to standard procedures. 5 to 10 randomly selected areas are then recorded with an epifluorescence microscope* equipped with a CCD camera using a low-resolution objective (e.g. 16x). Thereafter the DAPI stained nuclei can be easily counted on digital images (e.g. using ImageJ).

Doubling time t_d of the cell culture is then calculated by

$$t_d = \frac{\log 2 \times \Delta t}{\log N_2 - \log N_1}$$

where N_1 and N_2 are the number of counted cells per any given area on the coverslip fixed at time point 1 and 2 respectively, and Δt is the duration between the two fixations.

The doubling time is equivalent to the cell cycle length when 100% of the cells are in a proliferating state, as judged by immunodetection of Ki-67 protein (see below).

* In this case, dead cells are also excluded from counting as early apoptotic stages are easily identified by DAPI counterstain, whereas already detached dead cells are washed away before fixation.

3.10.2 Determination of cell cycle stages

Essential cell cycle parameters of a cell culture can be assessed by immunostaining of pKi-67 and BrdU, following a 15 min pulse labeling and fixation (see 3.6 and 3.8). Ki-67 protein has an intranuclear localization in proliferating cells, but is absent in G0 cells and therefore serves as a marker of the proliferative status (Kill, 1996; Bridger *et al.*, 1998b; Endl and Gerdes, 2000). In late G1, S, and G2 cells pKi-67 is localized mainly in the nucleoli and weakly in the nucleoplasm. In contrast, telophase and early G1 cells display a characteristic staining of numerous smaller spots distributed in the nucleoplasm, which can be used as a marker to distinguish between early and later stages of G1. In mitotic cells (from prophase to anaphase) Ki-67 protein is covering the surface of condensed chromosomes (Figure 6). Malignant transformed cell lines, such as SH-EP, HeLa or CHO cells, typically show pKi-67 positive staining in virtually 100% of nuclei. Hence, S-phase length can be calculated by the fraction of BrdU positive labeled cells.

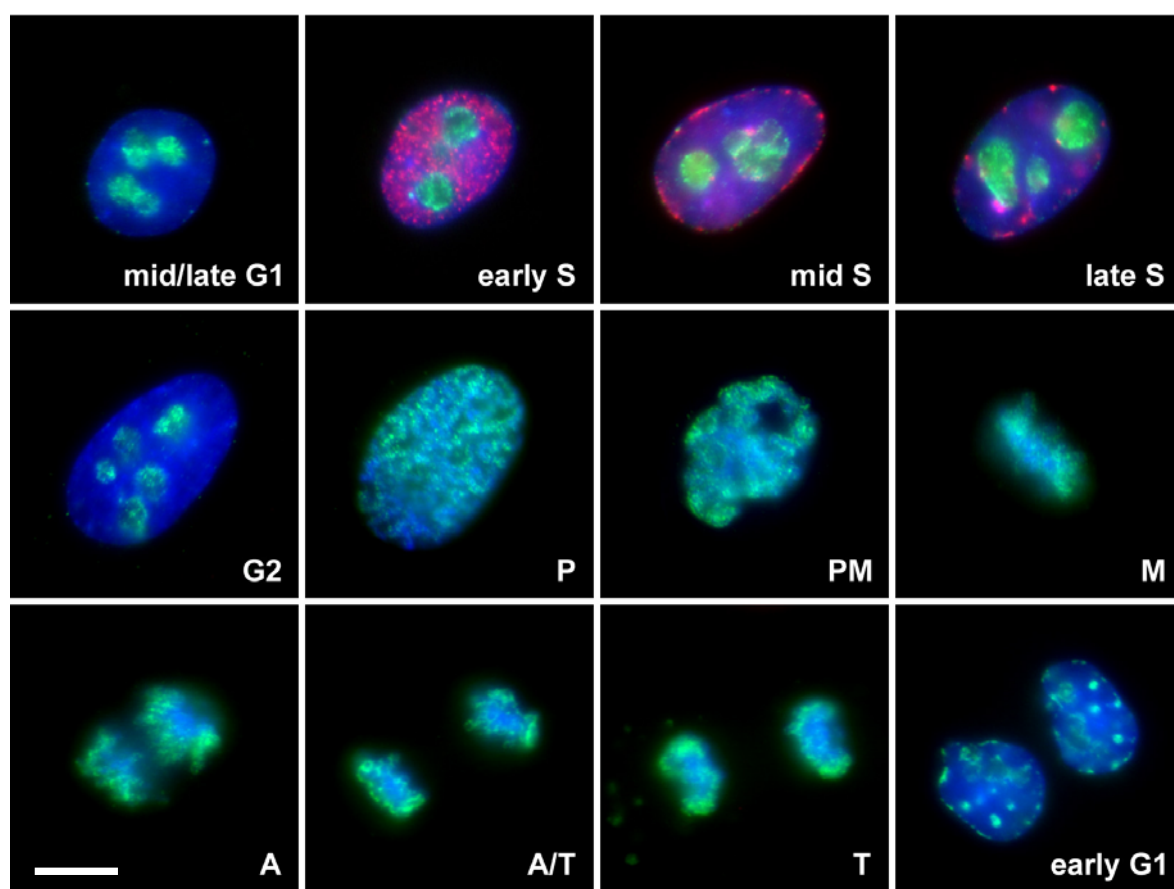


Figure 6. Simultaneous immunodetection of pKi-67 (green) and BrdU (red) in SH-EP N14 cells. Cells were 30 min pulse labeled with BrdU and then fixed with 4% formaldehyde and DAPI stained (blue). Cell cycle stages are indicated (P: prophase; PM: prometaphase; M: metaphase; A: anaphase; T: telophase). Bar: 10 μ m.

Similarly the length of the distinct S-phase stages can be estimated by the fraction of early mid and late replication pattern. The same applies for mitosis (mitotic index) and for early G1 (as defined by the specific Ki-67 pattern). G2 cells have no BrdU incorporated but are characterized by a significantly increased nuclear diameter and volume in comparison to G1 cells. The length of mitosis (M) and G2 are considered to be constant for all mammalian cells with roughly 1 hour and 2-3 hours, respectively. Taking into account this information, the average cell cycle parameters can be reconstructed. The data are shown in Table 3 for SH-EP N14 neuroblastoma cells and HeLa H2B-GFP, since these two cell lines were primarily used in the present thesis.

Table 3. Estimated cell cycle/stage lengths

	SH-EP N14		HeLa H2b-GFP	
t_d Ki-67 → cell cycle	99%	13 h (± 1 h) (n=303)	~13 h	>99% (n=330)
BrdU → S-phase pattern	47%	~6.1 h	36%	~6.5 h
I → early	44%	~3.2 h	51%	~3.6 h
I-II → mid	18%	~2.3 h	15%	~2.1 h
II-III → late	23%	~0.6 h	24%	~0.5 h
G2	(constant)	~2.5 h		~2.5 h
M	(constant)	~1 h		~1 h
Ki-67 → early G1	~15%	~2 h	~15%	~2.5 h
mid-late G1	(remaining)	~3.5 h		~5.5 h

3.10.3 Cell cycle parameter under live cell imaging conditions

The average cell cycle length of HeLa H2B-GFP cells under live cell observation conditions (as described in chapter 3.12) was 18-20 hours, as determined by the time interval between two mitotic events ($n = 24$). In these cases, cells were imaged at low spatial and temporal resolution to avoid phototoxic effects.

The duration of G1 was estimated by measuring nuclear volumes outlined by H2B-GFP (see 3.15): On average nuclei showed a ~2.5 fold increase in the nuclear volume during telophase and early G1. Between 1:45 h and 3:00 h after telophase the volumes reached a plateau-phase. The period from telophase until the beginning of this plateau phase was defined as early G1. The volumes then remained constant for ~4 - 5 hours (mid-late G1) followed by another 1.5 - 1.6 fold volume increase during S-phase and G2.

3.11 Synchronisation at G1/S transition

A number of agents have been described to synchronize mammalian cells at the transition from G1- to S-phase by reversibly inhibiting DNA replication. These include e.g. hydroxyurea, methotrexate, mimosin or aphidicolin (Merrill, 1998). Aphidicolin, an inhibitor of DNA-polymerase α and δ (Ikegami *et al.*, 1978; Lee *et al.*, 1985) was previously suggested to be the least cytotoxic of the above cited agents (Fox *et al.*, 1987) and has proved to be suitable for a large number of cell lines. Typically cells are incubated in an aphidicolin-containing medium for the duration of roughly one cell cycle, which enriches the fraction of cells that are at the onset of S-phase. Then cells are released from the block by washing and transferal to a normal medium.

Importantly, the final concentration of aphidicolin necessary for the cell cycle arrest can vary profoundly for each cell line and has to be determined in a first step. While a too low concentration will not completely block DNA replication, a too high concentration may impair DNA synthesis after release. Therefore, the optimal concentration should be assessed by a simple concentration row: coverslips with cells are incubated in medium supplemented with different concentrations of aphidicolin (e.g. 0,1 / 0,3 / 1 / 3 $\mu\text{g/ml}$) for several hours. BrdU is then added for 15-30 min during the block and in parallel shortly after release. The optimum concentration is found when cells show no BrdU incorporation when incubated in aphidicolin containing medium, but show high labeling intensity, similar to a non-treated control cells, after release.

A high fraction of S-phase cells is an attribute of quickly proliferating cell lines. After applying aphidicolin to such a cell line, numerous S-phase cells will stop immediately in an advanced S-phase stage, which causes incomplete synchronization. In cases when a higher synchrony is desired, particularly for double replication labeling experiments (see above), this limitation may be overcome by using a two-step protocol, where an enrichment of G1/G0 cells precedes the blocking of DNA replication. G1/G0 cells may be enriched either by serum deprivation or detachment of mitotic cells (mitotic shake off). Both methods have their limitations. Some cell lines do not withdraw from cycling when cultivated in serum-deprived medium (e.g. HeLa). Others stop cycling but as a result of G0, do not restart to proliferate in a synchronous fashion (e.g. BHK, fibroblasts). In these cases mitotic shake off may be indicated, which yields, however, only small amounts of cells.

SH-EP N14 neuroblastoma cells show an enrichment of G1/G0 cells upon ~24 h serum deprivation and quick regain of proliferation when serum is added. Hence, using a combination of serum deprivation and subsequent aphidicolin treatment, SH-EP N14 cells can be synchronized with extraordinarily high efficiency, where ~95% of cells are in early S-phase within 30 min after release from the block.

Solutions:

- RPMI 1640 complete medium (10% FBS), prewarmed and CO₂-adapted in incubator
- RPMI 1640-serum deprived medium (0% FBS); prewarmed to 37°C.
- Aphidicolin stock solution (5 µg/µl in ethanol or DMSO)
- PBS, prewarmed to 37°C

Method:*SH-EP N14 cells:*

1. Harvest confluent cells and seed them on sterile coverslips in appropriate dilution in RPMI 1640 complete medium (1:8, in the morning, if to be continued the same evening or 1:10 in the evening, if to be continued the next evening). Grow cells in CO₂-incubator until 40-50% confluence.
2. Aspirate medium and add RPMI 1640 serum deprived medium. Incubate in CO₂-incubator for ~24h*.
3. Exchange deprived medium with complete medium and add aphidicolin to a final concentration of 1 µg/ml, then incubate 12 - 15 h (over night).
4. For release wash twice with PBS and once with prewarmed complete medium and incubate in CO₂-adapted complete medium.

HeLa H2B-GFP cells:

1. Grow cells on coverslips to ~60-70 % confluence.
2. Add aphidicolin to a final concentration of 0,15 µg/ml and incubate ~15 h.
3. For release wash twice with PBS and once with prewarmed complete medium and incubate in CO₂-adapted complete medium.

* Generally, the duration is not critical but should be at least ~14h and not exceed 2 days.

Notes:

The degree of synchrony can be visually controlled under the phase contrast microscope. Synchrony during the block and short after release is indicated by the absence of mitotic cells. Ideally all synchronized cells should undergo mitosis at a defined time after passing S-phase and G2 and enter the next G1-phase concomitantly. Figure 7 shows a time series of synchronized SH-EP cells after release demonstrating that this is largely the case in this cell line. The method is hence useful to highly enrich cells in any desired cell cycle stage when they are fixed at a defined time point after release. As a result, the following time points (after release) were determined for SH-EP cells to assign these cells in a defined cell cycle stage: ~7 h for G2, ~8.5 h for G2 and mitoses, ~10.5 h for mitoses and G1, ~12 h for G1.

For a more detailed analysis of the progression through the different stages of S-phase - as indicated by the different replication pattern - a BrdU pulse labeling can be performed at different time points after release (see Figure 8 and Table 4 below for data obtained on SH-EP N14 cells).

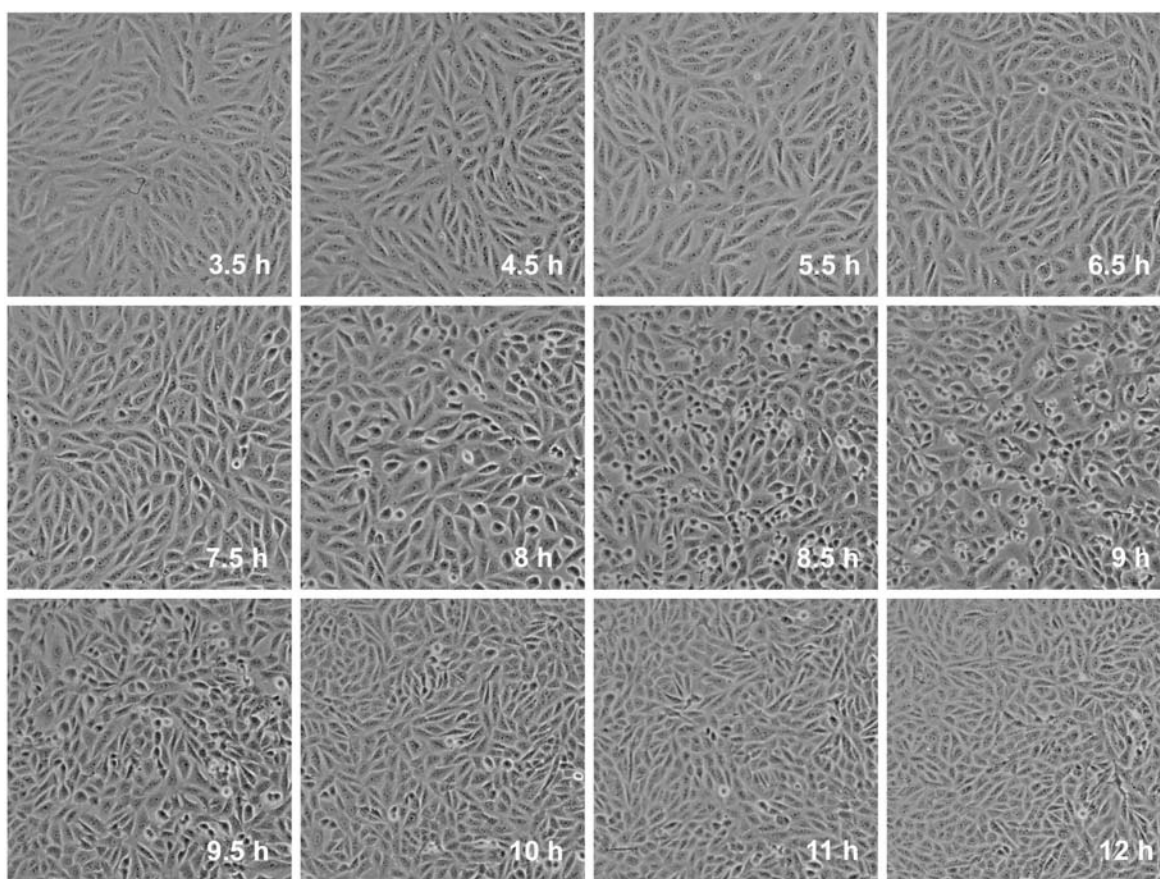


Figure 7. Time-series of two-step synchronized SH-EP cells. Cells were grown in serum deprived medium for 24 h and in complete medium supplemented with 1 µg/ml aphidicolin for 14 h. Phase contrast photographs were taken at the indicated time point after release from the aphidicolin block. Note that mitotic cells (indicated by round shape and partial detachment from the monolayer) are virtually absent until 6.5 h after release and a high number of mitoses between 8 h and 10 h. The somewhat elongated period for the onset of mitosis indicates that individual cells may have some variations in S-phase and G2 phase length. Very few cells already divide at earlier time points, indicating a low fraction of cells that were already in an advanced S-phase stage when the aphidicolin block was applied.

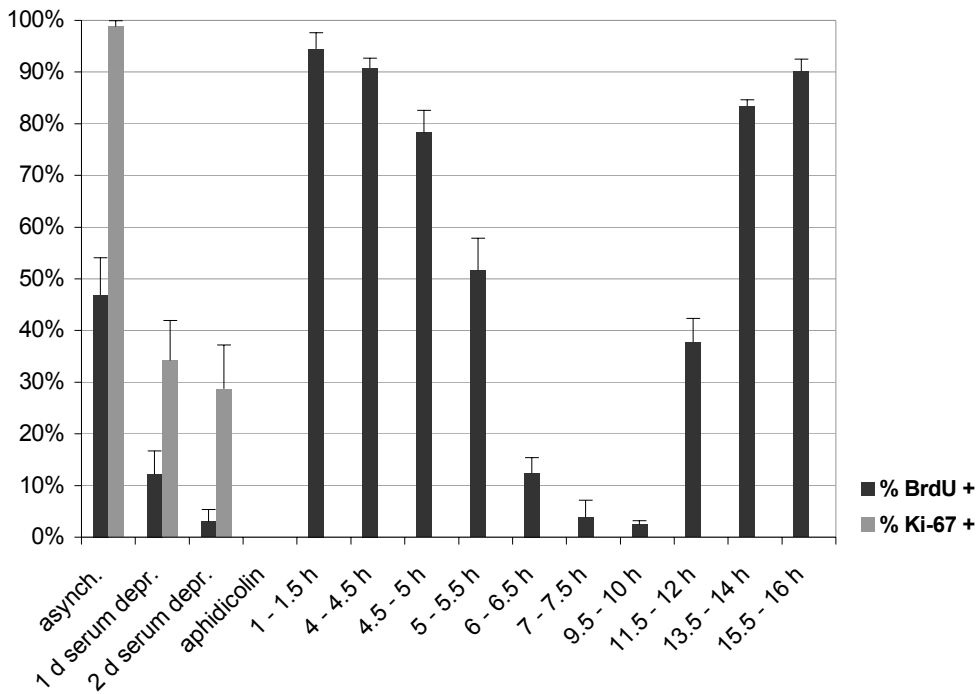


Figure 8. Quantitative evaluation of proliferation parameters. SH-EP N14 cells were grown on coverslips and 30 min pulse labeled with BrdU at the indicated times during and after synchronization. Asynchronous cells were BrdU labeled in parallel as control. After fixation and immunodetection, the fraction of BrdU positive cell nuclei in a total of approximately 500 cells was determined. (Error bar indicates the standard deviation of five randomly selected areas that were counted on the same coverslip) An additional Ki-67 immunostaining indicated the effect of a 24 h and 48 h serum deprivation on the number of non-cycling (G0) cells. In untreated control cells nearly all cell nuclei showed Ki-67 positive staining; ~47% were in S-phase (BrdU positive). Serum deprived cells show a significant decrease in Ki-67 positive cells (34% and 29%, after 1 day and 2 days respectively). Accordingly, the number of S-phase cells decreased (12% and 3%).

Table 4. Replication pattern of asynchronous and synchronized SH-EP N14 cells.

BrdU pulse [h after release]	BrdU positive	n (BrdU ⁺) (100%)	early (I)	mid (I-II)	mid (II)	late (II-III)	late (III)
(asynch.)		303	44.2%	18.5%	22.8%	10.9%	3.6%
1 - 1.5	94.5%	230	97.4%	0.9%	0.4%	0.9%	0.4%
4 - 4.5	90.7%	320	2.5%	2.2%	93.1%	2.2%	0.3%
4.5 - 5	78.3%	225	0.9%	1.3%	90.7%	6.7%	0.4%
5 - 5.5	51.7%	160	2.5%	5.0%	43.8%	36.9%	11.9%
6 - 6.5	12.4%	163	17.2%	7.4%	24.5%	25.2%	25.8%
7 - 7.5	3.9%	78	30.8%	19.2%	23.1%	16.7%	10.3%

The table demonstrates the influence of the synchronization protocol on the distribution of different replication patterns (experiment described in Figure 8). In an indicated number of BrdU positive cells the exact replication patterns (early, mid, late and intermediate stages) were determined. One hour after release nearly all BrdU positive cells show an early replication pattern indicating the high degree of synchrony. Between 4 and 5 hours after release more than 90% display a mid replication pattern. The highest amount of cells with late replication patterns is found ~6 h after release. Generally the distribution of the pattern becomes less distinct with progressing S-phase. This might be attributed to the shorter periods during which these patterns are most prominent and to some variability in S-phase duration of individual cells.

3.12 Microscopy of living and fixed cells

3.12.1 Confocal laser scanning microscopy of fixed specimen

Fixed specimens were usually imaged at a Zeiss LSM410 (located at the Institut für Kristallographie der LMU, Theresienstrasse, Munich). In some cases, however, a Leica TCS SP system (Zoologisches Institut der LMU, Luisenstrasse, Munich) or a Zeiss LSM 510 (Northwestern University Medical School, Chicago) was employed. Typically light optical image stacks were recorded with a lateral resolution (xy-pixel size) of 50-80 nm and a z-distance between each confocal section of 200 nm or 250 nm. To accomplish a high signal to noise (S/N) ratio, the laser power was adjusted as high as possible without causing photobleaching of the fluorescence signals, whereas the contrast (*i.e.* the voltage at the photo multiplier tube) was adjusted as low as possible to minimize electronic noise (see Table 5, right column for recommended imaging parameters for the Zeiss LSM 410).

Table 5. Recommended imaging parameters for the LSM 410.

	live cell observation	fixed cell observation
geometry	256×256 pixel	512×512 pixel
averaging	2×	4× or 8×
pixel size (xy)	150 - 200 nm	50 - 80 nm
z-step (# z-steps)	0.4 or 0.5 µm (20-30)	0.2 or 0.25 µm (variable)
pinhole	30	20
Attenuation (contrast)	GFP : T=0.001-0.0032 (290-320) Cy3 : At=30 (310-330) Cy5 : At=30 (330-340)	variable (250-300)
time interval	variable: 180 - 1800 sec	-
pump time	10 sec	-

3.12.2 Long-term confocal time-lapse microscopy of living cells

Successful observations of living cells under the microscope depend on several requirements: (a) for optimal growth, most mammalian cell types have to be kept within a distinct temperature range (36.5 to 37°C). While lower temperatures slow down cellular metabolism and therefore impair energy dependent processes, higher temperatures result in cellular damage and death. (b) The pH value of the medium should be kept within the physiological range (pH 7.2 to 7.4). In most growth media this is accomplished by a CO₂-NaHCO₃ based buffer system requiring a 5% CO₂ atmosphere. In addition, media may contain HEPES buffer to increase the buffer capacity. (c) Evaporation of water leading to a harmful increase of the ion concentration has to be prevented. (d) For long-term observations waste medium has to be replaced by fresh medium. (e) The microscope should be able to record time series of 3D image stacks automatically with a high aperture objective. Focus drift should be automatically corrected. Vibrations during imaging should be carefully avoided. (g) Light exposure of the cells should be kept to the possible minimum to avoid phototoxic effects.

During the course of the present work, a dedicated setup was established (in close cooperation with J. Walter) to fulfill these requirements. This setup is

based on a perfusible Bioptechs FCS2 live-cell chamber, which can be mounted on the microscope stage and kept at 37°C. The objective is typically operated with an objective heater as part of the FCS2 system to avoid a decreasing temperature gradient, which may cause thermal distortions and system instability. For shorter observation times of less than 8 hours a non-perfused, “closed” chamber might be sufficient to maintain cell viability. Observation periods longer than 8 hours, however, result in cell death possibly due to limited buffer capacity of the medium inside the FCS2 chamber (volume < 1 ml). Hence, for long-term observations the chamber is perfused with fresh medium using a flexible-tube pump in an airtight assembly that prevents the loss of CO₂ and keeps the pH value stable at 7.4. A 20 ml syringe connected to the pump and the chamber by a perfusion tube served as a reservoir for the CO₂ adapted medium (Figure 9).

To exchange medium, the pump (set to a flow rate of ~5 µl/s) is automatically switched on for 10 - 20 s after each imaging time point. Cells are protected against photodamage by adding 200 µM Trolox, a water-soluble vitamin E derivative, which acts as a scavenger of free radicals (Wu *et al.*, 1990), to the growth medium the day before observation. This set-up allows cell growth on the microscope stage over several days, from low density until confluence (Figure 10).

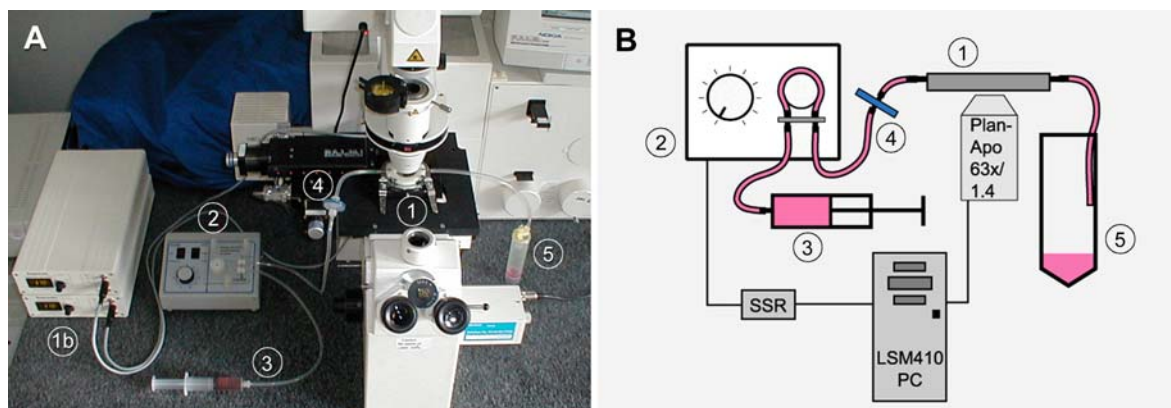


Figure 9. Experimental setup (A) and scheme (B) for long term live cell confocal microscopy. The system consists of a Biophtechs FCS2 live cell chamber (1), temperature control units for chamber and objective-heater (1b), flexible tube pump (2) connected to the control PC via a solid state relay (SSR), syringe for supply of fresh medium (3), disposable syringe filter (4), waste container (5). For further details see text.

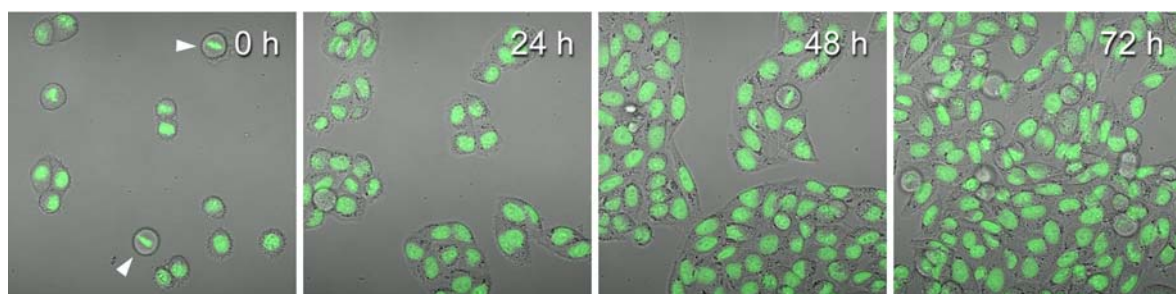


Figure 10. Live cell observation set-up does not impair cell growth. HeLa cells expressing GFP-tagged histone H2B were grown to confluence on the microscope stage within 3 days under low resolution imaging conditions (see also supplemental video 1). Arrowheads at time point 0 h indicate cells in mitosis.

A. Preparing cells for live cell observation

Equipment and solutions:

- Appropriate cell culture medium (with HEPES), prewarmed to 37°C
- PBS (37°C)
- Trypsin-EDTA solution (0,05%/0,02% in PBS); prewarmed to 37°C
- Trolox stock solution (100 mM), vortex before use
- Round coverslips (40 mm Ø)

Method:

Cells are typically seeded on round coverslips the day before live cell observation

1. Trypsinize cells and resuspend in fresh medium with appropriate dilution.
2. Place round coverslip (cleaned and flamed) into a 60 mm Ø tissue culture dish.
3. Add ~50 µl of the suspension in the center of the coverslip, covering an area of roughly 5-10 mm Ø.
4. Incubate 30 min at 37°C until cells have attached to the glass surface, than add 5 ml of fresh prewarmed medium supplemented with 0.2 mM Trolox. (When needed, synchronize cells by adding aphidicolin in appropriate concentration.)
5. Incubate cells at least 12h in Trolox supplemented medium before start of live cell observation

Note: CHO Lamin C-GFP cells synthesize the recombinant protein only at lowered temperatures. These cells therefore have to be transferred to a CO₂ incubator adjusted to 32°C at least 2 days before seeding onto coverslips and then kept at this temperature prior and during observation on the microscope.

B. Assembly of the live cell chamber**Equipment and solutions:**

- Appropriate cell culture medium (containing HEPES), pre-warmed and CO₂ equilibrated
- Cells grown on a 40 mm Ø coverslip (see above)
- Trolox stock solution (100 mM), vortex before use
- Bioptrix FCS2 live cell chamber system, including an electrical temperature sensor, upper plastic support (white, with perfusion tubes) upper silicone gasket (with holes), microaque duct slide, lower silicone gasket (0.75 mm thick) and self locking metal base
- 2×35 cm / 1×25 cm / 1×10 cm tubes (Tygon 2275, Øi 1.6 mm, Øe 4.8 mm, Ep. 1.6 mm)
- 1×12 cm flexible tube (Tygon 3350, Øi 1.6 mm, Øe 3.2 mm, Ep. 0.8 mm)
- 2×Tube connectors (Luer Lock for ID 1.6mm, female)
- 1×Tube connector (Luer Lock for ID 1.6mm, male)
- 2×Silicone fittings (delivered with the pump)
- Plastic valve (2-way Luer Lock, male and female)
- Sterile filter (0.20 µm or 0.45 µm pore size)
- 20 ml syringe (Luer lock)
- 2 fine forceps
- Immersion oil
- Gel-packs (adapted to 37°C in water bath) and styrofoam box (required for transport)

Method:*Preparation:*

1. Assemble 3 tubing pieces in following order*:
 2. *part 1* (from syringe via pump to filter): female Luer connector - 35 cm tube - 12 cm flexible tube connected with silicone fittings of the pump - 35 cm tube - male Luer connector
 3. *part 2* (from filter to chamber): female Luer connector - 10 cm tube
 4. *part 3* (from chamber to waste): 25 cm tube - 2-way plastic valve
5. Rinse all plastic and silicone parts thoroughly with d H₂O. Clean metal lid and microaque duct slide by wiping with 80% ethanol.
6. Autoclave upper (white) part of FCS2 chamber, gaskets and tubing at 115°C.
7. Put 25 ml culture medium in a 94/16 mm tissue culture dish and place it in the CO₂ incubator for a few hours (or overnight) to equilibrate temperature and CO₂ content.

* Assembled parts 1-3 can be reused again after rinsing with d H₂O and autoclaving.

Mounting the FCS2 chamber:

1. Assemble the supply tubing in the following order: part 1 - sterile filter - part 2.
2. Vortex Trolox stock solution (100 mM) and add 50 µl to the equilibrated medium to a final concentration of 200 µM, then load ~20 ml into a syringe.
3. Connect the syringe to the supply tube and press medium all the way through.
4. Assemble FCS2 chamber (top side down) in following order:
White, plastic support (with small perfusion tubes facing up, and the bulge for the temperature sensor to the left; underlay the backside of a forceps to level off the right side) - upper gasket (place into recess and align holes with the small perfusion tubes) - microaqueduct slide (with contacts down and grooved side up) - lower gasket (press around the perimeter creating a seal).
5. Wash and equilibrate the chamber by pipetting 1 ml medium onto the open chamber, discard medium.
6. Connect supply tube to the inlet port facing away from the white support. Connect the waste tube (part 3) to the outlet port facing to the front.
7. Press medium from the syringe to the chamber ensuring that no air bubbles remain in the supply tube. Fill the open chamber with ~1 ml medium so that a little meniscus is generated.
8. Place the coverslip cell-side down onto the medium until it is resting on the gasket. Excess medium should be sucked off with a paper wipe.
9. Take the metal base and assure that the screw is completely open and not uptight. (To open, screw clockwise with the brackets facing up.) Then turn the device upside and place it on top of the stack aligning the black electrical connector and the metal brackets with respective slots in the chamber top.
10. Screw carefully clockwise, brackets should then move to the left. If necessary use forceps to move the brackets. Further screwing seals the chamber.
11. Turn the chamber and wipe off any excess medium outside the chamber. Take care that the contacts of the microaqueduct slide are completely dry and that the screw is completely closed.
12. Place a small drop of immersion oil on the temperature sensor of the temperature control and screw the control to the chamber.

Note: For transport, place the whole assembly into a styrofoam box together with a pre-warmed heat pack. For more detailed information and instruction on the FCS2 chamber see <http://www.biotechhs.com/Products/FCS2/fcs2.html>.

C. Live cell microscopy and laser-photo-bleaching at the LSM 410

A macro (written by J. Walter) for the LSM 410 control software is employed, in order to record confocal time series automatically. This macro records time series of 3D image stacks from multiple regions of interest (ROI) at high zoom within a field of view selected at a low zoom (Figure 11). To compensate z-axis drift the interface between the coverslip and the cell culture medium is imaged in reflection contrast before each image stack is recorded. The reflected light intensity has a sharp maximum at a distinct z-position, which is then used as a reference position.

GFP and FITC are excited with an Argon-laser at 488 nm (15 mW) at 30% power, additionally attenuated to 0.1 - 0.3% and detected with a BP 502 - 542 nm band pass filter. Cy3 is excited with a 543 nm Helium-Neon-laser (0.5 mW) attenuated to 3% and detected with a LP 570 long pass filter. Cy5 is excited with a 633 nm Helium-Neon-laser (5 mW) attenuated to 3% and detected with a 665 nm long pass filter.

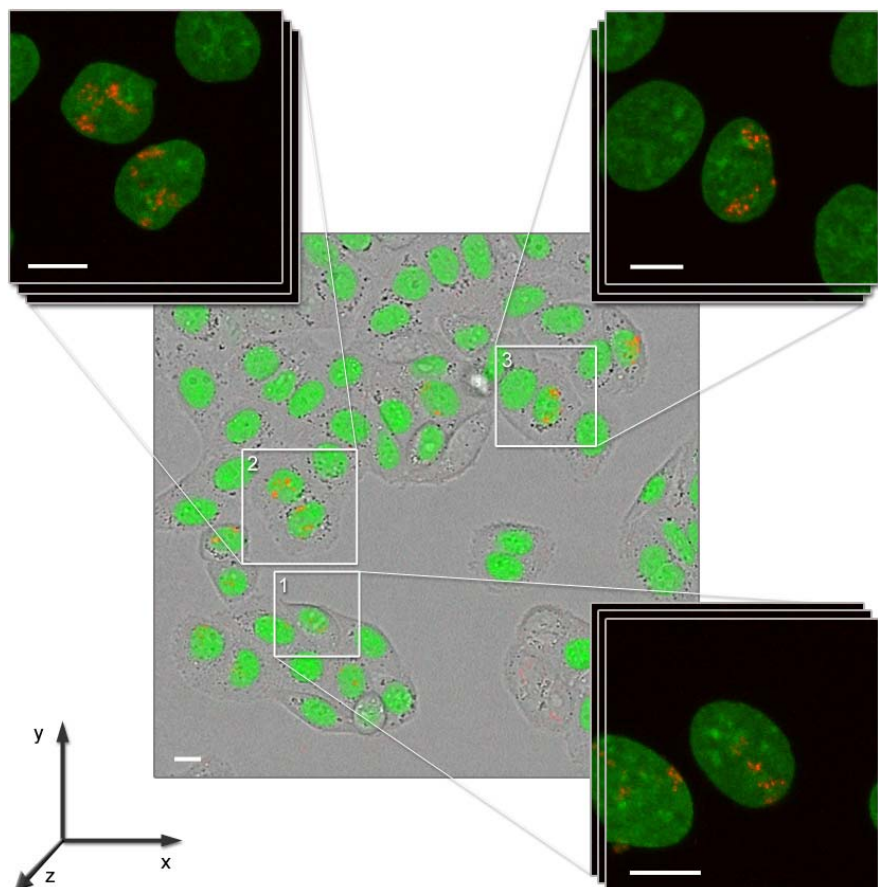


Figure 11. Macro for live cell microscopy at the LSM 410. The 4D-imaging macro records an overview image of the whole field of view and high-resolution z-stacks of selected ROIs at regular time intervals. Imaging parameters can be adjusted for each ROI individually. Bar: 10 μ m

Equipment:

- Zeiss LSM 410 using 63×/1.4 plan-apochromat objective and equipped with Biotech stage adapter, controlled with LSM 410 software and the macros “TIMEPR” for recording 3D time series (written by J.Walter)
- Assembled live cell chamber (see above)
- Biotech objective heater and electronic controller for chamber and heater (located at the microscope together with appropriate tools)
- Flexible tube pump (connected via a solid state relay (SSR) to the parallel port of the LSM 410 control PC)
- 50 ml FALCON tube and rack (for waste medium)

Method:

1. Calibrate electronic controller according to the manufacturer’s manual.
2. Attach objective heater to the objective and connect to the respective controller.
3. Add a drop of immersion oil onto the objective and mount the live cell chamber to the microscope stage (temperature sensor backward, outlet to the right), fix chamber to the stage adapter with the appropriate screw.
4. Clamp the flexible tubing part of the supply tube into the pump (see also Figure 9); set the pump speed to: *forward*, *slow*, 0.
5. Warm both, live cell chamber and objective to 37°C (in case of CHO LaminC-GFP to 32°C).
6. Adjust imaging parameters (see Table 5 for recommended values).
If only one fluorochrome is recorded, use “overl2” mode for simultaneous recording of fluorescence (channel 1) and transmission (channel 2), otherwise use “frame” mode.
For optimal transmission image, the light system should be “koehlered”. The macro “AUTO B+C” can be applied as long as “TIMEPR” was not started.
7. Image the cells in the overlay mode at low resolution (zoom 1 or less), and select an appropriate field of view.
8. Start macro “TIMEPR” (TIMEPR1, when imaging one fluorescence channel + transmission; TIMEPR2 for 2 fluorescence channels + transmission; TIMEPR3 for 3 fluorescence channels).
9. Adjust the parameters for the coverslip search (typically 633nm, attenuation: 300, contrast: 200-210, brightness: 9999, pinhole: 20, zoom 8). The coverslip search is performed automatically before each image stack is recorded and compensates focal drift.
10. Select the position of the first cell or region of interest (ROI), which is to be imaged.
11. Fine tune position and imaging parameters (“tune img” mode), confirm with “ok”.
12. Set imaging parameters within the TIMEPR macro (#z-sections / z-distance / z-offset / averaging / time interval / pump time).
13. Select the positions of the other cells / ROIs to be imaged. Parameters will be taken over from the first position. Fine tune, if required. In addition select one position in the center for an overview. Adjust parameter for the overview (recommended: 512×512, zoom 1, #z-sections 1, z-offset µm, open pinhole). Start 3D-time series now or proceed for bleaching experiments.

Photobleaching:

14. Record an image stack for each selected position.
15. Bleach one target cell at each position as follows:
 - Select position 1, change to the “tune img” mode.
 - Set parameters to 512×512 at zoom 8.
 - Select an ROI to be bleached. (Note: at the LSM 410 the ROI constrains scanning area in vertical direction only!)
 - Scan the ROI 2-4 times at different axial positions without attenuation. Use “single scan” mode and attenuation 1 or 2.
 - Set the laser attenuation and the image parameters back to the previous values and leave the “tune img” mode by confirming “ok”.
 - Record an image stack of the cell.
 - Repeat for the remaining positions, except for the “overview” position.
16. Start the 3D-time series.

Notes:

- For live cell experiments the pinhole is opened to 2 Airy units sacrificing some optical sectioning capability for efficient light collection.
- The scan time per stack may last up to 200 sec (for 3 channels, 30 z-sections with 2× averaging) and has to be taken into account when choosing the time interval and number of ROIs.
- The imaging parameters in Table 5 for live cell observations were found to be an optimal compromise between a low incidence of apoptosis and adequate resolution quality of images.

3.12.3 Short-term microscopy of living cells

For short-term live cell imaging with observation times not exceeding 1-2 hours a simple live cell chamber, developed at the EMBL (Heidelberg) can be employed. The chamber is made of an aluminium plate with the dimension of a conventional microscopic slide (26×76 mm), through which a hole was drilled with a diameter of 5 mm. A surrounding ring-shaped indentation (\varnothing 12 mm) allows a round coverslip (e.g. CELLocate coverslip) to fit in. The coverslip can be assembled and sealed using silicone vacuum grease (Bayer silicone, medium). The temperature of the chamber is adjusted and controlled by using an objective heater. This system is well suited for comparative observations of individual cells in living and fixed state. The grid on the CELLocate coverslip facilitates relocation of respective cells.

Method:

1. Prepare the chamber before mounting of the cells as follows: If necessary wipe off excess silicone from the chamber with a wipe, clean thoroughly with dH₂O and flame it before use. Attach a pre-cleaned and flamed 22×22 mm square coverslip on one side of the chamber by placing a thin, continuous layer of silicone on the contact site (e.g. using a pipette tip). On the opposite side apply a thin layer of vacuum grease around the opening of the chamber for gluing the coverslip with cells. Seal the perfusion holes at the side of the chamber with vacuum grease.
2. To mount the chamber, fill the well with approx. 100 μ l adapted medium and apply the coverslip with the cells.
3. Press slightly onto the coverslip with a forceps to press out excess medium and attach the coverslip to the chamber. The chamber should be completely sealed and airtight.
4. Clean the round coverslip with 80% ethanol and mount the chamber on to the microscope stage. The objective should be equipped with an objective heater adjusted to 37°C.
5. After live cell imaging, the round coverslip with the cells can be removed from the chamber with the help of a fine forceps and subsequently fixed in formaldehyde.

Note: Due to the small medium volume, the buffer capacity for maintaining the pH in a tolerable range is limited. The observation period is therefore limited to roughly 1 hour.

3.13 3D-FISH of HeLa cell clones

HeLa H2B-GFP cells were seeded at low density on photoetched coverslips (Bellco) to identify individual cells and cell clones. To ensure the clonal origin of the 2- and 4-cell clusters, transmission images of defined areas on coverslips were taken 1 hour after cell seeding. Single cells with a distance of at least 100 µm to the next cell were identified and further monitored for clonal growth. Since HeLa cells show very low motility, growing of clones was easy to track. Cells were fixed in 4% paraformaldehyde/1×PBS 28 or 48 hours after seeding, when most of the cells had formed 2-cell and 4-cell clones, respectively. Permeabilization steps, 3D-FISH, and probe detection were performed according to protocols described in detail elsewhere (Cremer *et al.*, 2001; Solovei *et al.*, 2002). 3D-FISH was performed with painting probes specific for chromosomes 7 (labeled with digoxigenin, detected with Cy3-conjugated antibodies) and chromosomes 10 (labeled with biotin, detected with avidin-Alexa 488). Nuclei were counterstained with TO-PRO-3 and embedded with antifade solution. Confocal image stacks for all three color channels were recorded with the Zeiss LSM 410 or a Leica TCS-SP (pixel size: 50 - 80 nm, z-step: 0.25 µm).

3.14 Image processing and 3D-reconstruction

Data was routinely Gauss- or median-filtered to reduce noise. Projections were made with the Zeiss LSM 410 software. Images were processed with Adobe Photoshop 5.5. 3D-reconstructions of confocal image stacks were performed with Amira™ 2.3.

3.15 Quantitative evaluation of nuclear volumes and CT movements

Intensity gravity centers were determined for CTs, as well as for the entire nucleus counterstained with H2B-GFP (CN = center of nucleus). Distances between these gravity centers (CT-CT and CT-CN) as well as nuclear volumes were measured with the plugin *Sync Measure 3D* (written by J.Walter, LMU) for ImageJ (Rasband, 2002). The threshold for CT segmentation was set visually. Isolated chromatin foci with low pixel intensities (below 1000 in 8-bit images) were not considered. To take into account intensity variations due to different degrees of chromatin condensation during the telophase-G1 transition, the threshold for the nuclear volume measurements was determined as follows: All image stacks were normalized to gray levels between 0 and 255. For each dataset one interphase nucleus was chosen, and a profile plot along a central line through a nuclear midsection was made. The mean gray level between the first local maximum within the nucleus and the background was taken as threshold for volume measurement. The measured distances (d) were corrected for the increase in nuclear volume as follows: a volume during the first plateau (mid G1) was set as reference volume (V_0) and ratios V_t / V_0 were calculated for all volumes V_t within a

series of measurements. The corrected distances (d_c) were calculated as

$$d_c = \frac{d}{\sqrt[3]{\frac{V_t}{V_0}}}$$

Median values of the maximum deviations ($\Delta_{(\text{Max-Min})}$) were compared with the Mann-Whitney U-test (Barlow, 1989). Differences in the proportion of nuclei with $\Delta_{(\text{Max-Min})} > 2 \mu\text{m}$ were scored with Fisher's exact test (Bland, 2000) using SPSS software.

3.16 Methodological limitations

Limitations of multi color *in vivo* labeling approaches

(1) In live cell observations after *in vivo* replication labeling, a progressive reduction of fluorescence intensities of labeled replication foci was noted. This might be partly due to the fact that the density of fluorescent molecules per focus was reduced 2-fold after separation of the labeled sister chromatids during the first mitosis. In addition, specific excision repair mechanisms involving the exchange of modified nucleotides might contribute to the observed effect. (2) Cy5-dye and especially FITC are much less photostable than Cy3, which generally limits their usability for long-term confocal observations. Alexa488-dUTP did not suite as alternative to FITC, as it proved less efficiently incorporated *in vivo*, resulting in only weak fluorescence signals. So far, only Cy3-dUTP continued to fluoresce over a period of several days after labeling, which made live cell observation of chromatin/CTs in labeling/segregation experiments possible. For fixed specimen, it is generally possible to compensate to some extent for the reduction of fluorescence intensity by raising the excitation energy of the confocal laser. However, in living specimen this would aggravate the problem of phototoxicity (see below). (3) Despite the generally high yield of labeled cells obtained with the SRL approach on highly synchronized cells, the labeling intensities of individual cells can vary considerably depending on the initial nucleotide pool. This effect was universal to all tested *in vivo*-labeling approaches. When two-color SRL was performed on highly synchronized cells, a relatively large fraction of cells (~10-20%) had incorporated both labels. However, the number of cells displaying equally strong labels after segregation – which would be important for live cell observation – was too low. (4) A labeling of complete chromosomes, e.g. to define the borders of a CT, is not possible with present *in vivo* labeling strategies. A more flexible method with defined labeling duration, analogous to BrdU labeling, would be advantageous in some respect. Development of alternative strategies for even labeling with optimum efficiency and improved flexibility is thus indicated to attain the initial goals.

Phototoxicity and limited resolution

The live cell observation setup described in the present work allows for unimpaired cell growth on the microscopic stage without using a technically demanding and expensive CO₂-incubator surrounding the stage. Thus the remaining factor limiting the length of an observation period as well as the image quality is the phototoxicity caused by laser excitation. It is a commonly known that illumination with a high amount of light in the visible range can lead to cell cycle

arrest and trigger apoptosis. This may be reduced in cancer cells, such as HeLa, in which cell cycle checkpoints and apoptotic mechanisms are less effective than in diploid cells.

The detrimental effects of illumination presumably increase when labeling with fluorescent dyes is involved (Shea *et al.*, 1989; Saetzler *et al.*, 1997). Although the mechanisms leading to cell damage are still poorly understood, the release of oxygen radicals seems to be a major factor (Martin and Logsdon, 1987). The addition of radical scavengers such as ascorbic acid or Trolox, a water-soluble Vitamin E derivative (Wu *et al.*, 1990), can thus help to reduce photodamage to some extent (Kessel and Luo, 1996). In the live-cell experiments described in the present work, a significant increase in the lifespan of the observed cells could be noted when adding 200 µM Trolox 12 h or more before the start of the observation period.

The most crucial criterion in live cell imaging is a minimized the dose of excitation light. The probability of the observed cell becoming apoptotic during observation rises with the excitation energy over the course of time. Therefore, the spatial and temporal resolution of a time series is limited, especially for multicolor confocal analysis. It requires a careful balancing of image quality (lateral and axial resolution, signal-to-noise ratio), the number of recordings (time resolution), and phototoxicity.

Typical imaging parameters found to be compatible with for two color (Cy3 + GFP) long-term live cell observation were: a voxel size of 150 nm × 150 nm × 400 nm, 26 sections per stack, 2× avaraging, ~15 µs pixel time. The laser-power was attenuated to a range of 1 µW-10 µW for each of the two laser lines. Additionally, one transmission image was recorded at each time point to monitor cellular morphology. The critical determinant seemed to be solely the total light dosage, while the time interval between the recordings of each stack did not seem to influence viability. At least 60 to 80 time points could be recorded with these imaging parameters without obvious damage to the observed cells. Numerous cells passed through mitosis and reintegrated into the cell layer showing inconspicuous morphology. No membrane blebbing or filopodias, indicating cellular damage, became obvious within this time. With more prolonged observation, the nuclear morphology of the cells in the observation field started to change and they finally became apoptotic. In contrast, when the 543 nm laser was attenuated to a 3 times lower value (10 instead of 30) to improve signal-to-noise ratio, the observed cells did not divide, they started showing suspicious morphology between time points 20 to 30 and subsequently become apoptotic indicating a limit in light energy which is tolerable for cells. Besides, the slow scanning speed of the employed Zeiss LSM 410 limited the time resolution in particular, since a typical stack (2 channels, 256×256 pixels, 30 sections, 2× averaging) lasted roughly 2 minutes resulting in notable spatial distortions within one stack.

Both, phototoxicity and low time resolution might be partly overcome by using latest CLSM generation equipped with more sensitive photomultipliers. Multi-pinhole spinning disk microscopes (UltraVIEW™ LCI, Perkin Elmer) that combine confocality with the high quantum efficiency of a CCD camera (90% versus 10-20% of a PMT tube) could become especially useful for live cell imaging as it promises lower excitation energy and shorter image acquisition times.

Finally, the brightness of the employed fluorochromes is of obvious importance as lower-power excitation can be used to reduce photo-induced effects. For long-term observations of cells with replication labeling, DNA Cy3-dUTP was found to be particularly useful both in terms of brightness and photostability. Future development of novel dyes, e.g. luminescent nanocrystal quantum dots (Jaiswal *et al.*, 2003) that display similar or even superior qualities with different spectral properties may provide suitable alternatives to presently available Cy5- and fluorescein-dyes.

Quantitative evaluation: the unsolved problem

High-resolution multi-color 4D microscopy creates huge data sets and it is obvious that a quantitative evaluation of such data is highly demanding. In order to characterize motion and to perform 3D-tracking of chromatin domains or CTs a number of parameters must conceivably be determined: (1) 3D coordinates of chromatin domains/CTs over time, change of distances and angles to each other and to the nuclear gravity center; (2) speed, diffusion constants (mean square displacements), volumes, confinement radii; (3) if possible correction for external influences on movements induced by changes of nuclear volume and shape ("bending energy"); (4) correlation of motion of chromatin foci (spot-like) and nuclear envelope invaginations (surface). A software solution should integrate several steps: (1) Extraction of a region of interest (ROI) and removal of undesired signals in all time points, (2) 3D alignment of successive time points to correct for translational and rotational nuclear movements, (3) filtering to reduce electronic background noise, (4) segmentation of defined objects (5) automated 3D-tracking to define the trajectories of these objects over time (6) evaluation and quantification and (7) visualization. To date, no satisfying, integrated (semi-)automated user-friendly software-solution could be provided. Although some of these parameters can be determined manually, it will become essential to develop such an integrated software solution due to the rapidly increasing importance of live cell data.

4. Results

4.1 *In vivo* replication labeling

Initially a protocol had to be established that served two purposes: The reliable labeling of individual chromosomes in living cells for studies of CT dynamics in long-term confocal microscopy and the simultaneous *in vivo* labeling of the early and the mid-to-late replicating chromatin compartment with spectrally distinct fluorochromes.

Recently, live cell chromatin studies were developed based on *in vivo* replication labeling of DNA with fluorochrome-conjugated dUTPs. (Pepperkok and Ansorge, 1995; Zink *et al.*, 1998; Manders *et al.*, 1999). The applied methods, microinjection and bead loading, however, yielded insufficient amounts of labeled cells to accomplish the goals of the present thesis. This led to the development of a modified scratch loading protocol, termed scratch replication labeling (SRL, see chapter 3.9.1 for details).

Figure 12 shows typical examples of SRL where scratches through a layer of human neuroblastoma cells were applied (see also Figure 4 on page 31). Cells from the scratched area were either pushed aside or lifted from the surface. Numerous cells along the “scratch line” showed labeling when fixed 30 min after SRL (Figure 12 A). Four hours later, a repopulation of the scratch line could be noted (Figure 12 B). When performed on a synchronized cell population shortly after release from G1/S block, many labeled cells divided within the same time range as evaluated for non-labeled cells (Figure 12 C compare also Figure 7), demonstrating only minor delay in cell cycle kinetics after single-color labeling in a large fraction of cells. The SRL protocol allows simplified labeling of adherent growing cell lines and has been successfully applied to numerous cell lines (including HeLa, CHO, BHK, SH-EP N14 neuroblastoma cells and primary fibroblasts).

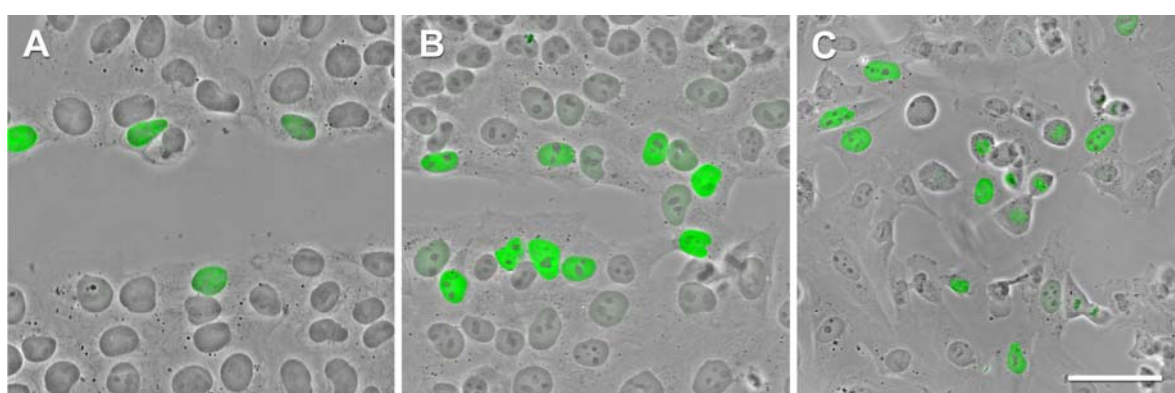


Figure 12. Scratch replication labeling (SRL) of SH-EP N14 cells. (A, B) Scratches through a layer of near confluent, asynchronously growing cells were performed with a hypodermic needle. Cells were fixed 30 min (A) and 4 hrs (B) after SRL with FITC-dUTP. (C) SRL performed on synchronized SH-EP cells and fixed 9 hrs after release. Numerous cells are dividing, demonstrating no major delay in cell cycle kinetics compared to non-labeled cells. Image of fluorescent nuclei (green) was overlaid with a phase contrast image. Scale bar: 50 µm.

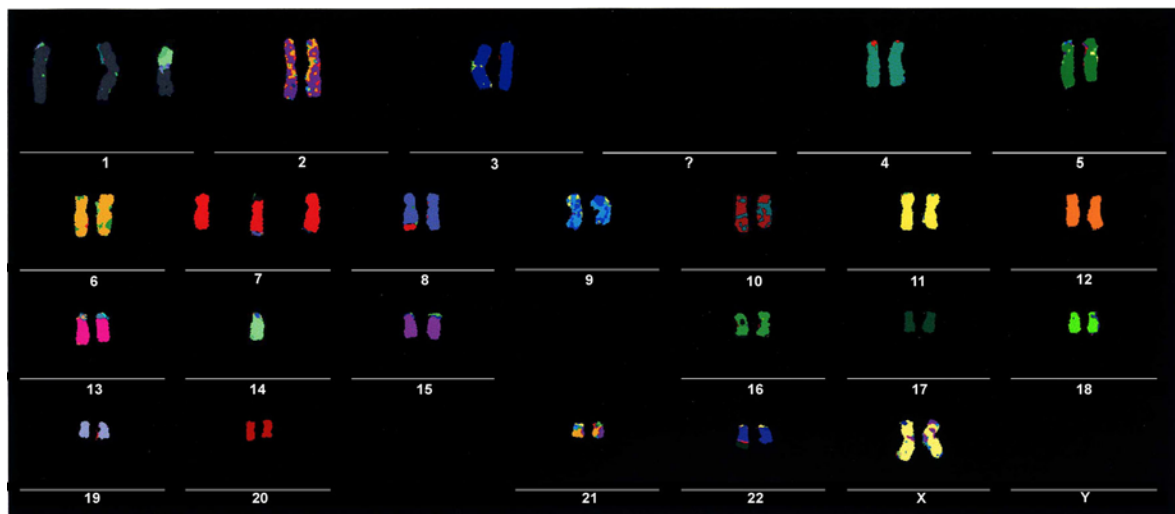


Figure 13. Karyogram of the SH-EP N14 cell line revealed by m-FISH. The karyotype (47, XX+7) displays only few translocations which were identified as follows: der(1;14)t(1;14) / der(7)t(7;8) / der(8)t(7;8) / der(22)t(17;22) (m-FISH was performed by C. Fauth, TU München and results were later confirmed with an independent experiment by S. Müller, LMU München).

Two-color labeling of early and mid-to-late replicating chromatin

Double pulse-chase labeling with IdU and CldU has been successfully employed for the simultaneous detection of early and late replicating chromatin in fixed cells (Aten *et al.*, 1992; Visser *et al.*, 1998; Zink *et al.*, 1998; Sadoni *et al.*, 1999; Visser and Aten, 1999). In the present work the feasibility of a double labeling of the early and the mid-to-late replicating compartment in an *in vivo* approach was to be assessed. This required not only an efficient labeling protocol (as was provided by SRL), but also a highly efficient synchronization of cells at the G1/S transition. This was provided by a two-step protocol, which was established for the neuroblastoma cell line SH-EP N14. The synchronization involved serum deprivation to enrich cells in G1/G0, followed by treatment with aphidicolin, an inhibitor of DNA polymerase α and δ subunit (Ikegami *et al.*, 1978; Lee *et al.*, 1985). This protocol facilitated the synchronization of SH-EP N14 cells with ~95% efficiency (see also chapter 3.11).

For two-color replication labeling, SRL was performed on synchronized SH-EP N14 cells 1 h after release to obtain early S-phase chromatin labeling, and 5.5 h* after release with nucleotide coupled to a different fluorochrome in order to achieve labeling of the mid-to-late replicating chromatin. Up to 80 % of cells (depending on the distance between scratches) were found to be labeled, and at least 15 % of labeled cells incorporated both labels (Figure 14 A). Figure 14 B shows a confocal mid-section through a number of labeled nuclei revealing the typical early replication pattern of cells labeled with Cy5-dUTP and the typical mid replication pattern in most of the FITC-dUTP labeled nuclei. Figure 14 C shows such a nucleus at high magnification. The high yield of (double-) labeled cells after SRL made the harvesting and seeding of treated cells at lower density possible.

* In BrdU pulse labeling experiments, the highest fraction of mid pattern was found between 4.5 and 5.5 hours. In two color SRL experiments, the second pulse was performed somewhat later to equalize a possible short delay induced by the first scratching procedure.

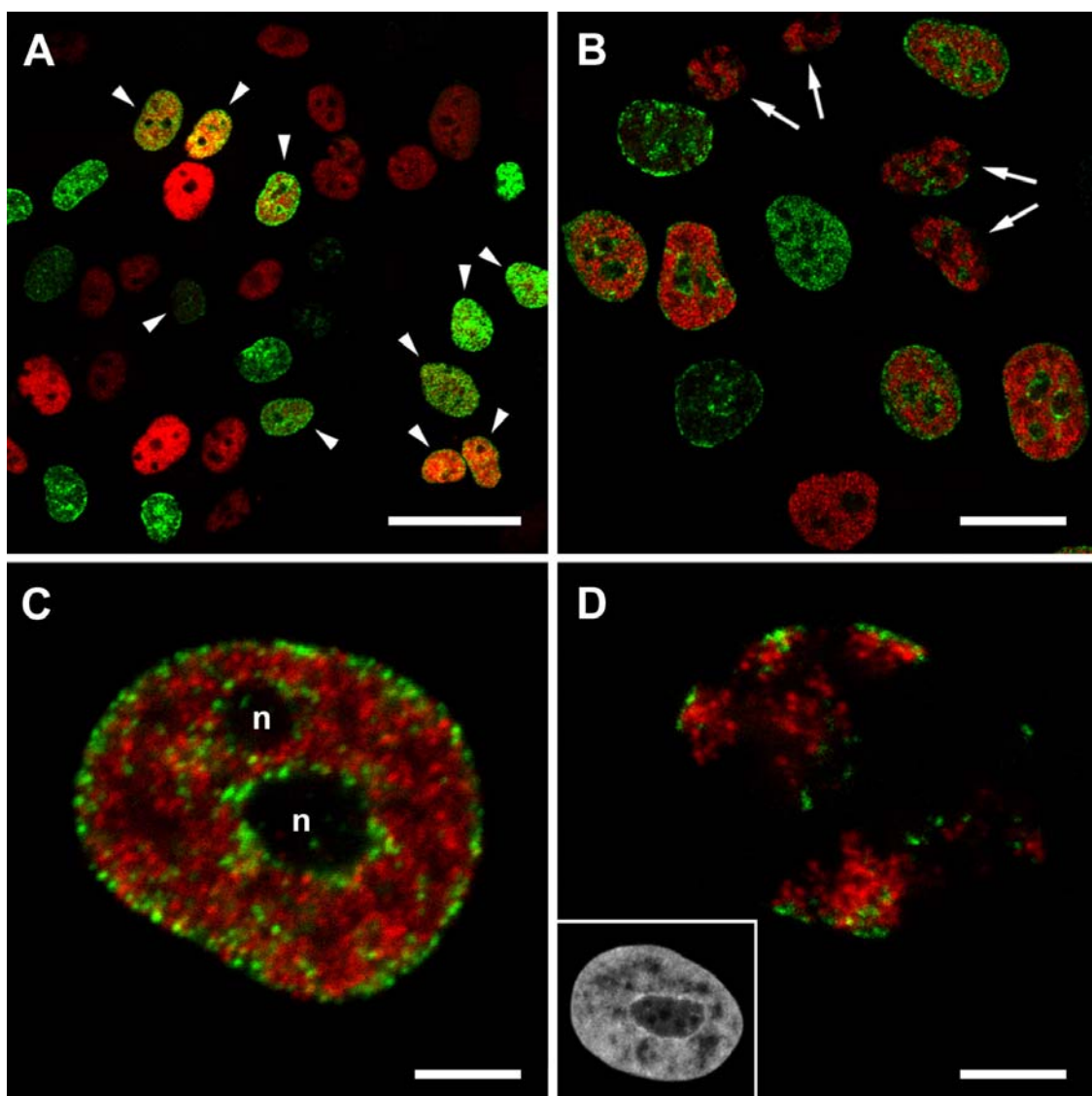


Figure 14. Confocal images of double-labeled nuclei of synchronized SH-EP N14 cells. (A and B) Cells were fixed 25 hrs after release from aphidicolin block and 19.5 hrs after completion of two-color SRL. Cells were labeled with Cy5-dUTP 1 hr after release and with FITC-dUTP 5.5 hrs after release. Note the high number of Cy5-labeled (red), FITC-labeled (green) and double-labeled (marked by arrowheads) nuclei in A. The confocal mid-section in B shows double-labeled nuclei at a higher magnification. Arrows indicate nuclei from cells, which have already divided twice and show segregated chromosome territories. (C) Light optical midsection through the nucleus of a SH-EP N14 cell fixed one day after two-color SRL shows the typical distribution of early (Cy5-dUTP, red) and mid-to-late (Cy3-dUTP, green) replication chromatin. Mid-to-late replicating chromatin is mainly located at the nuclear periphery and around nucleoli (n). Early replicating chromatin is distributed throughout the nuclear interior with exception of the nucleoli. (D) Light optical midsection through the nucleus of a SH-EP N14 cell fixed three days after two-color SRL shows polarized chromosome territories with typical early (Cy5-dUTP, red) and mid-to-late (FITC-dUTP, green) replication patterns. The majority of territories are unlabeled indicating that fixation was performed after at least three post-labeling cell cycles. Note that the topology of early and mid-to-late replicating chromatin was maintained through several cell cycles. Inset shows the same nucleus counterstained with propidium iodide. Scale bars: 50 μ m (A), 20 μ m (B) and 5 μ m (C, D).

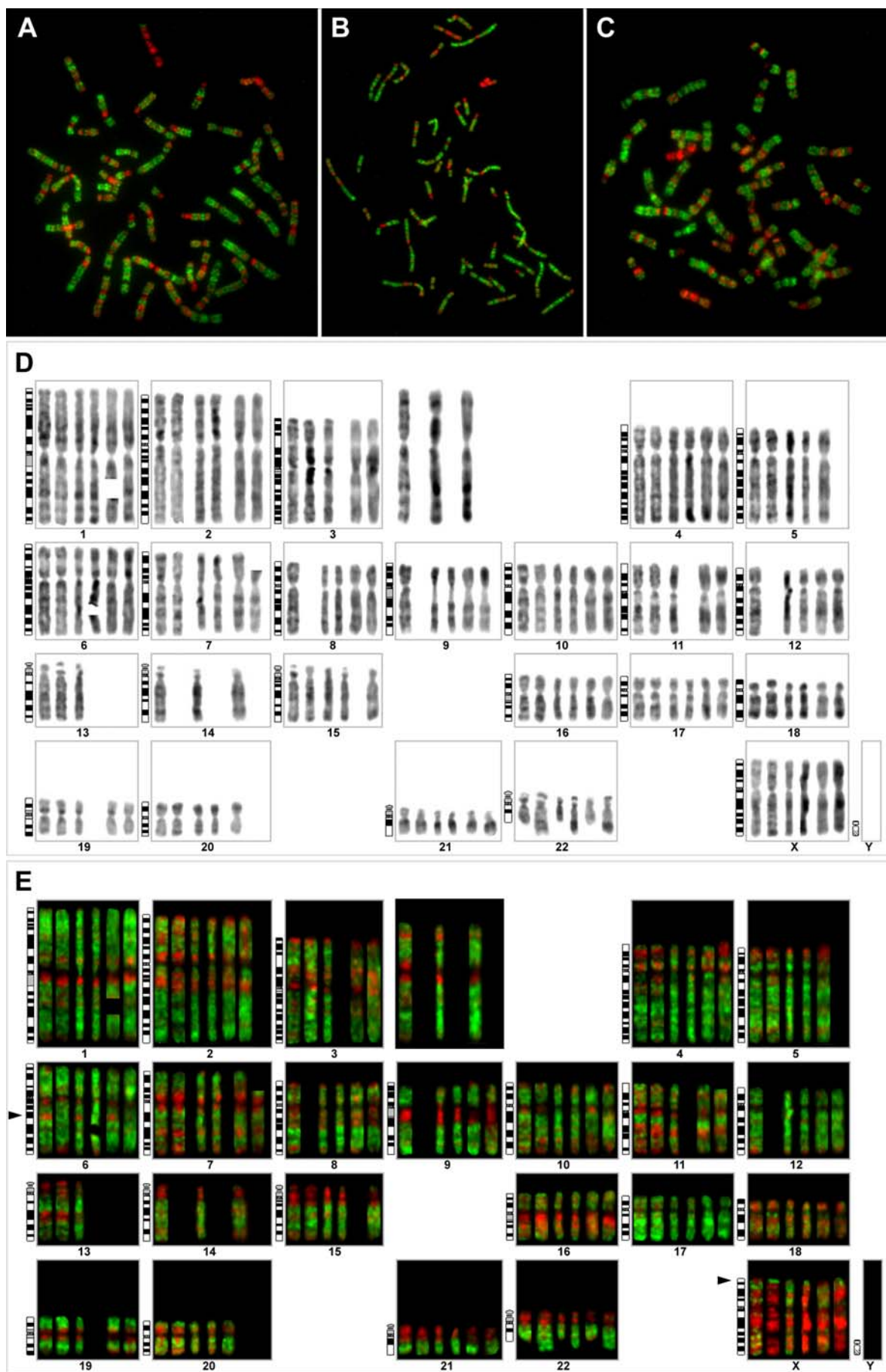
Double-labeled cells were able to continue cycling. As a consequence of semi-conservative replication, labeled and unlabeled chromatids were segregated at the second and subsequent mitoses following the labeling event, which resulted in nuclei with *in vivo* labeled chromosome territories (Figure 14 B and D). Double-labeled chromosome territories still showed the typical distribution of early replicating and mid-to-late replicating chromatin. This result clearly indicated that chromatin arrangements are stably transmitted over several cell cycles and that chromosomes reconstitute a “polarized” interphase CT arrangement after progression through mitosis.

Double labeled mitotic chromosomes

The characteristic pattern of early and mid-to-late replicating chromatin is generally thought to be correlated with R- and G-bands on metaphase chromosomes (Drouin *et al.*, 1990; Sadoni *et al.*, 1999). To confirm this assumption for the 2-color *in vivo* labeling approach synchronized SH-EP N14 cells were scratch labeled 30 min after release from the aphidicolin block with FITC-dUTP and 5.5 h after release with Cy3-dUTP. The cells were harvested 9.5 h after release (when a large fraction of labeled cells was undergoing mitosis) and fixed in methanol/acetic acid to obtain metaphase chromosome spreads. Consistent with the results from formaldehyde fixed interphase nuclei, most mitotic figures showed incorporation of either FITC-dUTP or Cy3-dUTP. In a considerable fraction (~15-20%) both labels were incorporated, however, one of the labels (either FITC or Cy3) was often found significantly less intense. Variable degrees of “injuries” of individual cells causing a variable influx of fluorescent nucleotides possibly explain this finding.

Figure 15 shows three double-labeled metaphase chromosome spreads with balanced fluorescence intensities, which were selected for a detailed analysis. The replication banding patterns found were in relatively good agreement with the alternating R- and G/C-bands as shown by the inverted DAPI staining (Figure 15 D and E). Most mid-to-late replicating (red) chromosome bands appeared to colocalize with a G-band. Centromeric heterochromatin was either Cy3-stained, and therefore presumably mid-to-late replicating (e.g. chromosomes 7 and 9) or unstained indicating later replication in very late S-phase (e.g. 10 and 12). Labeling of centromeric regions was especially prominent on NOR bearing human chromosomes 13, 14, 15 and chromosomes 21 and 22, which most likely accounts for the characteristic perinucleolar labeling of the mid-to-late replication pattern in interphase.

Figure 15. Replication banding pattern of metaphase chromosomes after two-color *in vivo* replication labeling. Synchronized SH-EP N14 cells were scratch labeled with FITC-dUTP (0.5 h after release, green) and Cy3-dUTP (5.5 h after release, red) and fixed with methanol/acetic acid 9.5 h after release. Metaphase spreads were prepared and DAPI stained. (A-C) Three metaphases that were selected for detailed analysis. (D and E) Chromosomes from the metaphase spreads shown in A-C were stretched and arranged in a karyogram using Quips CGH/Karyotyper 3.0 software (Vysis). The inverted DAPI staining is shown in D and the corresponding replication banding in E. The first homologous chromosome pair within each group corresponds to metaphase A the second to B, the third to C. Chromosomes that could not be clearly assigned by the inverted DAPI staining are not shown. Within each group the chromosomes were normalized to the same size. Arrowheads in E point to sites with likely asynchronous replication (for details see text).



These findings challenge a strict spatio-temporal allocation of facultative heterochromatin to the mid-to-late replicating compartment and constitutive (centromeric) heterochromatin to the very late compartment in this cell line.

In contrast to later replicating chromatin, early replicating DNA (green) appeared somewhat more dispersed, restraining a clear assignment to R-band bands. As expected, gene-dense chromosomes 17 and 19 were preferentially early replicating, while gene poor chromosomes, 18 and X were preferentially late replicating. Conflicting results were noted for chromosomes 16 and 11, which have an average gene density and were reported to have rather high gene expression levels (Caron *et al.*, 2001), but showed considerably large fractions of later replicating chromatin. In contrast, gene poor chromosomes 4 and 13, which were characterized by low expression levels, showed a relatively large fraction of early replicating chromatin. Likewise, some of the G-bands were clearly found early replicating. Despite taking into consideration the relatively low banding resolution, these findings indicate, that a too dogmatic commitment of replication timing and gene density and/or transcriptional activity should be considered with caution.

One of the two X chromosome homologues, likely the active X chromosome, showed additional early replicating bands (distributed over the whole length). In contrast, the second (inactive) X homologue was devoid of early replicating bands with exception of the pseudoautosomal region at the subtelomeric region of the short arm (Xp22.3). This region seemed to replicate earlier than its counterpart on the active X chromosome. Some bands on autosomes also displayed asynchronous replication, most prominently at 6q16. Allel specific differences in replication timing have been reported for imprinted regions, e.g. Prader-Willi syndrome / Angelman syndrome (PWS-AS) region on 15q11-13 (Simon *et al.*, 1999). However, no imprinting region has been mapped so far to 6q16. An alternative possibility might be a microdeletion in the respective region on one homologue of chromosome 6.

In a similar approach SH-EP cells were labeled in the same scheme but fixed 24 h after release when a large number of cells went through second mitosis. As a consequence of semi-conservative replication, metaphase spreads of these cells revealed chromosomes with only one labeled sister chromatid (Figure 16). Such metaphases were used to determine the frequency of sister chromatid exchanges (SCE). The average number of SCEs was found to be 6.2 ($n = 27$, single- and two-color labeled metaphases), which is somewhat higher than the SCE baseline frequency of 3.6 found in normal human peripheral lymphocytes (Tucker *et al.*, 1986). As the SCE baseline frequency of SH-EP N14 were not determined, it is not clear whether this increase is induced by the modified nucleotides. As a consequence of SCEs only fragments of CTs may be labeled in subsequent interphase nuclei.

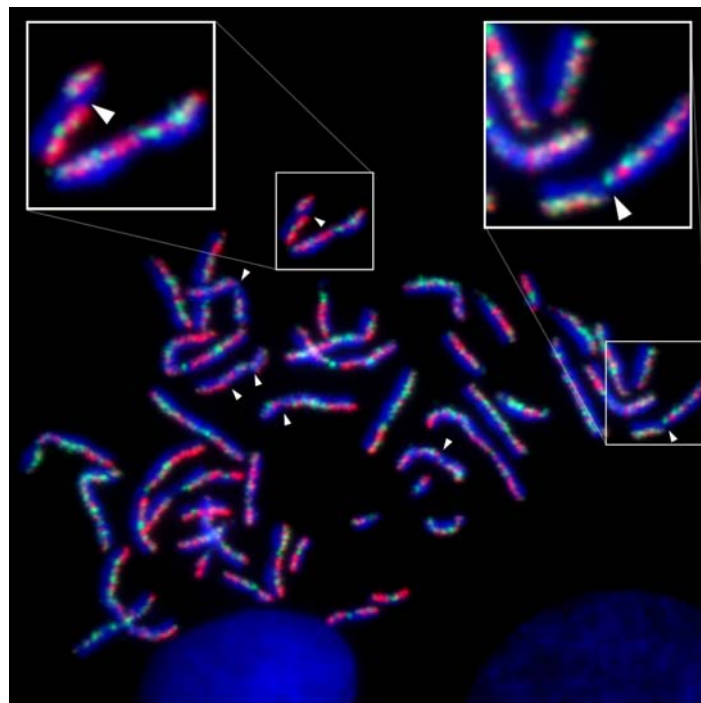


Figure 16. Second mitosis after two-color SRL. Synchronized SH-EP N14 cells were labeled as described for Figure 15, but fixed 24 h after release. Since no fluorescent nucleotides were present in the second S-phase, one chromatid on each chromosome is non-labeled and shows only the DAPI staining (blue). Arrowheads point to sister chromatid exchanges (SCE). Insets show two examples enlarged.

4.2 Dynamic behavior of chromosomes through the cell cycle

Because of its efficiency and easy applicability single-color SRL with Cy3-dUTP is ideal to study chromatin and chromosome dynamics in combination with green fluorescent protein (GFP). For the assessment of chromosome dynamics during the cell cycle, a HeLa cell line was employed that stably expresses GFP tagged histone H2B (Kanda *et al.*, 1998). Histone H2B-GFP is incorporated into nucleosomes without affecting cell cycle progression. HeLa cells expressing H2B-GFP show intense and stable green fluorescence staining of the nucleus, identical to that of DAPI.

Long-term observation of CT movement during interphase

To study the question whether major changes of CT positions in interphase nuclei may occur during more extended time periods, a single color scratch replication labeling with Cy3-dUTP was performed. During the second and subsequent post-labeling mitoses Cy3-labeled and unlabeled chromatids were segregated resulting in nuclei with a steadily decreasing number of labeled CTs. After labeling, cells were grown for 5-8 additional cell cycles resulting in nuclei with a low number of Cy3-labeled CTs. As described above the fluorescent nucleotides are incorporated into newly synthesized DNA for roughly 1 hour. Accordingly, each CT was represented only by a fraction of ~1 Mb chromatin domains that were replicated during the labeling period. Clusters of ~1 Mb chromatin domains were assigned to represent a single CT and the 3D-coordinates of the common intensity gravity center were calculated to represent its nuclear location. It is possible that a larger signal cluster was occasionally assigned to one CT although it corresponded to several neighboring CTs. Small signal clusters, which consisted of few ~1 Mb chromatin domains, possibly resulted from sister chromatid exchanges and therefore represented subchromosomal fragments. In spite of these limitations the calculated 3D-coordinates served the purpose of distinguishing whether individual CTs in HeLa cell nuclei can move to remote nuclear locations during interphase. The 3D intensity gravity center of the GFP-tagged nuclear chromatin served as the 3D-center of the nucleus (CN). 3D CT-CN distances as well as 3D CT-CT distances were measured at different time points of the total observation period.

Twenty-four cells exhibiting nuclei with 1-4 labeled CTs (Table 6) were chosen for the analysis of CT movements by time-lapse confocal microscopy with observation periods covering major parts up to a complete HeLa cell cycle of 18 - 20 hours. Evaluation periods in Table 6 represent the part of the total observation period used for a quantitative analysis.

Light-optical nuclear image stacks were sampled at high resolution with intervals between 6 min and 30 min. The simultaneous recording of H2B-GFP tagged chromatin allowed to monitor translational and rotational nuclear movements as well as changes in nuclear morphology and to measure the increase of the nuclear volume during interphase. In 12 cells the observation of a mitotic event preceded an evaluation period that covered G1 to mid S-phase. In 8 cells, a mitotic event resulting in two inconspicuous daughter nuclei was observed after the end of the evaluation period. In these cases, the end of telophase or the beginning of prophase was used as an indicator to estimate the interphase stages

Table 6. Nuclei included in the evaluation of CT-CT and CT-CN distances.

nucleus	approximate cell cycle phases covered	start of evaluation [h:min] after telophase (+) before prophase (-)	evaluation period [h:min]	volume increase during evaluation
fixed	-		6:00	+ 1%
1d1	telophase - early	+ 0:00	2:00	+ 116%
2d1	telophase - early	+ 0:00	2:15	+ 118%
3d1	telophase - early	+ 0:00	2:15	+ 82%
4	telophase - early	+ 0:00	2:36	+ 78%
5	early G1	+ 0:12	2:00	+ 46%
6d1	early G1	+ 0:15	2:45	+ 45%
7	early G1	+ 0:10	2:20	+ 42%
8	early G1	+ 0:15	1:30	+ 37%
1d2	early G1	+ 0:15	1:45	+ 29%
9	early G1	+ 0:12	1:36	+ 22%
10	early G1	+ 0:10	2:20	+ 25%
11	early G1	+ 0:10	2:40	+ 20%
9	mid G1	+ 1:48	2:12	+ 7%
2d1	mid G1 - late G1	+ 2:15	3:00	+ 4%
6d1	mid G1 - late G1	+ 3:00	3:00	+ 4%
12	mid G1 - early S	+ 2:30	5:00	+ 23%
4	mid G1 - early S	+ 2:36	5:24	+ 22%
5	mid G1 - early S	+ 2:12	6:00	+ 20%
13	mid G1 - early S	- 11:30	6:00	+ 16%
8	mid G1 - mid S	+ 1:45	10:00	+ 26%
10	mid G1 - late S/G2	+ 2:30 / - 17:20	12:20	+ 45%
11	mid G1 - late G2	+ 2:50 / - 17:00	16:30	+ 63%
14	mid G1 - late G2	- 15:15	15:00	+ 55%
3m	late G1 - late G2	- 13:30	13:00	+ 48%
15	lateG1/early S - G2	n.d.	10:00	+ 55%
16	lateG1/early S - G2	n.d.	10:00	+ 49%
1m	mid S - late G2	- 7:45	7:30	+ 36%
2m	late S - late G2	- 5:00	4:45	+ 27%
6m	late S - late G2	- 4:00	3:45	+ 19%
17	late S - late G2	- 4:00	3:45	+ 18%
18	late S - late G2	- 3:30	3:20	+ 12%
19	early- late G2	- 3:06	3:00	+ 1%

Each nucleus is named with an index number (column 1). Nuclei are arranged according to the cell cycle periods covered by the evaluation periods (column 2). Nuclei that were evaluated both during early G1 and later cell cycle stages are listed twice. In five of the nine nuclei recorded during early G1 the telophase stage could not be included in the evaluation since this stage was not completely recorded in z-direction. In 4 cases, where mother and daughter cell nuclei were evaluated, the mother nucleus is indicated by *m*, daughter(s) by *d1* (and *d2*). The start of the evaluation period is given in hours after telophase (+) or before prophase (-) (column 3). Column 4 indicates the length of the evaluation period. Column 5 shows the increase of the nuclear volume between the first and the last evaluated time point. A control nucleus was imaged for a period of six hours after fixation with 4% formaldehyde.

where CT movements were analyzed (Table 6) taking into account the approximate length of each cell cycle stage determined for HeLa cells (see chapter 3.10). In two cases (Table 6, nucleus 10 and 11) the total observation time encompassed two mitotic events. Two cells (Table 6, 15 and 16) did not undergo mitosis during an observation period of 10 hours but showed a nuclear volume increase typical for S-phase.

Figure 17 A-D shows, as a typical example, the results obtained from nucleus 3m (Table 6), which was evaluated from late G1 to late G2 over a time period of 13:00 h. Optical image stacks from the Cy3 and GFP channels were simultaneously recorded every 15 minutes. 13:30 h after the start of observation the cell went into mitosis yielding two inconspicuous daughter cells. During the evaluation period the nuclear volume increased from $1200 \mu\text{m}^3$ to $1780 \mu\text{m}^3$ (Figure 17 A-B). From a total of 52 3D image stacks, which were recorded during this time, 27 time image stacks with intervals of 30 minutes were used for a quantitative analysis of CT-CN and CT-CT distances. The results of these measurements are shown in Figure 17 C and D. The differences between the maximum and minimum distances ($\Delta_{(\text{Max-Min})}$) were taken as a measure of motility. Absolute distances fluctuated and increased slightly over time for distantly located CTs (Figure 17 C). This increase was probably a passive effect caused by the increase in nuclear volumes since it was no longer noticeable after correction for the nuclear diameter (Figure 17 D, see methods). Accordingly, the corrected $\Delta_{(\text{Max-Min})}$ values were smaller than the absolute values (compare Figure 17 C and D). Figure 17 D demonstrates that the relative positions of CTs were stably maintained during the entire evaluation period.

Figure 17. Stability of large-scale chromosome territory arrangements studied in nuclei with Cy3-labeled CTs. (A-D) Confocal time-lapse series of a HeLa cell (nucleus 3m in Table 6) with replication labeled CTs and its daughters recorded for a total observation period of 18 hours. CT movements in the mother cell nucleus were analyzed from late G1 to late G2 (13 hours evaluation period). Time point 0:00 indicates the start of evaluation. (A) The panel displays the superimposed maximum intensity projections of confocal serial sections from H2B-GFP (green) and Cy3-dUTP (red) together with a transmission image at the indicated time points. The start of evaluation was assigned to late G1 as the cell entered prophase 13.5 hours later. (B) Top and side view of 3D-reconstructions for time points 0:00 (h:min), 4:30, 8:30 and 12:30. Nuclei (outlined in gray) are displayed after correction for rotational movements, and nuclear volumes are indicated. Four signal clusters (shown in different colors) representing different CTs are shown in different colors for easier discrimination. (C, D) Absolute and corrected distances between the fluorescence gravity center of each CT and the center of the nucleus (CT-CN), as well as distances between all pairs of CTs (CT-CT) were evaluated at intervals of 30 min. $\Delta_{(\text{Max-Min})}$ indicates the difference between the maximum and the minimum distance measured within the complete evaluation period. (E-H) Confocal time-lapse series from another HeLa cell (nucleus 4 in Table 6) recorded with a time interval of 6 min. The 8-hour evaluation period started at telophase (time point 0:00) and is likely to have ended at early S-phase (8:00). The mother cell performed mitosis at time point -0:30. (E) Maximum intensity projections of confocal serial sections as described in (A) for indicated time points. (F) Top and side view of 3D-reconstructions from the evaluated nucleus (arrowhead) containing 3 CTs. (G, H) Absolute and corrected distances as described above for (C) and (D). CT-CN and CT-CT distances were evaluated at intervals of 12 min (early G1) and 30 min (mid G1-early S). The transition from early G1 to mid G1 is defined as the time point when the nuclear volume increase reaches a first plateau (see methods). Note the higher fluctuation of distances in early G1 in comparison to other cell cycle stages. Arrowheads in (A) and (E) indicate nuclei shown as 3D-reconstructions in (B) and (F). Bar: 10 μm .

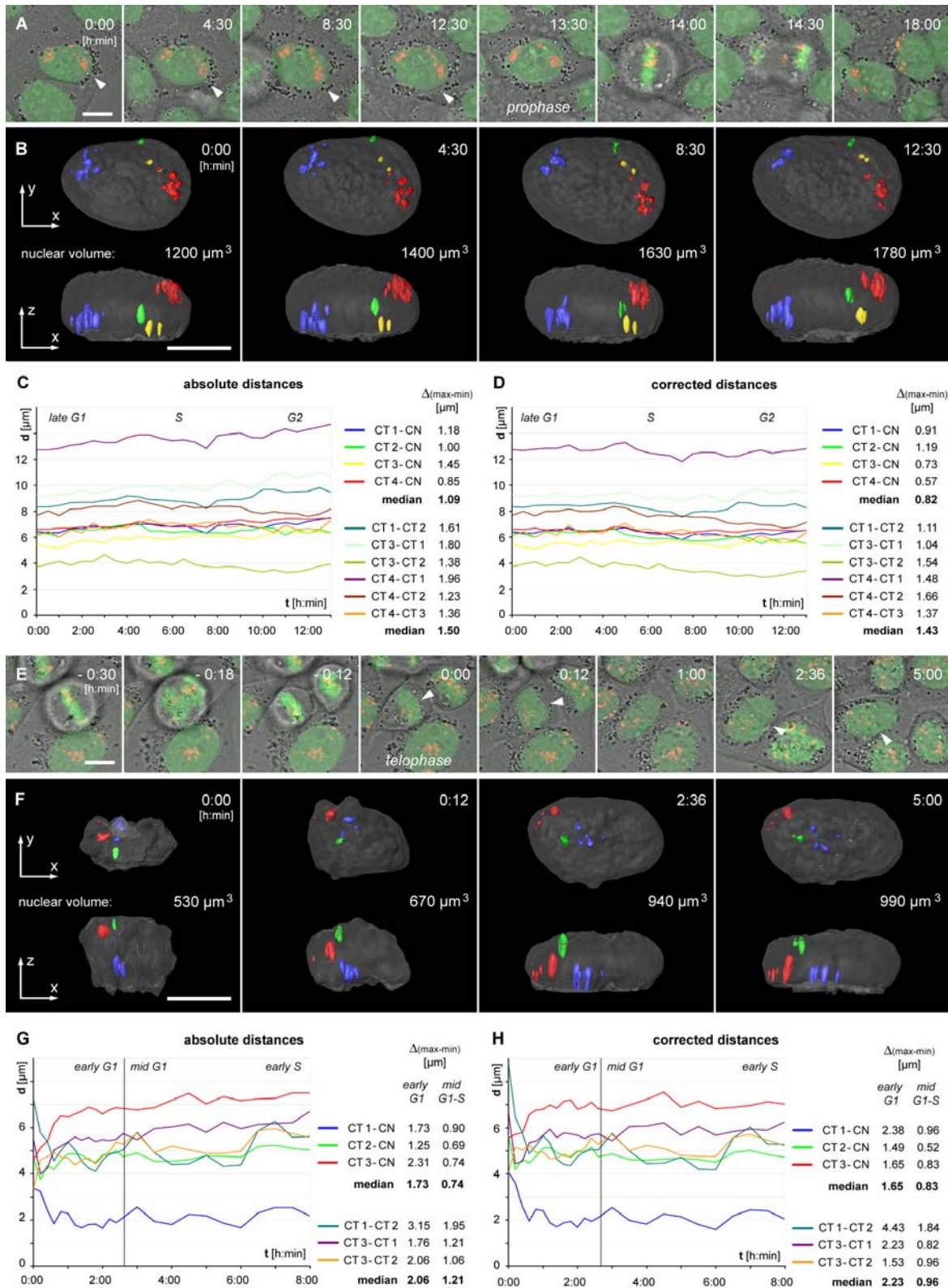


Figure 17 E-H shows nucleus 4 (Table 6), which exemplifies the analysis of CT movements covering a period of 8 hours from telophase into S-phase. From a total of 80 3D image stacks recorded at intervals of 6 min, 25 image stacks with intervals of 12 min during early G1 and of 30 min from mid G1 to early S phase were taken for a quantitative evaluation. Figure 17 G and H provide absolute and corrected CT-CN and CT-CT distance measurements. $\Delta_{(\text{Max-Min})}$ values measured during early G1 were higher than the values measured from mid G1 to early S.

The $\Delta_{(\text{Max-Min})}$ values determined for nucleus 4 during mid G1 to early S were similar to the values noted for nucleus 3m from mid G1 to late G2 (Figure 17 C, D). Accordingly, more extensive CT movements can occur during early G1 (see also supplementary video 2).

Table 7 summarizes the results from 3D distance analyses of 24 cells and confirms the findings described above for the two example nuclei. Movements of labeled CTs were locally constrained during interphase. However, $\Delta_{(\text{Max-Min})}$ values, which express the variability of the measured CT-CN and CT-CT distances, were significantly larger during early G1 (ranging from 0.47 to 4.44 μm for corrected CT-CT distances, 7/19 (37%) of the values were $> 2 \mu\text{m}$) compared

Table 7. Summary of CT-CN / CT-CT distance measurements

		number of nuclei	$\Delta_{(\text{Max-Min})}$ CT-CN [μm]		$\Delta_{(\text{Max-Min})}$ CT-CT [μm]	
			absolute	corrected	absolute	corrected
fixed	1	median (range)	0.09 (0.07 - 0.10)	0.11 (0.07 - 0.14)	0.15 (0.09 - 0.22)	0.16 (0.15 - 0.20)
		N($\Delta > 2 \mu\text{m}$)/N total	0 / 3	0 / 3	0 / 3	0 / 3
telophase	12	median (range)	1.34 (0.30 - 2.46)	1.26 (0.42 - 2.75)	1.76 (0.48 - 4.10)	1.53 (0.47 - 4.44)
- early G1		N($\Delta > 2 \mu\text{m}$)/N total	6 / 25 (24%)	3 / 25 (12%)	8 / 19 (42%)	7 / 19 (37%)
mid G1	20	median (range)	1.06 (0.32 - 1.76)	0.90 (0.24 - 1.53)	1.26 (0.40 - 2.59)	1.04 (0.25 - 2.11)
- late G2		N($\Delta > 2 \mu\text{m}$)/N total	0 / 48 (0%)	0 / 48 (0%)	4 / 45 (9%)	1 / 45 (2%)
		p (median)	0.047	0.001	0.135	0.01
		p ($\Delta > 2 \mu\text{m}$)	0.001	0.037	0.004	0.001

Distances between intensity gravity centers of CT pairs (CT-CT) as well as distances between CTs and center of nucleus (CT-CN) were measured for each nucleus. $\Delta_{(\text{Max-Min})}$ values are provided as a measure of CT motilities and represent the difference between the maximum and minimum CT-CN or CT-CT distances measured for each CT or CT pair during the indicated cell cycle phases. In addition to $\Delta_{(\text{Max-Min})}$ values calculated for absolute distances, the respective values for distances corrected for changes in total nuclear volume are presented. Displayed are the median values of $\Delta_{(\text{Max-Min})}$ from all CTs and the smallest and largest $\Delta_{(\text{Max-Min})}$ value (range) for a fixed control nucleus, for 12 nuclei in telophase to early G1 and 20 nuclei in mid G1 to late G2. The number of $\Delta_{(\text{Max-Min})}$ values exceeding 2 μm (N($\Delta > 2 \mu\text{m}$)), and the total number of measured $\Delta_{(\text{Max-Min})}$ values (N total) are shown. The p-values indicate the degree to which the differences in median and N($\Delta > 2 \mu\text{m}$) between nuclei in telophase to early G1 and nuclei in mid G1 to G2 are significant. The $\Delta_{(\text{Max-Min})}$ values obtained for a fixed control nucleus are within one magnitude of order smaller and indicate a minor contribution of mechanical instability in the microscope system. (A supplementary table with all $\Delta_{(\text{Max-Min})}$ values is presented with the supplementary material in chapter 7.1)

to subsequent interphase stages (0.25 to 2.11 μm for corrected CT-CT distances, only 1/45 (2%) of these values were $> 2 \mu\text{m}$). Notably, the mobility of individual CTs during early G1 varied largely (see supplementary table in appendix 7.1). From mid G1 to late G2 absolute distances increased slightly over time reflecting the increase in nuclear volume. During early G1 a significantly larger variability was noticed for both absolute and volume corrected distances. Furthermore, in spite of the increase in nuclear volume we observed occasional CT-CT and CT-CN distances, which became even smaller during early G1 (Figure 17 G, H). These findings indicate that the more pronounced CT movements during early G1 do not simply reflect the rapid increase of nuclear volume after telophase, but rather the movements of CTs to their final nuclear locations, which are then maintained within a range of 1 μm (maximum $\sim 2 \mu\text{m}$) from mid G1 to late G2. This corresponds to a radius of confinement of 0.5 - 1 μm .

In a further experiment a sequential two-color scratch replication labeling was carried out. During the first S-phase mother nuclei were labeled with Cy3-dUTP. During the next S-phase, daughter nuclei were labeled with Cy5-dUTP. Segregation of labeled and unlabeled chromatids during a post labeling growth of cells for four days resulted in nuclei with a subset of CTs stained in different colors (Figure 18, supplementary video 2). During observation periods of several hours neighboring differently colored CTs moved repeatedly closer and further apart confirming locally constrained CT movements in the order of 1 μm . We observed only very little color mixing indicating the separation of the bulk DNA from different CTs. The sensitivity of this approach, however, was not sufficient to exclude intermingling of a fraction of chromatin loops.

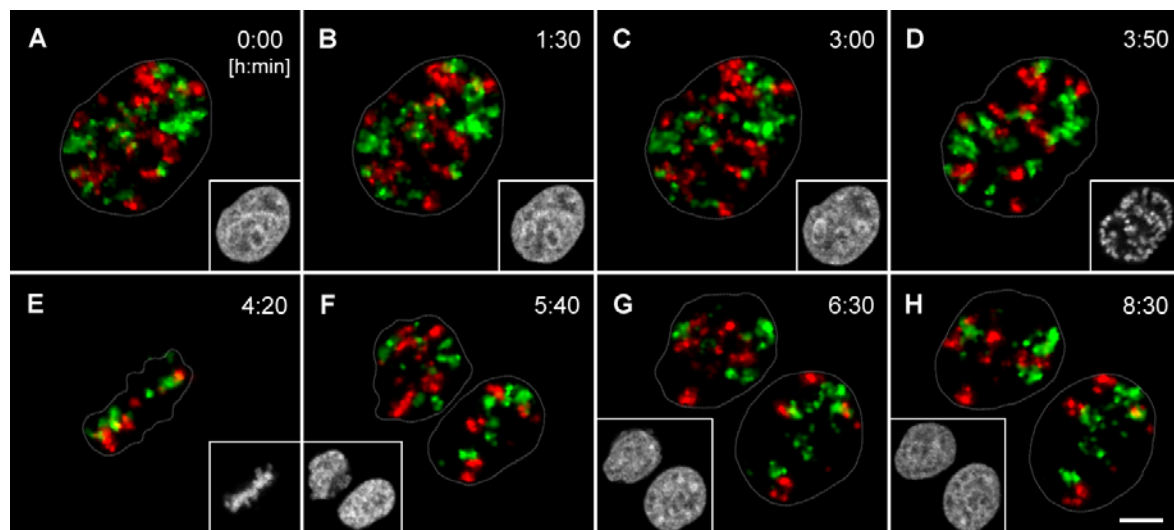


Figure 18. Stability of chromosome territory neighborhood during interphase of living HeLa cells. HeLa cells were replication labeled during S-phase of two consecutive cell cycles (first cycle: Cy3-dUTP, false color red; second cycle: Cy5-dUTP, false color green). Frames of maximum intensity projections from light optical serial sections are displayed for the indicated time points. Insets show GFP signals of confocal nuclear midsections in gray. Images are corrected for translational and rotational nuclear movements. Observation started 4.5 days after the second labeling event. After 3:50 h the cell entered prophase. Note that chromosome condensation is a locally confined process with little changes of chromosome arrangements (compare C and D). After completion of mitosis daughter nuclei were followed for another 3:30 h. Locally constrained movements, but no major rearrangements of differently colored chromatin domains were detected (see supplementary video 3). Bar: 5 μm .

Changes of chromosome neighborhoods occur during mitosis

To find out whether higher order chromatin arrangements change from one cell cycle to the next, we synchronized HeLa cells in early S-Phase. Five to six hours after release from the block, when most of the cells were in late S phase or had entered G2 (Figure 19, column I), we bleached the GFP-tagged chromatin, leaving a single, contiguous zone of unbleached chromatin at one nuclear pole (Figure 19, column II). The cells were then followed by time-lapse confocal microscopy through mitosis into the next G1 phase. 34 cells yielded daughter nuclei with sufficient contrast of unbleached chromatin patches reflecting the local decondensation of unbleached chromosome segments. Ten cases were excluded because one or both daughter cells showed nuclei with morphological abnormalities. The remaining 24 cases were analyzed in detail.

The area of unbleached nuclear chromatin retained its location and shape at the nuclear pole until the onset of prophase. At prophase several unbleached chromosomal segments became visible within this zone (Figure 19 C, column III). Mitotic rosettes were typically arranged perpendicularly to the surface on which the cells grew. Unbleached chromosome segments clustered within a single area in 9 rosettes (Figure 19 A, column IV), whereas some or most of these segments were observed in distant locations in 13 rosettes (Figure 19 B, C, column IV). Two rosettes could not be evaluated, as the light optical serial sections did not cover the unbleached segments.

In the 48 daughter cell nuclei the degree of clustering of unbleached chromatin was scored on maximum intensity projections. Twenty nuclei showed a nuclear subregion with a single cluster of unbleached chromatin patches (Figure 19 A, column V and VI). These cases reflect the best restoration of CT order between the mother nucleus and its daughter nuclei. Nevertheless, the restoration was far from complete since patches of unbleached chromatin were separated by zones of bleached chromatin suggesting that bleached chromosome segments had moved between unbleached chromosome segments. In 15 daughter cells most unbleached chromatin patches were clustered, but some patches were located in a remote nuclear area (Figure 19 B, column V and VI). In 13 nuclei patches of unbleached chromatin were distributed over the major part of the nucleus (Figure 19 C, column VI). Controls excluded the possibility that fluorescent patches simply reflected areas of high chromatin density rather than unbleached chromosome segments. DNA staining of fixed daughter cells with propidium iodide (PI) showed no spatial correlation of intense PI signals with sites of strong GFP fluorescence. In nuclei which were bleached completely and followed through mitosis, fluorescent patches were not detected (data not shown). These experiments demonstrate that significant changes of CT order occur during mitosis.

In addition to the visual analysis, the degree of nuclear clustering of unbleached chromatin was quantitatively evaluated by calculating a radial autocorrelation function (RAC developed by J. Walter for details see Walter *et al.*, 2003). The RAC analysis fully confirmed the conclusion derived from the visual inspection: The positions of unbleached chromosome segments studied in daughter nuclei differed significantly from the positions in the mother cell nuclei.

In conclusion, the experiments described in this section support Boveri's hypothesis that changes of chromosome neighborhoods occur when cells pass through mitosis. In the majority of cases (18 of 24) both daughter nuclei showed the same pattern of unbleached patches, suggesting that anaphase-telophase

chromosome movements retain a certain level of symmetry. In six cases, however, scattering of unbleached chromatin patches was much more pronounced in one daughter nucleus than in the other (data not shown), suggesting that different movements of unbleached sister chromatid segments during anaphase/telophase or in early G1 nuclei contributed to this apparent loss of symmetry.

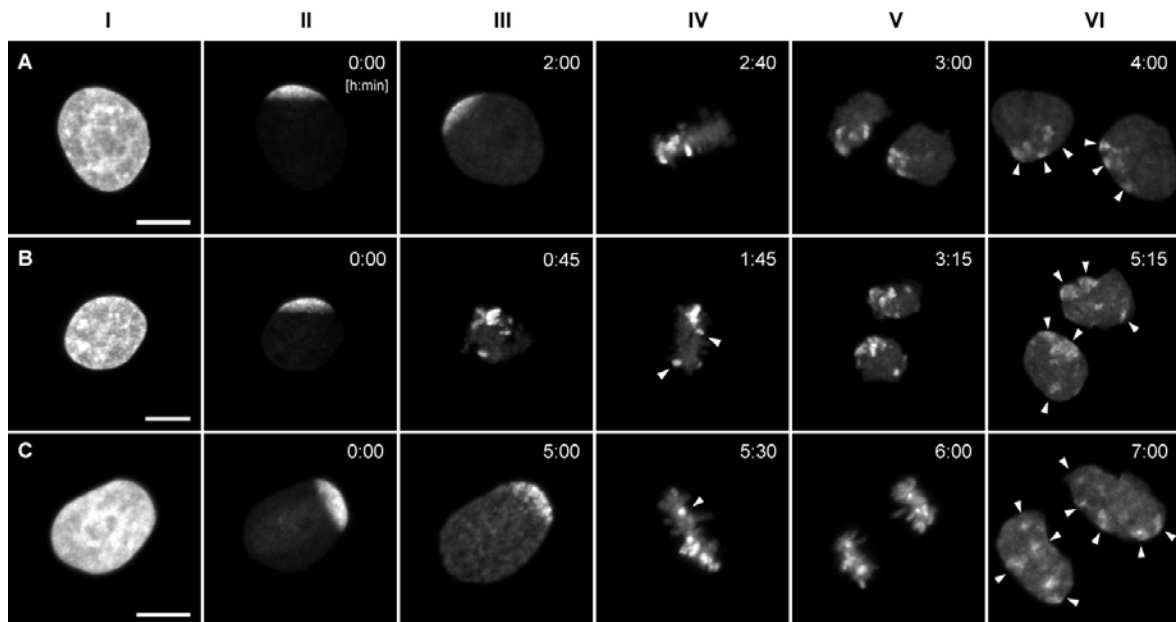


Figure 19. Large-scale chromosome territory arrangements in HeLa cell nuclei change from one cell cycle to the next. Panels A - C show examples of live cell confocal image series from three HeLa cells (for movie sequences see supplementary video 4). After bleaching of GFP labeled chromatin apart from a contiguous unbleached region at one nuclear pole, cells were followed through the remaining part of interphase and through mitosis till the formation of daughter nuclei. All images are maximum intensity projections of confocal image stacks. The degree of the redistribution of unbleached chromatin patches in G1 daughter cells (column VI, arrowheads) can vary from “clustered” (panel A) to “partially clustered” (panel B) to “scattered” (panel C). Column I: GFP pattern of HeLa nuclei before bleaching; column II: the same nuclei after partial bleaching; column III: last frame recorded prior to the formation of the metaphase plate; column IV: metaphase plate, arrowheads in B and C point to unbleached chromosomal fragments that are remote from the bulk of unbleached chromatin. Column V and VI: daughter nuclei in anaphase (column V, C), telophase or very early G1 (column V, A and B) and in early G1 (column VI). Bars: 10 µm.

Changes of chromosome territory arrangements during clonal growth

To study the variability of arrangements of specific CTs in 2-cell clones from independent mitotic events, as well as between the two pairs of daughter nuclei in 4-cell clones, we performed two color 3D-FISH experiments on HeLa cell clones fixed at these stages. Painting probes for chromosomes 7 and 10 were chosen, since these chromosome types were present as three free copies and not involved in translocations (data not shown). Confocal serial sections were obtained from twelve 2-cell clones and ten 4-cell clones and projections were visually compared for translational and mirror like similarities of CT arrangements (for examples see Figure 20 and Figure 21). Additionally, 3D-reconstructions of

daughter nuclei were made which could be freely rotated allowing the comparison of their CT arrangements from any angle (Figure 21 B, supplementary videos 5-8). The CT arrangements in the nuclei of 2-cell clones showed an obvious albeit far from perfect symmetry in most clones, whereas different mitotic cells yielded daughter nuclei with largely different CT arrangements (Figure 20). In 4-cell clones, pairs of nuclei were identified that showed a notable symmetry of their CT arrangements, whereas strong differences were noted between the two pairs (Figure 21). In agreement with Boveri's findings (compare Figure 3 B), CT arrangements in 4-cell clones already differed largely.

Figure 20. CT #7 and #10 arrangements in nuclei of 2-cell clones. Projections of confocal image stacks obtained after painting of chromosome 10 (red) and 7 (green). DNA counterstain: blue. A, B, and D represent daughter nuclei with an obvious although not perfect symmetry of the relative CT arrangements. F provides an example of a pronounced deviation from a symmetrical arrangement. To facilitate assessment of symmetry some of the nuclei were rotated and / or mirrored. Bars: 10 µm.

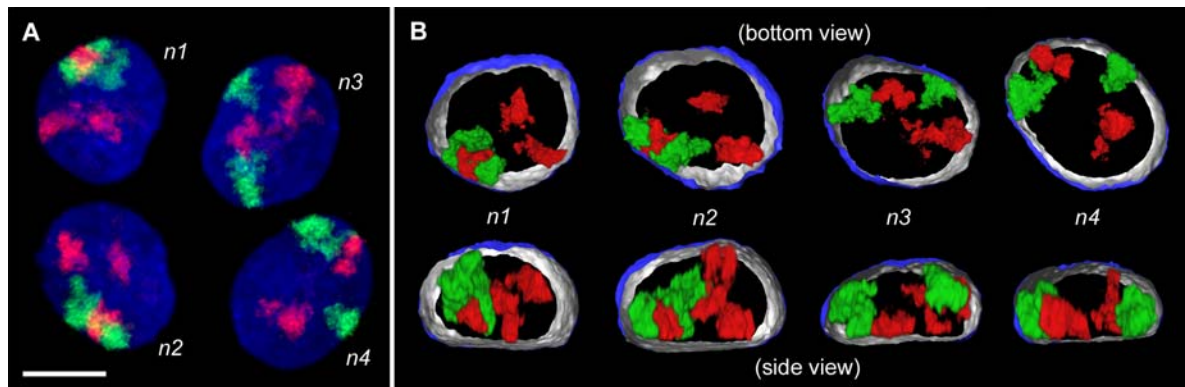
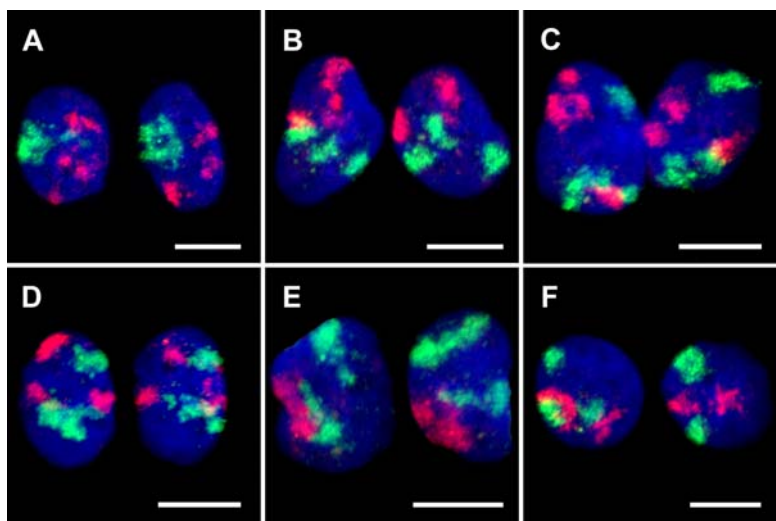


Figure 21. CT #7 and #10 arrangements in a 4-cell clone. (A) Projection of a confocal image stack through nuclei n_1 to n_4 after painting of chromosome 10 (visualized in red) and 7 (visualized in green). DNA counterstain: blue. (B) 3D-reconstructions of n_1 to n_4 by volume rendering. Part of the nuclear border is indicated by reconstruction of the counterstain periphery (outside: blue, inside: silver-gray). The upper row shows the bottom view, the lower row the corresponding side view. To show the symmetry of CT arrangements in nuclei n_1 and n_2 more clearly, the x-axis of n_2 was inverted. Bar: 10 µm. (For interactive animation of nuclear reconstructions see supplementary videos 5-8).

4.3 Mid-to-late replicating chromatin associates to the nuclear lamina

To gain insight into the interconnection between distinct chromatin compartments and the nuclear lamina *in vivo*, initial experiments were performed combining replication labeling and visualization of the nuclear lamina in fixed and living cells. First experiments approaching functional assay, were performed on replication labeled baby hamster kidney (BHK) cells using a dominant negative lamin A protein (Δ NLA) which causes a reversible disruption of the nuclear lamina (Spann *et al.*, 1997). Therefore, labeling of the nuclear pore complex (NPC) was performed in some experiments to assess the possibility of using NPC as a marker of the nuclear envelope during disruption of the lamina.

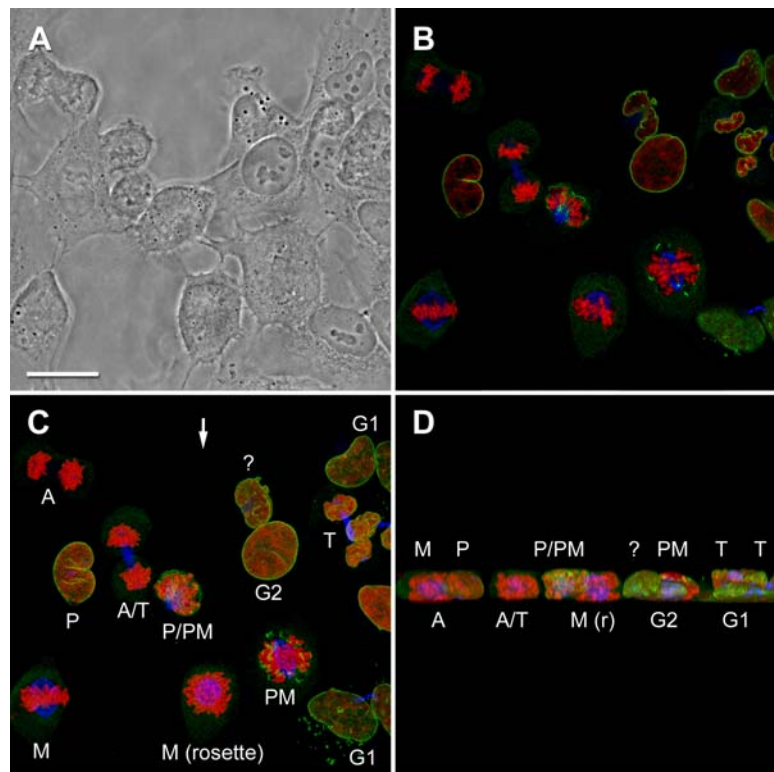
Morphology of the nuclear lamina during cell cycle of SH-EP N14 cells

SH-EP cell interphase nuclei immunostained with antibodies against lamin A/C or lamin B often showed irregular nuclear shapes with enfoldings and invaginations of the nuclear envelope and sometimes tube-like channels as has been described for other mammalian cells (Fricker *et al.*, 1997). The invaginations were mostly oriented perpendicularly to the coverslip as has been described for CHO cells (Broers *et al.*, 1999). G1 nuclei typically displayed a higher number of invaginations, which seemed to decrease with progression through the cell cycle. Consequently, S-phase and G2 cell nuclei were characterized by a more regular, oval shape and little or no invaginations. Apart from the prominent nuclear rim staining, both A-type and B-type lamins showed a diffuse or small-dotted “veil” staining of the nucleoplasm excluding the nucleoli (Moir *et al.*, 2000b).

The high degree of synchrony obtained for SH-EP N14 neuroblastoma cells after two-step synchronization (described above) was utilized to investigate nuclear morphology at various stages of the cell cycle, in particular during mitosis. Synchronized SH-EP cells were fixed in 3.7% formaldehyde 8.5 h after release from aphidicolin block. At this time point a large fraction of cells were undergoing mitosis (Figure 22; see also Figure 7) with all types of mitotic figures highly enriched. In addition, G2 cells as well as early to mid G1 cells, but virtually no S-phase cells were present. G1 cells can be unequivocally distinguished from G2 cells by their size and morphology. In general, such an experimental scheme nicely complements live cell studies as it facilitates high-resolution microscopy of all mitotic stages on fixed cells, avoiding apparent detrimental effects of high-resolution live cell microscopy.

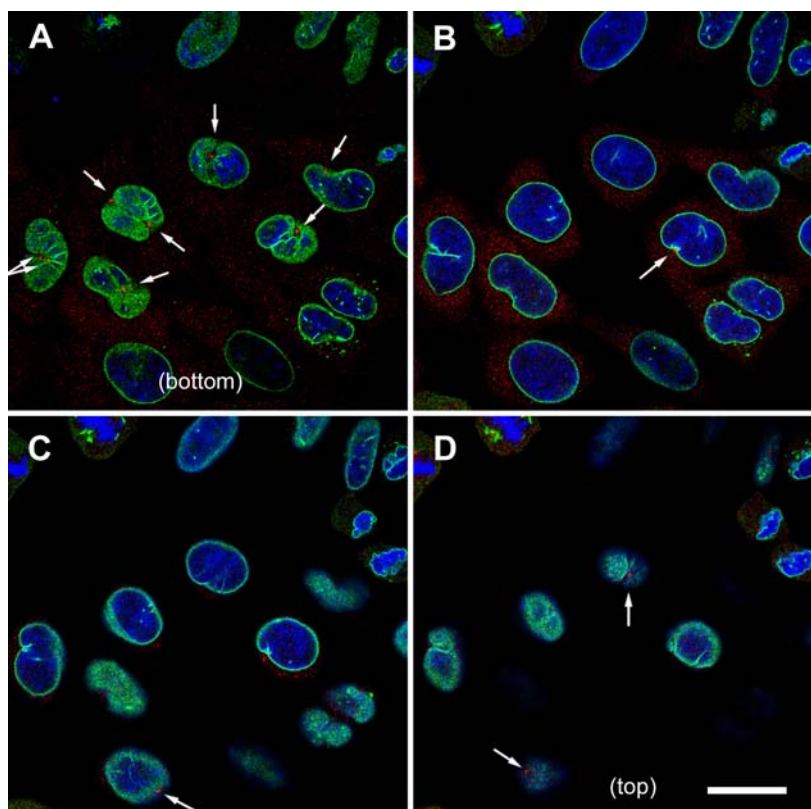
Cells were immunostained with antibodies against lamin B (or A/C) in combination with antibodies against β -tubulin (to mark the mitotic spindle), γ -tubulin (centrosomes) or with nuclear pore complex (NPC) specific antibodies (mAb 414). DNA was stained with TOTO-3, TO-PRO-3 or PI. TOTO-3 as well as PI also have a strong binding affinity to RNA, thus RNase treatment was performed in most cases.

Figure 22. Overview of mitotic stages in SH-EP cells. Two-step synchronized SH-EP N14 cells were fixed 8.5 hrs after release from aphidicolin block and immunostained with antibodies against lamin B (green) and β -tubulin (blue). DNA was stained with TOTO-3. Due to the high degree of synchrony, mitotic cells are highly enriched at the time point of fixation. Here all mitotic stages can be identified within one field of view. (A) Phase contrast, (B) confocal mid section, (C) 3D-projection in xy direction (D) 3D-projection in xz (axial) direction. Arrow in C indicates view direction. (For a detailed view and description of the mitotic stages see Figure 24). Bar: 25 μ m.



At the onset of mitosis, in early prophase cells, a characteristic indentation of the nuclear lamina was typically observed at the site where the (already duplicated) centrosomes were positioned (Figure 23). With separation of centrosomes, a branching invagination of the nuclear envelope was induced by the microtubules of the early spindle (Georgatos *et al.*, 1997; Beaudouin *et al.*, 2002). With proceeding prophase, the chromatin of condensing chromosomes was relocated towards the lamina leaving a relatively large space devoid of chromatin in the nuclear interior (Figure 24). At the end of prophase, individual chromosomes became visible, which were mainly positioned alongside the periphery and were especially concentrated along the branching invagination of the nuclear envelope, indicating a physical attachment to the still contiguous lamina. In general, two characteristic prophase figures were found (here referred to as type I and II). In type I (Figure 24 C, M, N and Figure 25 A) the forming spindle is oriented perpendicularly to the substrate. These nuclei typically display one central transnuclear, branched lamin invagination. In type II prophase nuclei, the spindle forming is oriented parallel to the surface and two deep indentations can be observed, both on one side, typically at the bottom (Figure 24 D, O and Figure 25 B). This suggests that type I prophasess would be preceded by a “classical” metaphase rosette (with a perpendicular spindle, for an example see indicated cell in Figure 23), which is then followed by subsequent 90° tilting of the spindle and metaphase plate. In contrast, in type II prophasess tilting is obviously dispensable.

Figure 23. Centrosome location in prophase cells. Synchronized SH-EP cells immunostained with antibodies against lamin B (green) and γ -tubulin (blue), which is present in centrosomes and involved in microtubule nucleation. DNA was stained with TOTO-3. A-D shows four confocal sections with an axial distance of 1.6 μ m from the bottom (glass) side to the top. In prophase nuclei, characteristic indentations of the nuclear lamina where the centrosomes are positioned can be seen (arrows). In most cases the daughter centrosomes have already migrated to distant poles. Bar: 25 μ m.



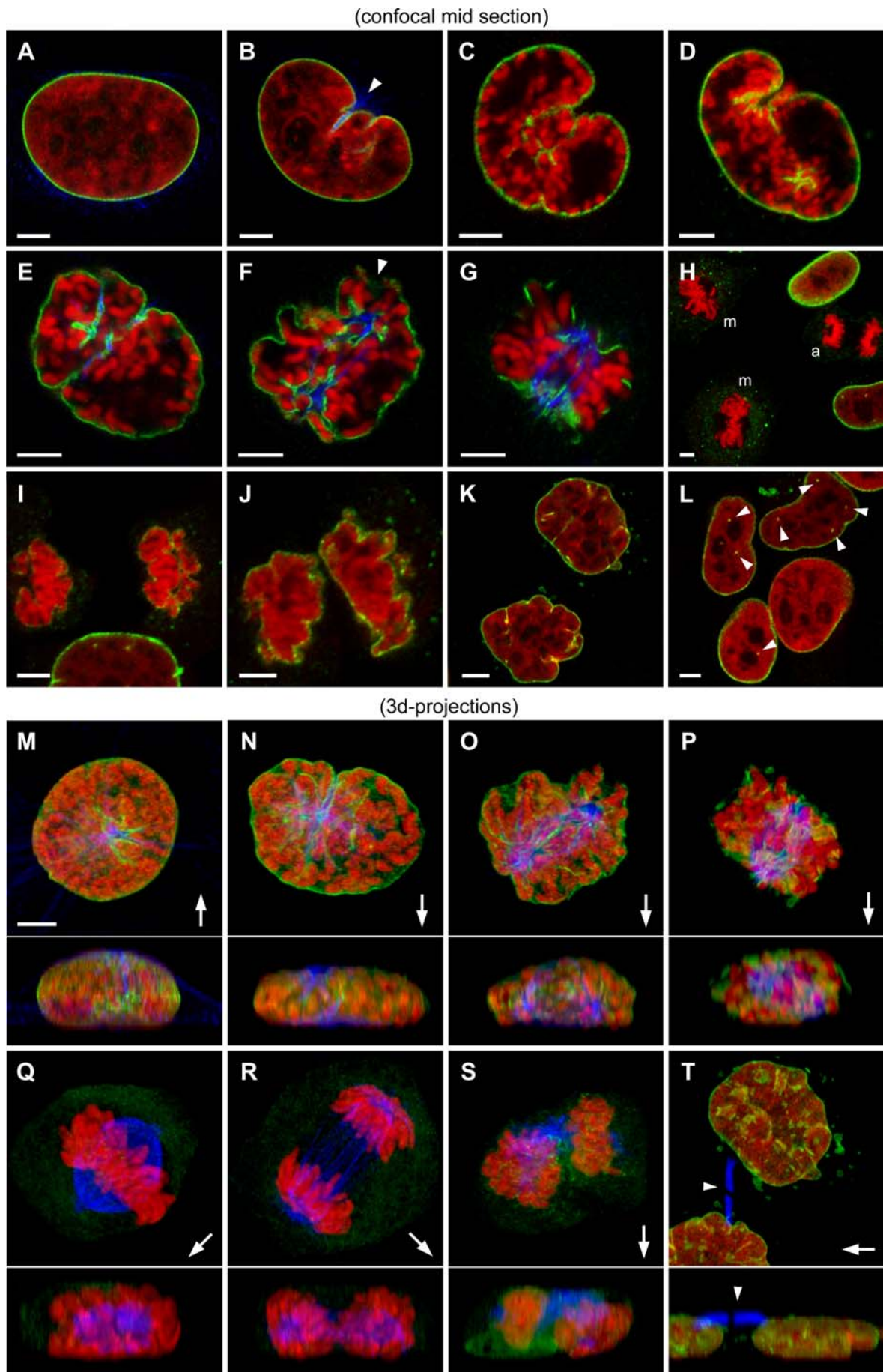
With transition to prometaphase (Figure 24 E, F, N), the lamina lost its tension force causing a flattening of the nucleus. Finally the lamina disrupted into fragments at a time point when all sister chromatids were attached to the spindle (Beaudouin *et al.*, 2002).

In comparison to lamin B, NPC revealed different disassembly kinetics. During interphase as well as in prophase (Figure 25 B), NPC and lamin B were both colocalizing along the nuclear periphery as well as on lamin invaginations (Figure 25 C). However, in prometaphase, NPC diffused into cytoplasm while lamin B was still forming a contiguous layer around the condensed chromosomes. Interestingly, lamin A/C, unlike lamin B, also disassembles in a diffusive manner and at an earlier stage in prometaphase (Georgatos *et al.*, 1997). Hence, lamin B disassembly has to be considered a late event in the mitotic breakdown of the nuclear envelope.

During metaphase, chromosomes were typically found aligned in the equatorial plate located in the center of the horizontally oriented spindle (Figure 24 H, Q). Here, as well in the subsequent anaphase, the nuclear envelope was dissolved and lamins B, like NPCs, were completely dissociated in the cytoplasm (Figure 24 H, Q, R). In early telophase, reassembly of the nuclear envelope started with the formation of the nuclear membrane and assembly of nuclear pores as an early event. At this stage NPC specific antibodies showed a strong rim staining around still condensed chromosomes and weak cytoplasmic signals, whereas lamin B showed only weak rim staining and relatively strong cytoplasm staining (Figure 24 I, S, Figure 25 D). In subsequent stages of late telophase and early G1, deep invaginations or channels became visible

(Figure 24 J, K, T). Consequently, invaginations and tube-like structures found in G1 nuclei (Figure 24 L) are likely to be remnants of the concomitant chromatin decondensation and the formation of the nuclear envelope. In G2 cells, invaginations are less common (Figure 24 A), indicating receding internal lamin structures during progression of interphase. This process might be accompanied with movement of attached chromatin domains towards the nuclear periphery.

Figure 24. Different mitotic figures of SH-EP cell nuclei. Synchronized SH-EP cells were formaldehyde-fixed 8.5 hours after release from aphidicolin block. Chromatin (red) was stained with TOTO-3 (A, B, E-F) or propidium iodide (C, D, H-L) and lamin B (green) was immunodetected. In a subset (A, B, E-G and M-T) β -tubulin was detected simultaneously (blue). (A-L) Confocal mid sections, (M-T) 3D-projections of confocal serial sections in xy-direction (upper panel) and z-direction (lower panel) are shown. Arrows indicate viewing direction of the z-projection. (A) G2 nucleus that displays a regular oval shape without invaginations of the nuclear envelope. β -Tubulin containing microtubules from the cytoskeleton surround the nucleus. (B) Early prophase nucleus showing a characteristic indentation caused by mechanical tension of microtubules of the early spindle (arrowhead). A beginning chromatin condensation becomes apparent around the indentation. (C, D, M) Characteristic mid prophase figures: type I (C and M) shows one strongly convoluted indentation and perpendicularly oriented spindle penetrating the nucleus. Type II (D) displays two indentations with the spindle apparently forming parallel to the surface. The condensed chromosomes are located along the still contiguous nuclear lamina leaving a chromatin-free space in the interior. (E-G, O, P) During prometaphase the nuclear lamin B meshwork breaks down in fragments. Chromosomes that are now attached to the spindle are drawn towards the spindle center. (H, M) In metaphase cells (m) chromosomes are aligned in a wheel-shaped equatorial plate. Lamin B is completely dissociated into the cytoplasm. (H, R) In anaphase (a), the sister chromatids are pulled towards the spindle poles. (I, T) In early telophase, a weak lamin staining indicates the beginning of the lamina formation while chromosomes start to decondense (nuclear membrane and NPC are already assembled at this time point, see also Figure 25 D). Microtubules of the spindle concentrate as consequence of cytokinesis. (J, K, T) In late telophase/early G1, the lamina is highly convoluted with enfoldings and invaginations. Early G1 cells (T) are still connected by a tubulin-bridge (arrowhead). In later stage of G1 (L), SH-EP cell nuclei often display mostly vertically oriented invaginations (seen as dots in the confocal mid-section, arrowheads) Bars: 5 μ m.



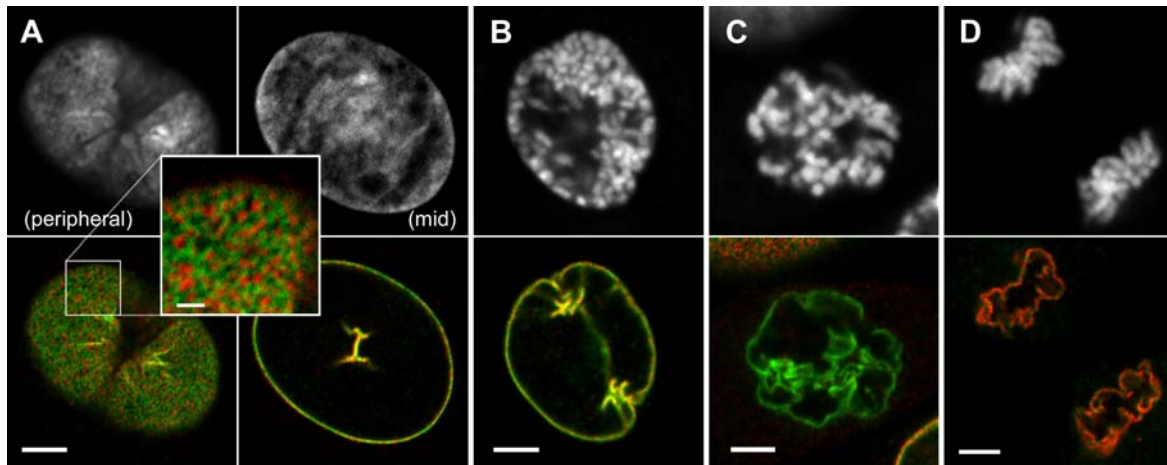


Figure 25. Lamin B and nuclear pore complex (NPC) in mitotic cells. Synchronized SH-EP cells were stained with antibodies against lamin B (lower panel, green) and NPC (mAb 414, red). DNA was stained with TOTO-3 (upper panel). (A) Early prophase SH-EP cell nucleus with typical indentation and beginning chromatin condensation. In the peripheral section the staining of lamin B shows a discontinuous meshwork pattern while NPC shows distinct dots of roughly 200 nm size; both signals are mutually exclusive (inset, bar: 1 nm). In the mid section both fluorochromes appear to colocalize, due to the limited z-resolution of the CLSM. NPC are also present with the invagination. (B) Prophase nucleus displays both epitopes still present on the nuclear envelope. (C) During prometaphase NPC disassembles while lamin B is still associated with the disrupting envelope. (D) In contrast, NPC reassembles already in late telophase, preceding reformation of the lamina in telophase (compare Figure 24 I). Bars: 5 μ m (inset 1 μ m).

Lamin is associated with mid-to-late replicating chromatin

It is generally accepted that mid-to-late replicating chromatin is mainly located at the nuclear periphery and around nucleoli. However, a small subset of chromatin domains is often seen in the nuclear interior at some distance to the perinucleolar space as well as to the nuclear periphery. Although an association of mid-to-late replicating chromatin domains with the nuclear lamina is plausible, a detailed analysis is lacking, especially in light of a possibly more convoluted nuclear lamina. Analysis of single- and two-color direct-labeled SH-EP cell nuclei that were formaldehyde-fixed and immunostained with lamin B revealed a close association of mid-to-late replicating chromatin domains. In contrast, early replication chromatin domains showed virtually no contact to the periphery (Figure 26 A-C). Intriguingly, many (although not all) intranuclear mid-to-late replicating domains (that were also not part of the perinucleolar compartment) were found in close proximity with invaginations and transnuclear tube-like structures of the nuclear lamina (Figure 26 C, E, F). This observation implicates that a subset of the “peripheral” chromatin compartment can be located in the nuclear interior when associated with a lamin invagination.

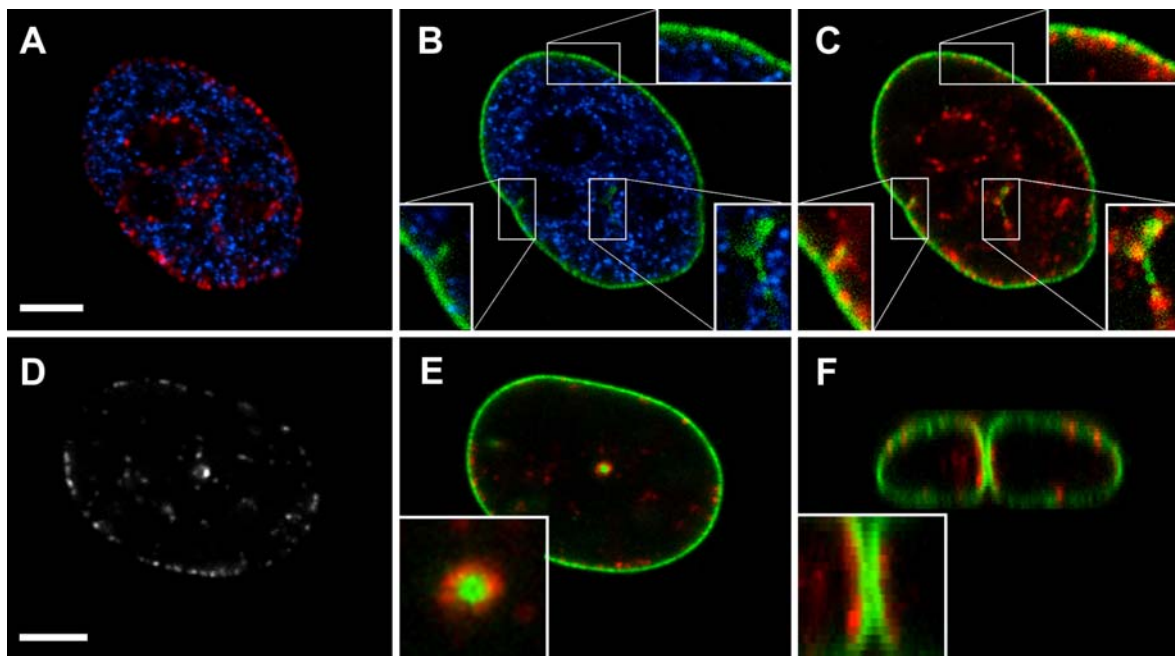


Figure 26. Association of mid-to-late replicating chromatin domains with the nuclear lamina. (A) Confocal mid-section through the nucleus of a SH-EP cell fixed 20 h after direct two-color labeling of DNA with Cy3- and Cy5-dUTP at early and mid-S-phase, respectively, shows typical early- (blue) and mid-to-late replicated chromatin (red). (B and C) Confocal mid section through the same cell nucleus shown in A immunostained with lamin B (green). A comparison of B and C shows that mid-to-late replicating ~1-Mb chromatin domains (C, red) are closely associated with the peripheral lamina but also with invaginations extending into the nuclear interior, in contrast to the early-replicating domains (B, blue). (D) Confocal mid-section of a SH-EP cell nucleus 3 days after direct labeling with Cy3-dUTP displaying a segregated mid-to-late replication pattern. (E and F) Immunostaining of lamin B (green) reveals a transnuclear tubular structure of the nuclear lamina. The confocal mid-section in E and z-projection in F demonstrate a clear association of the labeled chromatin (red) with the lamin-tube. Bar: 5 μ m.

Chromatin movement may be influenced by movements of lamin invaginations

A dynamic behavior of lamin invagination has been demonstrated in live cell observations of CHO cells expressing lamin A-GFP and lamin C-GFP (Broers *et al.*, 1999). To test if the observed movements may also involve the movement of possibly attached mid-to-late replicating chromatin domains, lamin C-GFP expressing cells were *in vivo* replication labeled with Cy3-dUTP. Following several cell divisions confocal time-series were recorded. The time series of such a nucleus, shown in Figure 27, revealed concomitant movements of a prominent tubular lamin structure and an associated mid-late replicating chromatin domain. This initial experiment clearly supports a physical attachment of specific chromosomal segments and indicates the possibility of a lamin driven directed movement of chromatin domains.

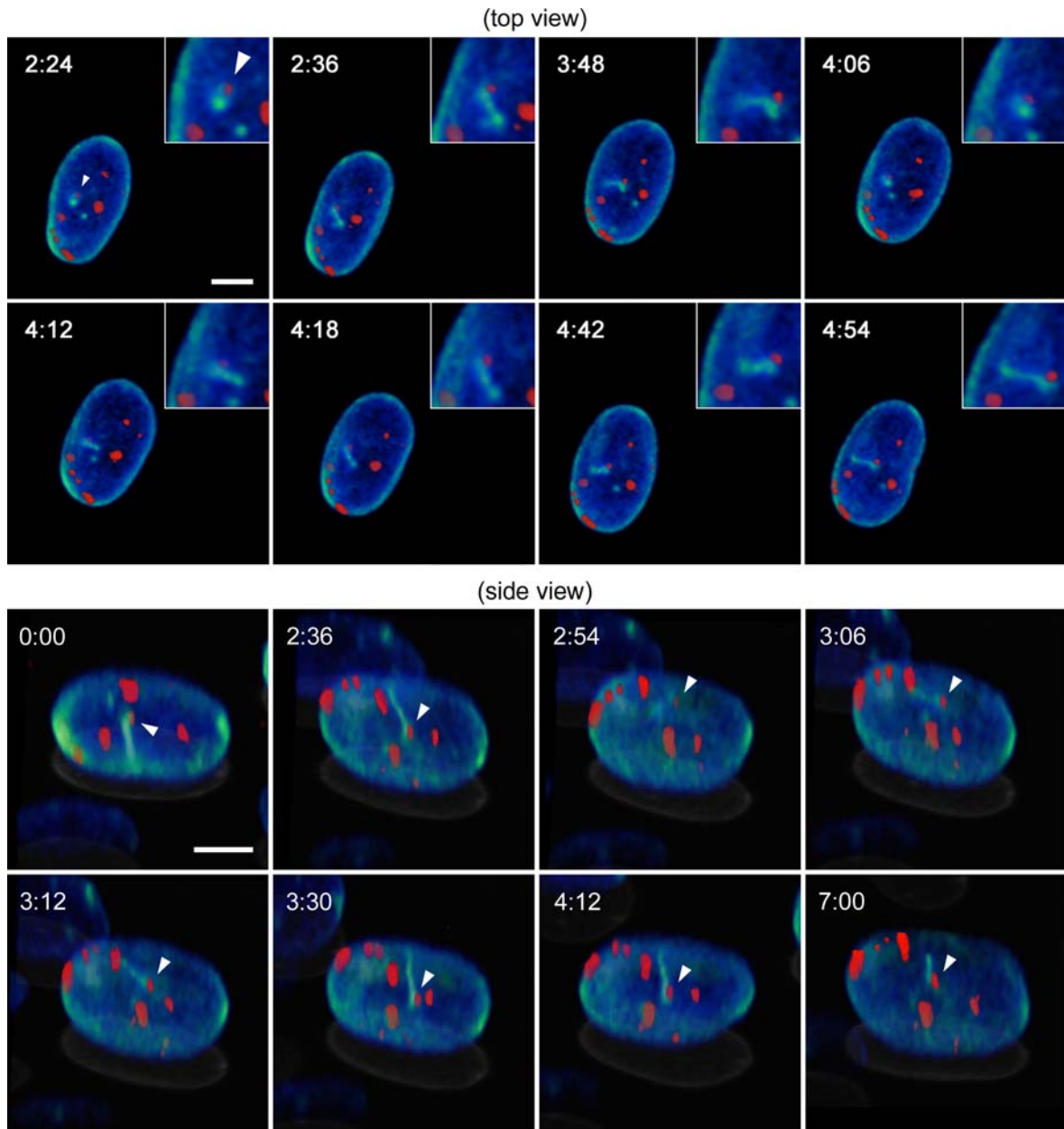


Figure 27. Synchronous movements of lamin invagination and associated mid-to-late replicating chromatin domain. Confocal time series of a CHO cell expressing lamin C-GFP that was scratch replication labeled with Cy3-dUTP 4 hours after release from aphidicolin block. Observation started several days after the labeling event. The series was recorded at 6 min time intervals for a total of 7 hours. 3D-volume renderings of selected time-points are shown (upper panel, top view and lower panel, side view). During the first two hours the nucleus performed a ~180° nuclear rotation around the z-axis (compare time point 0:00 and 2:36 in lower panel, see also supplemental video 9). Mid-late replicating chromatin domains of segregated CTs are found to be associated to the nuclear lamina. One single, more internally located chromatin domain (indicated by arrowhead) shows a clear association to a prominent lamin invagination and synchronous movements can be observed of this particular domain together with the invagination indicating a physical attachment. In contrast, the other domains appear to be more stable as they do not change their relative positions. (Bar: 5 μ m)

Lamin disruption on chromatin labeled BHK-21 cells

Initial lamin A knock-down experiments by microinjection of a dominant-negative mutant lamin protein (Δ NLA) were performed on *in vivo* replication labeled BHK-21 fibroblast cells. The objective of this approach was to investigate whether peripheral mid-late replicating chromatin loses its association to the nuclear envelope upon lamin disruption.

BHK cell nuclei are normally characterized by a rather regular, elongated shape. In a non-synchronized culture, numerous cells showed intensely stained internal lamin foci that did not contact the peripheral lamin rim. Invaginations of the nuclear lamina were also found in some nuclei (predominantly in G1); however, invaginations were less frequent than in SH-EP or CHO cell nuclei. Replication labeled nuclei display the typical pattern described for other mammalian cells (data not shown).

For the disruption experiments, BHK-21 cells were grown on gridded coverslips until 30-40% confluence was reached and subsequently scratch labeled with Cy3-dUTP. 1-2 hours later Δ NLA protein (1 mg/ml in PBS) was microinjected into the cytoplasm of some 10-20 cells. Alternatively, SRL with Cy3-dUTP was performed on subconfluent grown BHK-21 cells on conventional coverslips and cells were harvested and replated on gridded coverslips 3h after labeling and microinjected approximately 18 h later. The cells were fixed with 4% formaldehyde 1.5 h or 2.5 h after microinjection of Δ NLA protein and Lamin A/C was immunodetected. Simultaneously, either lamin B was detected or DNA staining was performed with TOTO-3.

The nuclei of injected cells showed a variable degree of deformation, probably dependent on the dose of mutant protein. In heavily deformed nuclei, lamin A/C aggregated into big foci that were either compacted or ring shaped. In a less disrupted state these lamin foci were still attached to the peripheral rim. In a more advanced state of disruption the rim became less and less visible and lamin aggregates were found inside the nucleoplasm apparently loosing contact to the periphery. Nuclei with highly disrupted lamina adopted remarkably flat and lobulated shapes, underlining the importance of the lamin filament meshwork for the nuclear shape and rigidity. The extension in z-axis reduces from ~ 6 - 8 μ m in normal state to < 3 μ m in nuclei with completely disrupted lamina (Figure 28, z-projections). Nuclei of injected cells also showed a general increase of internal lamin A/C staining (excluding nucleoli), probably due to an excess of mutant lamin A that has been imported into the nucleoplasm.

Concomitant with the deformation of the nuclear shape, nucleoli also acquire a more irregular shape than in undisrupted state (Figure 28 A). This indicates that the disruption is not restricted to the peripheral lamina but may also impact internal structures, corroborating the view of functionally and structurally relevant internal lamin fraction (Goldman *et al.*, 2002).

Both A-type and B-type lamins were affected by the mutant lamin A protein, however, simultaneously immunostained nuclei did not show a complete colocalisation of both lamins through all stages of disruption. In particular, nuclei that were in an earlier state of disruption revealed differences in the distribution of lamin A/C and lamin B. For example, the nucleus shown in Figure 29 A displays a prominent enfolding of lamin B which is devoid of lamin A/C. Other cells (Figure 29 B, C) were still showing a continuous lamin B layer whereas the lamin A/C rim was partially dissolved or had formed internal aggregates.

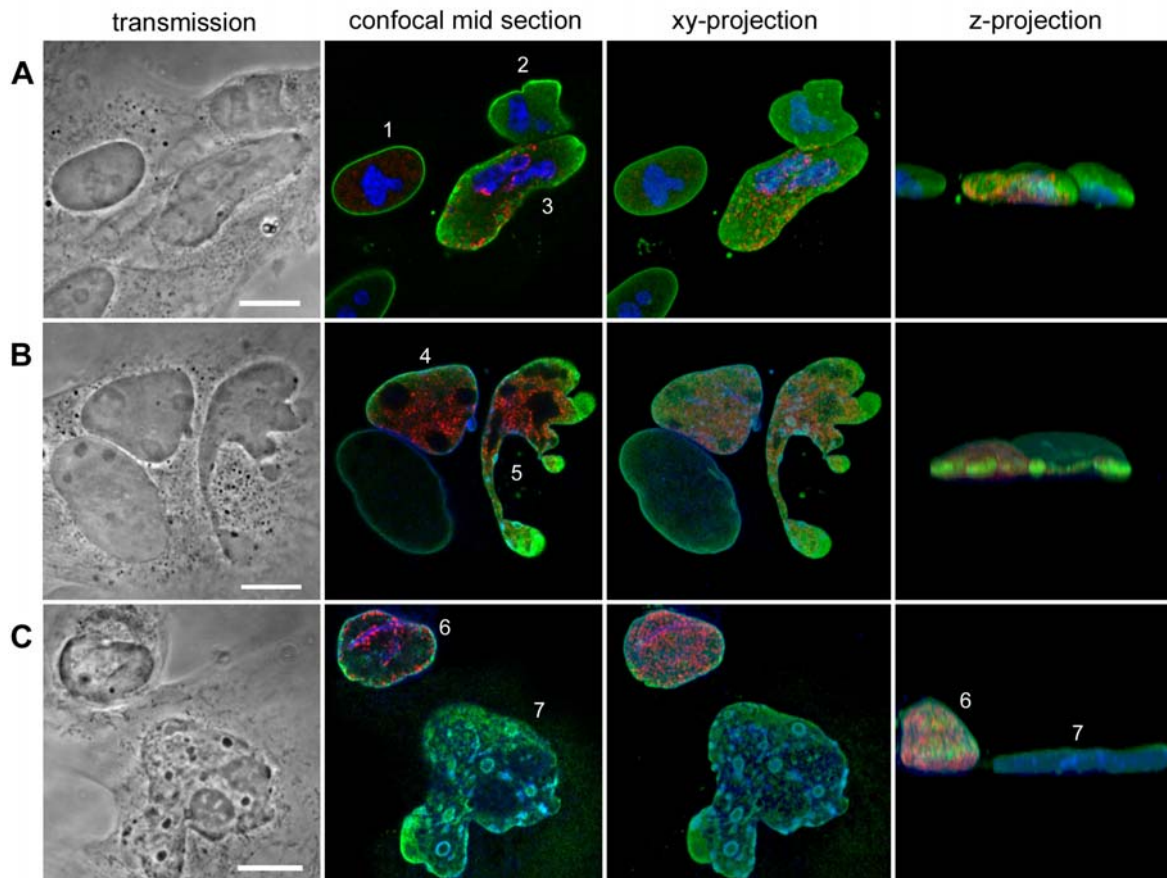


Figure 28. Dramatic changes of nuclear morphology accompany disruption of the lamina. BHK-21 cells (scratch replication labeled with Cy3-dUTP, red) were microinjected with mutant Δ NLA protein and formaldehyde-fixed 2.5 h later. (A) Nuclei with lamin A/C immunostained (green) in combination with nucleic acid counterstaining by TOTO-3 (blue). Nucleoli are intensely stained as no RNase treatment was performed. Disruption of the lamina is accompanied by deformation of nucleoli. (B, C) Simultaneous immunostaining of lamin A/C (green) and lamin B (blue). Generally, various degrees of disruption can be found amongst injected nuclei. Nuclei with incomplete disruption still show a strong rim staining but a beginning deformation of nuclear shape (nuclei 2, 4, 6). With progressing disruption nuclei may display highly lobulated shapes and an increase in internal lamin staining (3, 5). Heavily disrupted nuclei (7) are characterized by an extremely flat shape and a high number of focal or vesicle-like internal lamin structures, also visible in phase-contrast transmission image.

However, in completely disrupted cells lamin B again seemed to colocalize with lamin A/C. No apparent association of mid-late replicating chromatin with internal lamin A/C aggregates was detected in disrupted nuclei. In contrast, partially disrupted cells, which exhibited a differential pattern of both lamin types, often showed a striking association of mid-late replicating chromatin and lamin B. (Figure 29 B, C). This finding indicates that mid-late replicating chromatin might have a higher tendency to associate with lamin B (or associated proteins LAP2 or LBR) rather than with lamin A/C.

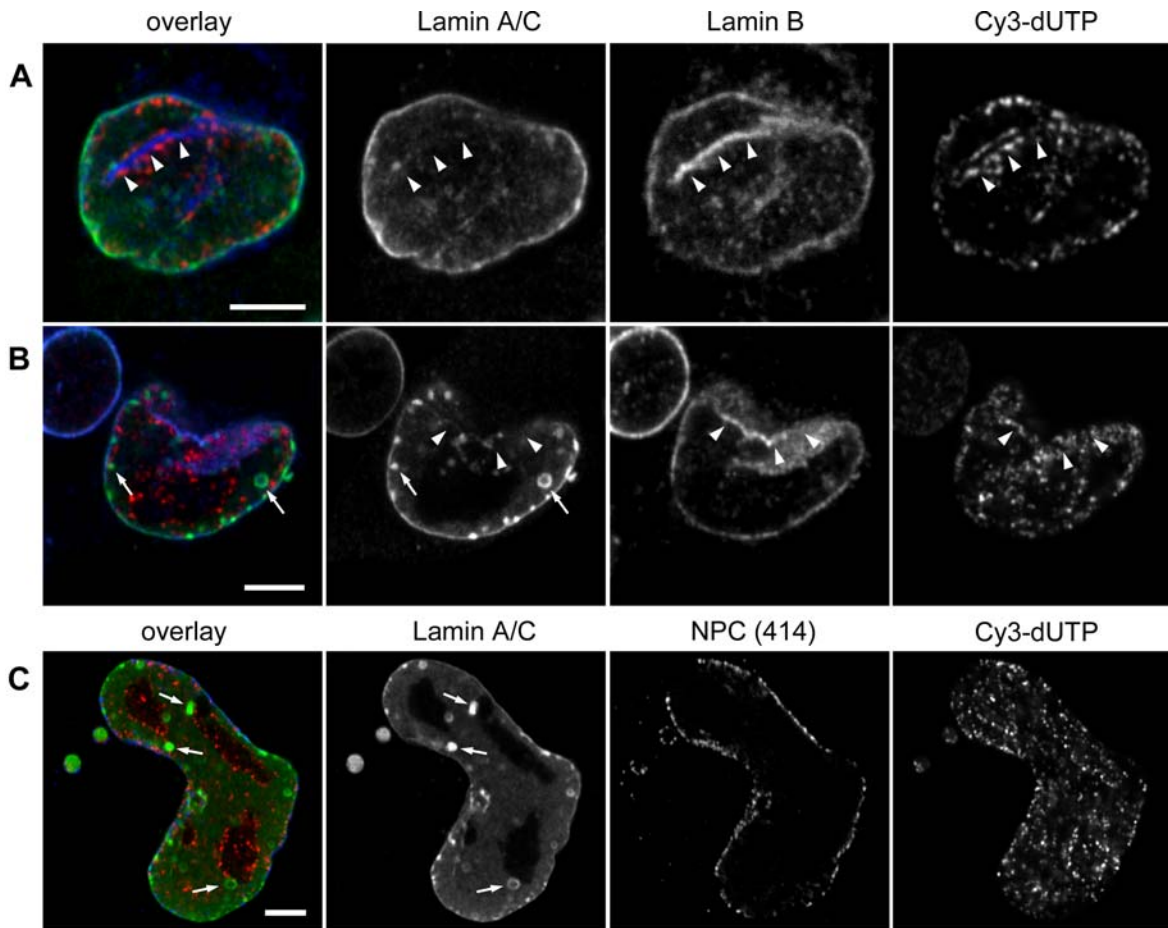


Figure 29. Detailed view of disrupted replication labeled BHK cell nuclei. (A, B) Simultaneous immunodetection of lamin A/C (green) and lamin B (blue) was performed on cells in early stage of disruption. Confocal mid-section reveals only partial overlap of both epitopes. Mid-to-late replicating chromatin domains preferentially associate with structures containing only lamin B (arrowheads) whereas internal lamin A/C aggregates (arrows in B and C) are apparently not associated with labeled chromatin domains. (C) Simultaneous immunostaining with NPC specific antibodies demonstrates that the nuclear membrane maintains a peripheral location whereas lamin A has dissociated and formed internal aggregates (arrows). Hence, NPC is a useful marker of the nuclear membrane during disruption. Bar: 5 μ m.

Simultaneous immunodetection of lamin associated proteins, such as LBR and LAP2, are indicated to test for specific association with chromatin after disruption, which could point to a possible influence on chromatin organization. Moreover, the use of a mutant lamin B (Δ NLB instead of Δ NLA) could provide further insight into specific interactions of different types of lamins with chromatin.

The preliminary experiments described above provided the basis for future live cell experiments including quantitative motion analysis, which will then make it possible to track the conceivable relocalization of individual chromatin domains in different states of lamin disruption and, moreover, to test for changes in mobility and confinements upon lamin disruption.

4.4 Cell cycle dependent redistribution of centromeres

The experiments described in chapter 4.2 demonstrated a high degree of stability of CTs arrangements from mid G1 to late G2. However, this does not exclude a higher mobility of some chromosome subregions. Mobility of gene clusters upon transcriptional activation for example, has been reported in mammalian cells (Volpi *et al.*, 2000; Williams *et al.*, 2002). Several studies reported centromere repositioning during the cell cycle, however, with controversial results (Bartholdi, 1991; Ferguson and Ward, 1992; Weimer *et al.*, 1992; Vourc'h *et al.*, 1993; Hulspas *et al.*, 1994).

Centromeres were detected using human anti-CREST serum (obtained from patients suffering from progressive systemic sclerodermia) reacting against kinetochore proteins. In eight analyzed G2 cells and one S-phase cell, the centromeres were positioned preferentially at the nuclear periphery with the exception of 3-5 internal centromeres that were mostly associated with a nucleolus. In all nine cells, a striking asymmetry of centromere distribution was observed, with 15-17 centromeres on one side (either top or bottom) and 24-28 centromeres on the opposite side. When entering prophase, the centromeres lost their peripheral position as chromosomes condensed (Figure 30). Although chromatin condensation generally seemed to be directed towards the lamina (compare Figure 24) the centromeric chromatin at this stage is obviously not strictly associated with the nuclear periphery. With the progressive assembly of chromosomes in the metaphase plate, the centromeres took a position in the center of the metaphase plate forming a ring around the spindle. In anaphase the centromeres were further compacted at the poles of the spindle. This polarization persisted also in telophase but gradually dissolved with transition to early G1. In G1 cells, centromeres were either positioned at the periphery of one side or in the nuclear interior. The clear “bipolar” distribution (described above for G2 nuclei) was established later in early S phase (Figure 30 B). These findings indicate a directed movement of a fraction of centromeres from telophase until late G1. With the exception of a few, mainly nucleolus associated centromeres, a strictly peripheral position might be fully established in late G1/early S-phase, which is then maintained during S- and G2 phase.

A dedicated study has been performed in collaboration with Irina Solovei and co-workers that included detailed statistical evaluations of centromere rearrangements during cell cycle in SH-EP cells and three other cell lines (Solovei *et al.*, 2003).

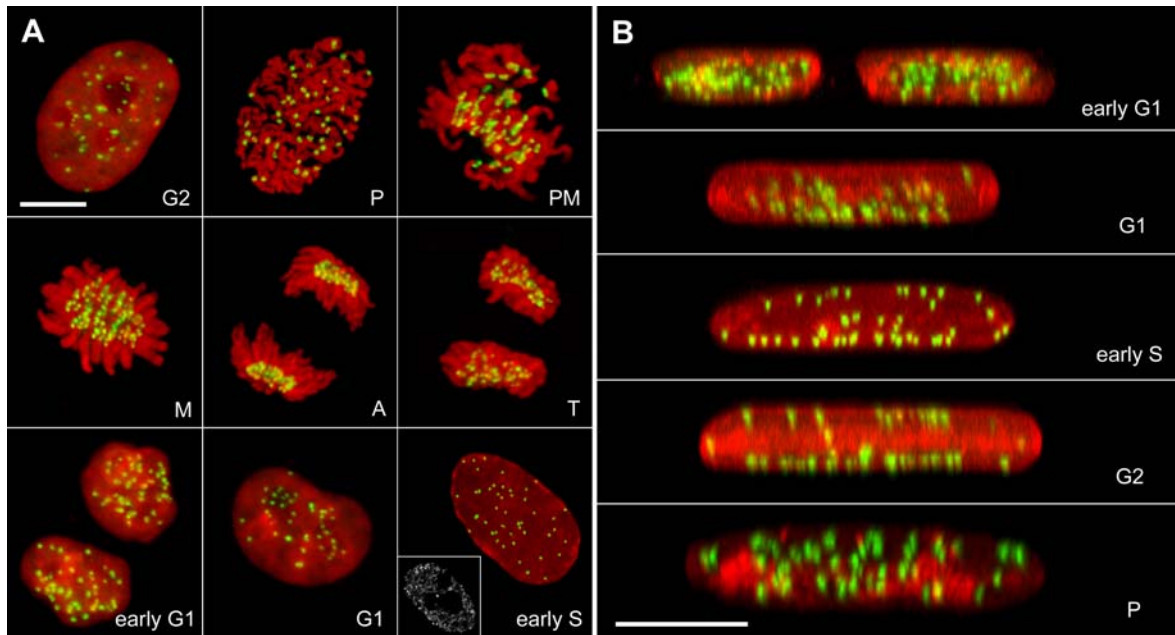


Figure 30. Centromere distribution in SH-EP N14 cells during cell cycle. To obtain mitotic cells including late G2 and early G1 nuclei, synchronized cells were fixed in formaldehyde 8.5 hours after release. For the detection of S-phase nuclei, unsynchronized cells were replication labelled with BrdU before fixation. Centromeres were detected using human anti-CREST serum and FITC coupled secondary antibodies (green); DNA was counterstained with TOTO-3 (red). (A) 3D-projection (xy) of nuclei from different cell cycle stages. P: prophase; PM: prometaphase; M: metaphase; A: anaphase; T: telophase. Inset in “early S” shows the corresponding replication pattern. (B) Z-projection of selected nuclei displayed in A. Bar: 10 µm.

5. Discussion

Two major questions were addressed in this thesis. Firstly, is there a global inheritance of chromosome territory neighborhoods in mammalian cell nuclei or can chromosomes acquire new neighborhoods, and if so, at which stage of the cell cycle do positional changes take place? Secondly, does functionally distinct chromatin of the early and mid-to-late replicating compartment exhibit different dynamic properties in relation to other nuclear structures, in particular, to the nuclear envelope, and how does the nuclear lamina contribute to a nuclear higher order structure? To address these questions, novel *in vivo* labeling strategies were developed and a live cell observation setup was established that facilitated semi-automated long-term 4D confocal microscopy.

5.1 Chromosome dynamics in interphase nuclei

In previous studies of chromatin dynamics in mammalian cells, live cell observations were restricted to a limited time window ranging from a few minutes up to five hours. These studies could not exclude the possibility of slow “drifting” movements of chromosome territories during interphase that could result in major changes of the chromosome territory order from early G1 to late G2.

With the long-term *in vivo* study of Cy3- or Cy5-labeled CTs presented in this work the observation periods could be extended significantly to cover a complete cell cycle of 18 hours or more. Quantitative distance measurements over time showed that CTs were confined within a radius of about 0.5 - 1 µm from mid G1 to late G2, which is in agreement with earlier studies on chromatin dynamics in mammalian cells (Shelby *et al.*, 1996; Abney *et al.*, 1997; Zink and Cremer, 1998; Bornfleth *et al.*, 1999; Chubb *et al.*, 2002; Lucas and Cervantes, 2002). However, more extended positional changes (occasionally exceeding 4 µm) were observed during the first 2 - 3 hours after mitosis. This increased mobility cannot simply be attributed to the rapid volume increase during telophase-G1-transition as the data were corrected for this effect. Moreover, distances between different CTs occasionally became smaller during telophase/early G1, indicating a directed relocalization of CTs. Heterochromatic associations involving large-scale reorganization of chromosomes during G1 were previously described in *Drosophila* larval nuclei (Csink and Henikoff, 1998). In a study of painted CTs in fixed human diploid fibroblast nuclei Bridger *et al.* (2000) found that the final locations of CT#18 were established during the first 2 - 4 hours of G1. Evidence for an increased mobility during early G1 compared to later interphase stages was also presented for GFP-tagged centromeres in living HeLa cells (Shelby *et al.*, 1996) and for a GFP-tagged heterochromatic chromosomal site in CHO cells (Tumbar and Belmont, 2001). Together, these results support the idea of a time window of increased chromatin mobility during early G1 until structural components, essential for the stability of CT arrangements are fully established.

More extensive movements during early G1 may also reflect a necessity of CTs to home in to their final nuclear locations and to establish a “polarized” orientation (Sadoni *et al.*, 1999). In all normal and malignant mammalian cell types studied so far, gene-poor chromatin, which replicates in mid S, is preferentially arranged in the nuclear periphery and around the nucleoli, whereas gene-dense, transcriptionally active early replicating chromatin is located in a zone which expands between these two transcriptionally silent compartments (Dimitrova and Berezney, 2002). Interestingly, it was possible to show that replication-timing program is also established in early G1, 1-2 hours after metaphase concomitant with repositioning of chromosomal domains (Dimitrova and Gilbert, 1999; Li *et al.*, 2001). In these studies, CHO cell nuclei isolated at different stages of cell cycle were incubated in a cell-free replication competent *Xenopus* egg extract. The proper spacio-temporal order of replicated chromatin domains was found when nuclei were isolated in late G1, a random order of replication domains was, however, observed when nuclei were isolated in early G1.

A comparison of the data presented here with other published studies of chromatin movements in nuclei of living cells should be performed with caution: The long-term measurements of constrained movements of whole CTs performed in the present study with sampling intervals ranging from 6 to 30 min for total observation periods of many hours cannot be directly compared with movements of small chromatin sites analyzed in other cell systems using intervals of minutes or seconds for much shorter evaluation periods. For *lac*-operator repeats integrated into different chromosomal sites of human HT-1080 cells, Chubb *et al.* (2002) found that the maximum range of movements depend on the subnuclear localization totaling 0.9 μm for a site located in the nuclear periphery and 1.5 μm for a nucleoplasmic site. Diffusion coefficients were in the range of $10^{-4} \mu\text{m}^2/\text{s}$ or lower. In HeLa cell nuclei initial evaluations of diffusion coefficients for ~1 Mb chromatin domains and entire CTs recorded with sampling intervals of 20 min imply values in the order of $10^{-5} \mu\text{m}^2/\text{s}$ (Bornfleth *et al.*, 1999; Edelmann *et al.*, 2001).

In contrast to mammalian cells, a higher mobility with diffusion coefficients in the order of 10^{-3} to $10^{-2} \mu\text{m}^2/\text{s}$ was reported for fluorescence tagged chromosomal sites in *Drosophila* and yeast (for reviews see Gasser, 2002; Marshall, 2002). In *Drosophila* early embryos, confinement radii $\leq 0.9 \mu\text{m}$ were reported for a heterochromatic site (Marshall *et al.*, 1997). In *Drosophila* spermatocyte nuclei, Vazquez *et al.* (2001) described long-range motions of integrated *lac*-operator sites to be confined to a radius of 3 μm in mid G2 and ~0.3 μm in late G2 nuclei. In yeast, the movements of centromeric and telomeric sites were confined to radii $\leq 0.3 \mu\text{m}$ independent of the cell cycle. In contrast, chromosomal regions close to transcribed genes were found to be less constrained in G1 with a radius of 0.7 μm , showing particularly fast movements of up to 0.5 μm within 10 sec. In S-phase, these movements became constrained to a radius $\leq 0.3 \mu\text{m}$ due to a replication dependent mechanism (Heun *et al.*, 2001). Notably, in this study on HeLa cells, no changes in the confinement of CTs during S- and G2-phase were observed.

To interpret higher order chromatin dynamics observed in human, *Drosophila* and yeast cells, differences in size of their chromosomes (human: 50-250 Mb; *Drosophila*: 4.3-70 Mb; yeast: 0.2 - 1.5 Mb) and genome structure have to be considered. For example, the fraction of transcriptionally active chromatin in

yeast amounts to ~90% compared to ~10% in humans. This may correspond to differences in chromatin compaction and rigidity / flexibility of higher order chromatin structures. A “free” yeast chromosome of 1 Mb may behave differently to a human ~1 Mb chromatin domain which is part of a much larger CT.

It was shown that motility of a measured target depends on its chromosomal localization (Heun *et al.*, 2001) and its nuclear position (Chubb *et al.*, 2002). The latter study reported lower chromatin mobility near the nucleoli and the nuclear periphery indicating a function of these structures in maintaining the 3D arrangements of chromatin. While the lamina-coated nuclear envelope is a proven site for chromatin attachments (see below), it is not clear whether the tethering of chromatin to a matrix of branched matrix core filaments plays a major role in constraining chromatin movements (Ma *et al.*, 1999; Cremer *et al.*, 2000). Alternatively, the stability of large-scale chromatin arrangements may also be maintained without the help of an internal nuclear matrix. Movements of a given CT could become constrained mainly by its neighboring CTs.

Major CT movements were observed neither in long term live cell observations after *in vivo* labeling / segregation in normal diploid fibroblast nor in SH-EP neuroblastoma cells (data not shown) or mouse myoblasts (A. Brero, personal communication) indicating that the large-scale stability of CT order seen in HeLa cell nuclei probably illustrates a general feature of mammalian interphase nuclei. Such stability does not exclude more extended, rapid and possibly directed movements of subchromosomal regions and genes. Initial experiments on the centromere distribution in neuroblastoma cell nuclei at different stages of cell cycle presented in this work also point to an increased mobility of centromeric chromatin. Consistently, this motion is mostly restricted to G1 when most centromeres assume a position at the nuclear periphery.

Functional implications of changes in higher order chromatin architecture are strongly supported by the finding that transcriptional activation / gene silencing is correlated with the repositioning of genes and gene clusters (for review see Baxter *et al.*, 2002, see also Figure 1 and references in the corresponding legend).

5.2 Changes of CT order from one cell cycle to the next

Similarities of CT arrangements in daughter nuclei as well as changes of chromosome arrangements during mitosis were analyzed both by tracking of unbleached chromatin regions through mitosis and by chromosome painting of 2-cell and 4-cell HeLa cell clones. Initially, histone H2B-GFP-tagged chromatin was photobleached leaving a coherent segment of unbleached chromatin at one nuclear pole of late S or G2 nuclei. The unbleached zones retained their location and shape until the onset of mitosis. This further confirms the stability of large-scale interphase chromatin arrangement and is consistent with results from Abney *et al.* (1997) who demonstrated the local persistence of bleached spots in dihydroethidium-stained chromatin of mammalian cells over at least one hour.

In prophase, the unbleached chromatin locally condensed into several unbleached chromosome segments. In daughter nuclei, these segments were recognized as locally decondensed chromatin patches. The observation that locally constrained chromatin movements are sufficient for the transition of interphase into mitotic chromosomes and vice versa are consistent with findings reported by other groups (Manders *et al.*, 1999; Lemke *et al.*, 2002).

In metaphase plates, unbleached chromosomes were often found clustered, however 13 of 22 analyzed metaphase plates also showed unbleached chromosomes relocated to remote sites. The originating daughter nuclei typically also showed distantly located patches of unbleached chromatin demonstrating the occurrence of major changes in the chromosome arrangement from one cell cycle to the next. According to Boveri's hypothesis, this suggests that rearrangement of chromosomal positions can occur during prometaphase congression when chromosomes are released from the constraints of the nuclear envelope after break down of the lamina and concomitantly become attached to the microtubules of the mitotic spindle and pulled to the equatorial plate. The opportunity of positional changes does not exclude a higher probability of neighbored prophase chromosomes becoming attached by nearby spindle microtubules and being pulled to nearby positions in the metaphase plate (Figure 31 A).

As a result of the perfectly symmetrical chromatid movements during anaphase/telophase one would expect to see daughter nuclei with a translational or mirror-like symmetry in their CT arrangements. In both chromatin bleaching and 3D-FISH experiments pairs of daughter nuclei did indeed often show a notable symmetry of the labeled higher order chromatin structures, however, this symmetry was never perfect and in few cases pairs without any obvious translational or mirror like symmetry were noted. Failure to achieve a symmetrical CT distribution may result from an imperfect symmetry of chromatid movements during anaphase. The finding that CT movements were significantly more pronounced in nuclei studied in early G1 compared to nuclei followed from mid G1 to late G2 provides an additional possibility for movements, which disturb this symmetry.

A comparison of randomly selected pairs of daughter nuclei showed clearly diverging arrangements of painted CTs. 3D nuclear reconstructions from 4-cell clones demonstrated major differences already in the granddaughters of a cloned cell. In conclusion, the variability of CT arrangements in HeLa cell cultures (data not shown) is caused by sometimes drastic changes of CT neighborhoods from one cell cycle to the next and does not necessarily depend on the accumulation of small positional changes during many cell generations.

Arguments against global inheritance of chromosomal order

The presented data demonstrates that mitosis is of major importance in explaining the variability of CT arrangements in interphase nuclei and is thus in conflict with earlier findings by Nagele *et al.* (1995; 1999) which claimed a highly ordered reproducible arrangement of chromosomes with two antiparallel haploid sets in prometaphase rosettes and interphase nuclei of human fibroblasts and HeLa cells. It also substantially conflicts with a recent publication by Gerlich *et al.* (2003) who described a global inheritance of chromosome positions through mitosis in normal rat kidney (NRK) cells. These authors bleached half of the nuclear volume in early prophase of histone H2B-YFP and H2B-CFP co-expressing cells and followed bleached and unbleached chromatin into next G1. In metaphase plates, a separation of bleached and unbleached chromatin was found when the bleaching axis in prophase was parallel to the spindle, however, intermixing was noted when the bleaching axis was perpendicular to the spindle. On the other hand, a separation of unbleached and bleached chromatin into two halves was observed in telophase/early G1 irrespective of the situation in the metaphase plate (Figure 31 B and C). Furthermore, the tracking of about six EGFP-CENP-A

tagged centromeres that could be followed unambiguously from prophase to metaphase, led to the conclusion that only linear movements take place during this period. Likewise, the tracking of ~10 centromeres during telophase/early G1 expansion inferred that exclusively isometric chromosome movements occur in this period excluding positional changes. Gerlich *et al.* proposed a model in which differences in the timing of sister chromatid separation, which is genetically controlled by differences in centromere sequences, causes reestablishment of the global chromosomal order in anaphase. This model creates a testable prediction insofar as the resulting daughter nuclei should display a polarization, with the early dividing chromosomes at the distal end and the late dividing chromosomes at the end near to the cleavage furrow. This implies that (at least some) homologue chromosomes should be in closer proximity on either side than expected from a random distribution. Such a non-random distribution of homologues, however, is in contrast to several studies measuring distances and angular separation of homologues in different human cell lines and indicating a random distribution (Lesko *et al.*, 1995; Sun *et al.*, 2000; Cremer *et al.*, 2001; Bolzer, 2002). Moreover, the sister chromatid cohesion model would implicate a mechanism to ensure that in the subsequent mitosis the spindle is formed in the same orientation. A 90° deviation, for instance, would lead to a metaphase plate with a polarity of early and late dividing chromosomes, which would be likely to cause a zipper-like appearance in early anaphase when the first chromatids on one pole start to separate (Figure 31 D).

If the centromere were decisive for the location of chromosomes that display a highly non-random location (like the peripheral location of chromosome 18 and interior location of chromosome 19 in human lymphocyte nuclei) then exchange of centromeres between chromosomes by a translocation should lead to a significant relocation of the respective chromosome segments. However, this is clearly not the case as chromosomal segments of 18 and 19 keep their preferential location irrespective whether they are involved in translocations or not (Croft *et al.*, 1999; Cremer *et al.*, 2003).

A conceivable reason for the observed variances from the data presented here might be the different size of unbleached segments (polar segment of roughly 1/5 to 1/6 of the nuclear volume *versus* one half). Smaller changes may remain unrecognized when larger segments are marked. Different observation times or differences in cell type may also account for some variations.

In support of a cohesion-based mechanism Gerlich *et al.* demonstrated a complete randomization of bleached and unbleached chromosomes (as predicted by computer simulation) after treatment with Hoechst 33258, an intercalating agent that disrupts heterochromatin formation. This observation clearly indicates an important function of heterochromatin in the preservation of some constraints and favors the cohesion model at first glance. The data presented in this work also shows the maintenance of some degree of order (and functional heterochromatin might be one factor among others), but, more importantly, also allows some degree of reshuffling, which will, in any case, lead to major changes after a few rounds of cell division. This rather probabilistic view does not predict a functional relevance of chromosomal neighborhoods as would be implied by a deterministic model of global inheritance. The presented FISH data on HeLa cell clones further support this view. A current study on CT arrangements in cell clones from HeLa and other cell lines, including non-transformed diploid cells, and quantitative evaluations performed in the group of T. Cremer confirmed the rapid

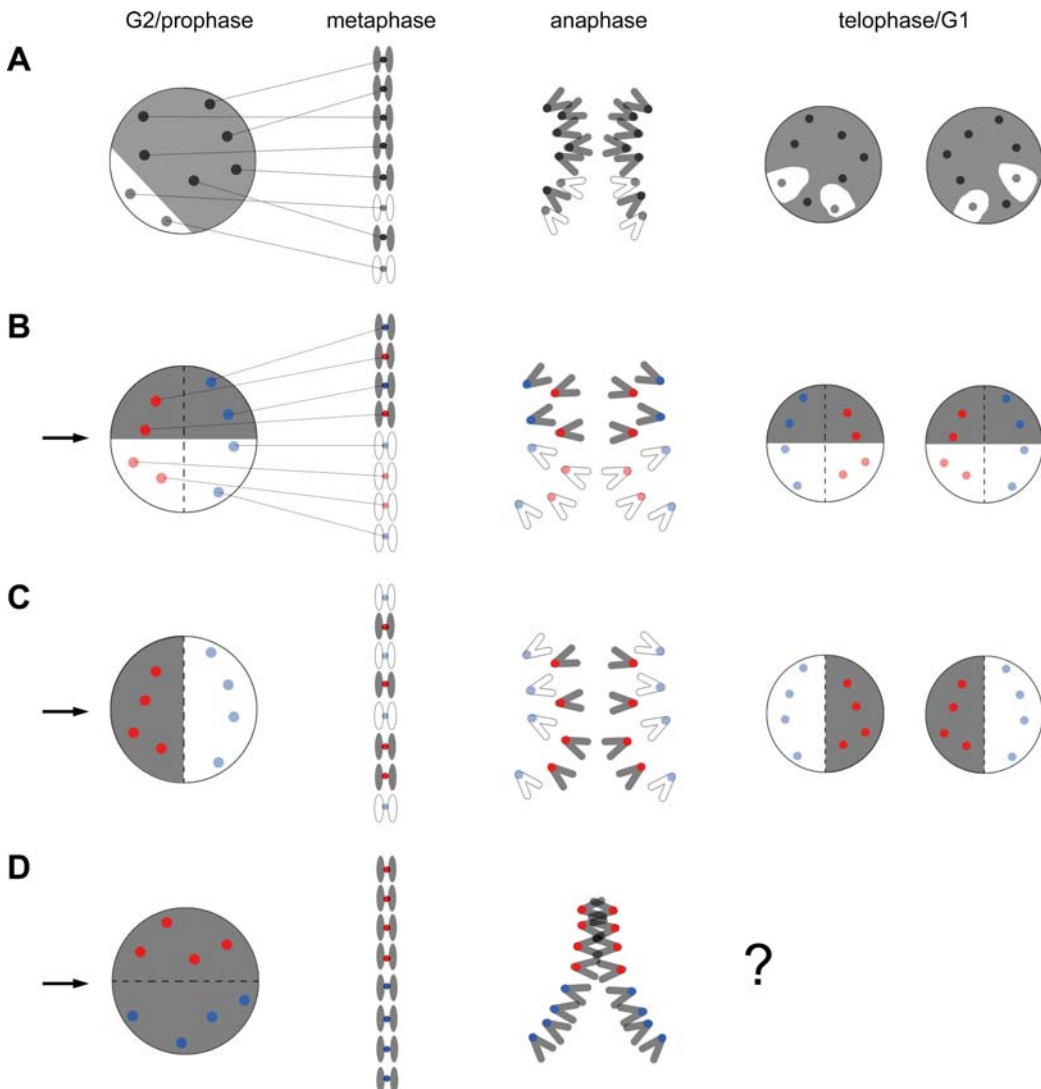


Figure 31. Changes or maintenance of relative chromosomal positions during mitosis? (A) A schematic representation of the bleaching experiments described in this thesis. A segment of unbleached chromatin (light area) is followed through mitosis. Occasional repositioning during transition from prophase to metaphase can lead to changes in chromosomal side-by-side arrangements in the metaphase plate. (Gray lines indicate the trajectories of centromeres indicated by dark dots). Accordingly, patterns of unbleached chromatin in G1 daughter nuclei deviate from the pattern in the mother nucleus. As a consequence of the constrained movements in anaphase, the patterns in the daughter nuclei are largely symmetrical, however additional movements in telophase/early G1 may lead to some distortion of this symmetry. (B, C) Schematic representations of experiments performed by Gerlich *et al.* The bleaching pattern is reestablished in the daughter cells irrespective of whether bleaching is performed parallel (B) or perpendicular (C) to the spindle orientation (indicated by arrow). Movements of chromosomes occur only along the spindle axis, thus the metaphase represents a projection of the prophase nucleus. The global inheritance of chromosomal positions is explained by reproducible differences in separation timing of sister chromatids. Blue dots indicate centromeres of early-separating chromosomes, red of late-separating. As a consequence of this model, mother as well as daughter nuclei should display a polarity of chromosomes with early- and late-separating properties (indicated by the dotted line), which implies a non-random distribution of homologous chromosomes. (D) Hypothetical zipper-like appearance of anaphase rosette if the spindle orientation in the subsequent mitosis would deviate 90° from the previous. (For further details see text.)

perturbation of the chromosome order in the clonal progeny of HeLa cells and other cell types, indicating a universal feature (D. Koehler, personal communication). Such studies will answer the question as to whether the number of cell cycles required to perturb chromosome order to an extent reflecting the variation observed in an entire cell culture depends on the cell type. Notably, Gerlich *et al.* also found exceptions with a less strict transmission of order and they predict that the “order will be diluted further over several cell cycles”. This prediction is somewhat contradictory to the hypothesis of a genetically controlled global inheritance of chromosome positions.

5.3 Nuclear lamina and heterochromatin: an intimate relationship

Several observations support a physical tethering of chromosomes *in vivo* by specific interactions with the nuclear envelope: (1) The condensation of chromatin during prophase is directed towards the nuclear periphery. The attached prophase chromosomes concentrate at the branched invagination of the lamina around the developing spindle. (2) In interphase nuclei, a preferential association of mid-to-late replicating chromatin domains was demonstrated not only to the peripheral lamin rim but also to tubular lamin structures invaginating into the nuclear interior. (3) Initial live cell experiments revealed concomitant movement of lamin invaginations and associated chromatin foci.

Earlier live cell studies reported occasional directed movements of Cy3-dUTP labeled replication foci (Zink *et al.*, 1998; Bornfleth *et al.*, 1999) as well as of centromeres, labeled by GFP-tagged CENP-B (Shelby *et al.*, 1996). In light of the observation described here tethering to invaginating and dynamic structures of the nuclear envelope could provide one possible mechanism for such movements. Increased chromatin movement, as described for CTs and centromeres during telophase and G1, may in part be induced by the concomitant formation of heterochromatin domains comprising the establishment of physical attachments and the retraction of lamin invaginations from an initially more lobulated nuclear envelope to a more regular nuclear shape in later stages.

Nuclear lamins and nuclear envelope associated integral proteins of the inner nuclear membrane have been demonstrated to bind to DNA and chromatin *in vitro* (Wilson, 2000). Despite these biochemical evidences and the fact that numerous studies described interaction in fixed cell studies (Paddy *et al.*, 1990; Belmont *et al.*, 1993; Marshall *et al.*, 1996; Ferreira *et al.*, 1997), it is still unclear at present what the exact nature of this interaction is *in vivo* and how it affects the spatial organization of chromosomes and influences and/or constrains chromatin movements. Generally, it seems more likely that the physiological interaction is mediated by (hetero-)chromatin associated proteins rather than by specific DNA sequences and possibly more than one type of anchoring mechanisms act together.

Chromatin may either be connected to lamin B (Luderus *et al.*, 1992; Moir *et al.*, 1994) or to integral proteins of the nuclear lamina, most prominently LAP2 (Furukawa, 1999; Cai *et al.*, 2001) and lamin B receptor (LBR). The latter has been shown to interact with HP-1 suggesting a possible docking mechanism for peripheral heterochromatin (Pyrpasopoulou *et al.*, 1996; Ye and Worman, 1996). Two recent papers described a direct interaction of different isoforms of HP-1

with pKi-67 (a well-known cell cycle marker with yet unassigned function, see also chapter 3.10) *in vitro* and *in vivo* (Kametaka *et al.*, 2002; Scholzen *et al.*, 2002), and a transient colocalization of HP-1 and pKi-67 in heterochromatin foci was observed during telophase and early G1. During metaphase, HP-1 largely dissociates from chromosomes and reassembles at the polar surfaces of anaphase chromosomes (Kourmouli *et al.*, 2000), whereas pKi-67 remains closely associated to chromosomes during this period (compare Figure 6). It is therefore tempting to speculate that pKi-67 may play a role in reestablishing heterochromatin domains during telophase/early G1 in a coordinated way with HP-1 during the same time that a HP-1 mediated binding of heterochromatin to the forming nuclear envelope via B-type lamins and/or LBR is established. A function for pKi-67 in the reestablishment (but not maintenance) of heterochromatic structures, which is restricted to early G1, could explain the characteristic focal distribution pattern in early G1 in contrast to the nucleolar distribution in later stages (which may either serve a second unknown function or a simple storage function) and complete absence in G0.

Clearly, more data and corresponding quantitative evaluations are required to elucidate whether dynamic movements of the nuclear lamina of intranuclear invagination, in particular, can cause changes in relative chromatin positions. Moreover, it will be interesting to see whether observed cell type specific differences in the number of internal structures have any functional relevance. Most importantly, functional assays, in particular, knock-down studies addressing the *in vivo* function of potential key players (lamin B, LBR, LAP2, HP-1, pKi-67 and others) will provide insight as to how these proteins influence the establishment of higher order chromatin compartments and their radial arrangement in early G1 as well as their preservation in later cell cycle stages. As the nuclear envelope was shown to constrain chromatin motion (Chubb *et al.*, 2002), it will also be interesting to see if general mobility of chromatin domains changes upon disruption of possible tethering mechanism. The preliminary experiments described in the present work, involving mutant lamin A, may provide a guideline, as to how such experiments could be approached.

Order in randomness

Bleaching and FISH experiments infer that chromosomal side-by-side neighborhoods are not determined but highly variable. This is in line with several other studies describing a predominantly random location of chromosomes with respect to each other (Lesko *et al.*, 1995; Habermann *et al.*, 2001; Bolzer, 2002; Cornforth *et al.*, 2002). This does not exclude cell type specific preferential relative positioning of some chromosomes as was shown by Parada *et al.* (2000) who found chromosomes 12, 14 and 15 clustered in nuclei of mouse splenocytes and lymphoblastoma cells. A conceivable factor for such a non-random localization might be that a subset of chromosomes shares common non-chromatin domains or nuclear bodies, such as Cajal- or PML-bodies. Most prominently, NOR bearing acrocentric chromosomes which constitute the nucleolus will probably have a higher preference to be located in proximity of each other (Parada and Misteli, 2002).

The variability of CT order in HeLa cell nuclei begs the question as to whether CTs may be arranged in an entirely random fashion in this cell line, however, this is clearly not the case. In agreement with the non-random radial distribution pattern of the gene-dense CTs #19 and gene-poor CTs #18, which

was demonstrated in diploid nuclei of lymphocytes and lymphoblastoid cells from man and other primates (Croft *et al.*, 1999; Cremer *et al.*, 2001; Tanabe *et al.*, 2002), a more interior location of gene-dense chromosome 19 material was found in HeLa cell nuclei as well as in a number of other normal and cancer cell lines, compared to chromosome 18 material despite of rearrangements involving these chromosomes (Cremer *et al.*, 2003). Gene density has been shown to be the major determinant for the radial position of a chromosome (Boyle *et al.*, 2001).

Another argument in favor of a non-random radial higher order is provided by the two-color direct replication labeling experiments on SH-EP cells described in this work. These experiments demonstrate that the radial arrangement of early and mid-to-late replicating chromatin (which is largely concordant with transcriptionally competent euchromatin and inactive heterochromatin) is stably transmitted over several cell cycles, as was already proposed by earlier studies using halogenated thymidine analogues (Ferreira *et al.*, 1997; Sadoni *et al.*, 1999; Zink *et al.*, 1999). Hence, after transfer through mitosis chromosomes are reformed to build a “polarized” CT arrangement.

A model for a non-random radial CT positioning dependent on nuclear shape

A striking exception of a gene-density related radial arrangement, are human fibroblasts and amniotic fluid cells (epithelial cells derived from the fetal urinary tract, Ochs *et al.*, 1983). Both cell types show a size-correlated distribution with small chromosomes (e.g. chromosomes 18, 19 and Y) predominantly located towards the center, and large chromosomes at the periphery (Sun *et al.*, 2000; Cremer *et al.*, 2001; Bolzer, 2002). How can the differences in distribution be explained?

In mammalian cells, centromeres create a central ring around the spindle axis. Hence, the mass center of small chromosomes in rosette-stages should be located more towards the center. This assumption was confirmed for primary human fibroblasts (Bolzer, 2002). This feature may, therefore, represent a second fundamental motive for chromosomal order which is simply based on physical constraints effective in mitosis when chromosomes are attached to the microtubules of the mitotic spindle.

In early telophase, the chromosomes become surrounded by the newly forming nuclear envelope. At this stage the chromosomes are still condensed and the nuclear envelope is highly lobulated. With chromatin decondensation during telophase and into early G1, heterochromatin compartments become established and comprise chromosome segments of constitutive and/or facultative heterochromatin of one or several chromosomes. This process is likely to be mediated by HP-1 or related protein factors (possibly in a coordinated way with pKi-67), which at the same time establish interactions with the lamina. Such interactions, however, do not occur with transcriptionally active chromatin domains. Chromosomes that contain a larger fraction of sequences with “heterochromatic properties”, which is preset in the mother nucleus and transmitted through mitosis via epigenetic marks such as DNA methylation and/or histone modifications, will have a higher probability of contacting the envelope and establish stronger attachments than chromosomes with a larger transcriptionally active chromatin fraction. Notably, the binding mechanism may be transient (“steady state”), as HP-1 was recently shown to exchange constantly rather than to remain static (Cheutin *et al.*, 2003; Festenstein *et al.*, 2003).

With further chromatin decondensation and beginning transcriptional activity, the nuclear volume increases and the nuclear envelope adopts a more regular shape. In cells with spherical or oval nuclei that have a relatively large z-extension ($> 6 \mu\text{m}$), such as lymphocytes or HeLa cells, the nuclear expansion will pull chromosomes to the periphery that have established a stronger attachment to the lamina. Accordingly, mid-to-late and much of the very late replicating chromatin is preferentially located at the nuclear periphery or at remaining lamin invaginations (“internalized periphery”). In contrast, gene-rich chromosomes with less heterochromatin will be more likely to remain within the interior. An exception may be NOR bearing acrocentric chromosomes 13-15, 21 and 22. NORs from variable chromosomes, each harboring clusters of tandemly repeated rDNA genes, reconstitute nucleoli in a self-organizing manner by polymerase I driven transcription and ribosome biosynthesis. This process may create a constraint for the pericentric heterochromatin proximal to the NORs, which could be competitive to the otherwise preferred peripheral attachment. Alternatively, yet unknown differences in epigenetic marks and/or protein compositions may be specific to the perinucleolar compartment. Either would lead to the typical bipolar (peripheral and perinucleolar) distribution of mid-to-late replicating heterochromatin.

The separation of chromosomes in correlation to gene-content during nuclear expansion and the corresponding non-random radial location of a given chromosome is notably probabilistic in terms of a statistical likelihood. It does not exclude that some gene-rich chromosomes in individual nuclei can incidentally be found in a peripheral position and vice versa. Such a mechanism could also account for the changes in relative CT positions detected in early G1 and the imperfect symmetry of CT arrangements in daughter cell nuclei in HeLa cells. According to this model, the main factor for the establishment of a non-random radial higher order are non-transcribed regions of the genome/heterochromatic sequences while gene-dense chromosomes occupy the remaining space. This would imply that the radial positioning of chromosomes is determined by heterochromatin content rather than by gene density. Also consistent with this view is the observation that the establishment of a peripheral mid-late replication pattern after mitosis is not prevented upon transcriptional repression, which excludes gene expression as driving force (Ferreira *et al.*, 1997).

Some cell types, such as fibroblast or amniotic fluid cells, that feature a strong adherence to the substrate and increased mobility are characterized by having rather flat nuclei with z-extension not exceeding $3-4 \mu\text{m}$. The shape of the nucleus to some extent reflects the shape of the cell, which is in turn influenced by the filaments of the cytoskeleton essentially composed of actin, intermediate filaments (such as vimentin or cytokeratin) and tubulin. These filaments possibly create a tension on the flexible structure of the nucleus causing a flattening. During mitosis the constraint of the cytoskeleton is released. Accordingly, the mitotic cell is elevated from the substrate and adopts a spherical shape. The metaphase rosette is typically oriented perpendicularly, the mitotic spindle parallel to the substrate. In anaphase, the rosette (with radial separation of small and large chromosomes) will either “fall” on the pole side with the bulk of centromeres facing the substrate or on the opposite side with centromeres facing up. As the cytoskeleton becomes reestablished soon after completion of mitosis it creates its constraint on the telophase/early G1 nucleus at the same time as heterochromatin domains and their attachments to the nuclear envelope are established. As the volume increase in early G1 will not lead to a significant increase in z-extension in

flat nuclei, a separation of heterochromatin rich (gene poor) and gene rich chromosomes is impeded and the situation of the metaphase arrangement is preserved into interphase (with small chromosomes clustered in the center). This will not prevent the chromosomes from establishing the same heterochromatin-nuclear envelope associations as in spherical nuclei, the separation might just not become evident. With increasing flatness the surface / volume ratio increases and more chromosomes will in any case contact the periphery on either the top or bottom side. Accordingly, separation of chromosomes 18 and 19 should increase with roundness. A testable prediction of this model is that chromosomes 18 and 19 should become more separated with chromosome 18 in a more peripheral location when the flat fibroblast nuclei become released from the constraints of the cytoskeleton to adopt a spherical shape. This could be achieved by detachment after trypsinization and short reattachment on poly-L-lysine coated coverslips possibly combined with moderate hypotonic treatment. On the other hand, disruption (knock-down) of putative attachment factors (as proposed above) during early G1 may lead to a deviating distribution of the chromosome 18 and 19 in cells with spherical nuclei.

It will also be interesting to determine the difference between peripheral heterochromatin and perinucleolar heterochromatin originating from the pericentric heterochromatin of the NOR bearing acrocentric chromosomes, which does, apparently, not touch the nuclear envelope. This might be either due to different chromatin composition (HP-1?) or by a competitive effect of the nucleolus organization due to rDNA transcription and ribosomal processing. If a competitive effect is causative then disruption of nucleolus assembly in telophase/early G1, for instance by inhibition of polymerase I, should lead to a relocation of the pericentromeric heterochromatin of acrocentric chromosomes to the nuclear periphery.

A future task will be to better characterize early G1 movements possibly by tracking more specific chromatin sites (e.g GFP-tagged *lac*-operon repeats inserted in special chromatin environments). Such experiments should be combined with a simultaneous visualization of the nuclear lamina in a multi-color live cell approach. This will be highly demanding as a higher resolution in space and time will be needed, which was not possible with the currently available equipment. Furthermore, software tools will be required for a feasible and reliable quantitative analysis especially with regard to 3D-tracking analysis (see also 3.16).

5.4 Concluding remarks

There is a convincing line of evidence favoring a higher order genome compartmentalization in the metazoan cell nucleus, both on structural and functional levels, suggesting the importance in gene regulation. Replication labeling reveals fundamental persistent focal substructures. An early replicating internal compartment opposes a later replicating peripheral compartment. Structurally compacted heterochromatin compartments oppose more accessible euchromatic compartments folding into different (presently unknown) higher order structures. On the metaphase chromosome, a linear succession of R- and G/C-bands is seen with differential staining resulting from diverging base pair composition and/or differential packaging of the metaphase chromosome. On the transcription level, mapping of the transcriptosome to chromosomes revealed

clusters of highly expressed genes alternating with transcription-depleted areas. Chromatin structure is fundamentally affected by a network of epigenetic modifications on DNA and histone level, creating neighborhoods of transcriptionally permissive and repressed environments. Finally, insulator/boundary elements may be physical barriers of such domains.

Rigid chromosomal side-by-side neighborhoods seem less likely to be a motive for higher order nuclear architecture. Propagation of a certain degree of side-by-side arrangement through mitosis might to some extent be probable but not functionally necessary and as some more or less extended changes can take place, the neighborhoods will become highly divergent after a few rounds of replication and cell divisions. Hence, positioning of chromosomes follows a probabilistic principle in terms of a statistical likelihood rather than being deterministic. Regarding the surprisingly high mobility of a majority of the nuclear proteins involved gene expression, a functional necessity of chromosomal neighborhoods appears rather unlikely. More important, however, might be the establishment of chromatin environments that either repress or permit transcription regardless of the contributing neighboring chromosomes.

Future studies will have to address following open questions: (1) how does the increasing network of epigenetic modification influence nuclear topology (or vice versa)? (2) Are observed changes in nuclear structure the cause or consequence of gene expression and other nuclear functions? In other words, how do changes in chromatin structure interact with changes in the transcriptional status of a given gene or gene cluster?

High-resolution morphological analyses and exact quantitative evaluations are an important requirement for describing the phenomenology. New *in vivo* labeling tools and advanced microscope systems will facilitate analysis of living cells with enhanced resolution and the tracking of possible relocations of higher order nuclear structures during development and terminal differentiation, which are predicted to accompany a global change of the gene expression pattern. In combination with functional studies employing biochemical and molecular tools, the task in the next years will be to bring the variety of higher order motifs together to obtain an integrated view on nuclear structure and function.

6. References

- Abney, J.R., B. Cutler, M.L. Fillbach, D. Axelrod, and B.A. Scalettar. 1997. Chromatin dynamics in interphase nuclei and its implications for nuclear structure. *J Cell Biol.* 137:1459-68.
- Alberts, B., A. Johnson, J. Lewis, M. Raff, K. Roberts, and P. Walter. 2002. Molecular Biology of the Cell. Garland Science, New York.
- Allison, D.C., and A.L. Nestor. 1999. Evidence for a relatively random array of human chromosomes on the mitotic ring. *J. Cell Biol.* 145:1-14.
- Aten, J.A., P.J. Bakker, J. Stap, G.A. Boschman, and C.H. Veenhof. 1992. DNA double labelling with IdUrd and CldUrd for spatial and temporal analysis of cell proliferation and DNA replication. *Histochem J.* 24:251-9.
- Baltimore, D. 2001. Our genome unveiled. *Nature.* 409:814-6.
- Barlow, R. 1989. Statistics. Wiley, Chichester, UK.
- Bartholdi, M.F. 1991. Nuclear distribution of centromeres during the cell cycle of human diploid fibroblasts. *J Cell Sci.* 99:255-63.
- Baxter, J., M. Merkenschlager, and A.G. Fisher. 2002. Nuclear organisation and gene expression. *Curr Opin Cell Biol.* 14:372-6.
- Beaudouin, J., D. Gerlich, N. Daigle, R. Eils, and J. Ellenberg. 2002. Nuclear envelope breakdown proceeds by microtubule-induced tearing of the lamina. *Cell.* 108:83-96.
- Belmont, A.S. 2001. Visualizing chromosome dynamics with GFP. *Trends Cell Biol.* 11:250-7.
- Belmont, A.S., and K. Bruce. 1994. Visualization of G1 chromosomes: a folded, twisted, supercoiled chromonema model of interphase chromatid structure. *J Cell Biol.* 127:287-302.
- Belmont, A.S., S. Dietzel, A.C. Nye, Y.G. Strukov, and T. Tumbar. 1999. Large-scale chromatin structure and function. *Curr Opin Cell Biol.* 11:307-11.
- Belmont, A.S., Y. Zhai, and A. Thilenius. 1993. Lamin B distribution and association with peripheral chromatin revealed by optical sectioning and electron microscopy tomography. *J Cell Biol.* 123:1671-85.
- Berezney, R., D.D. Dubey, and J.A. Huberman. 2000. Heterogeneity of eukaryotic replicons, replicon clusters, and replication foci. *Chromosoma.* 108:471-84.
- Bernardi, G. 1995. The human genome: organization and evolutionary history. *Annu Rev Genet.* 29:445-76.
- Bland, M. 2000. The analysis of cross-tabulations. In An Introduction to Medical Statistics. Oxford University Press.
- Boggs, B.A., P. Cheung, E. Heard, D.L. Spector, A.C. Chinault, and C.D. Allis. 2002. Differentially methylated forms of histone H3 show unique association patterns with inactive human X chromosomes. *Nat Genet.* 30:73-6.
- Bolzer, A. 2002. Analyse der Chromosomenverteilung in menschlichen Fibroblasten mittels 3D-Vielfarben Fluoreszenz in situ Hybridisierung. In Dissertation an der Fakultät für Biologie der LMU, München.
- Bornfleth, H., P. Edelmann, D. Zink, T. Cremer, and C. Cremer. 1999. Quantitative motion analysis of subchromosomal foci in living cells using four-dimensional microscopy. *Biophys J.* 77:2871-86.
- Boveri, T. 1909. Die Blastomerenkerne von Ascaris megalcephala und die Theorie der Chromosomenindividualität. *Archiv für Zellforschung.* 3:181-268.

- Boyle, S., S. Gilchrist, J.M. Bridger, N.L. Mahy, J.A. Ellis, and W.A. Bickmore. 2001. The spatial organization of human chromosomes within the nuclei of normal and emerin-mutant cells. *Hum Mol Genet.* 10:211-9.
- Bridger, J.M., S. Boyle, I.R. Kill, and W.A. Bickmore. 2000. Re-modelling of nuclear architecture in quiescent and senescent human fibroblasts. *Curr Biol.* 10:149-52.
- Bridger, J.M., H. Herrmann, C. Munkel, and P. Lichter. 1998a. Identification of an interchromosomal compartment by polymerization of nuclear-targeted vimentin. *J Cell Sci.* 111:1241-53.
- Bridger, J.M., I.R. Kill, and P. Lichter. 1998b. Association of pKi-67 with satellite DNA of the human genome in early G1 cells. *Chromosome Res.* 6:13-24.
- Bridger, J.M., I.R. Kill, M. O'Farrell, and C.J. Hutchison. 1993. Internal lamin structures within G1 nuclei of human dermal fibroblasts. *J Cell Sci.* 104:297-306.
- Broers, J.L., B.M. Machiels, G.J. van Eys, H.J. Kuijpers, E.M. Manders, R. van Driel, and F.C. Ramaekers. 1999. Dynamics of the nuclear lamina as monitored by GFP-tagged A-type lamins. *J Cell Sci.* 112:3463-75.
- Brown, K.E., S. Amoils, J.M. Horn, V.J. Buckle, D.R. Higgs, M. Merkenschlager, and A.G. Fisher. 2001. Expression of alpha- and beta-globin genes occurs within different nuclear domains in haemopoietic cells. *Nat Cell Biol.* 3:602-6.
- Brown, K.E., J. Baxter, D. Graf, M. Merkenschlager, and A.G. Fisher. 1999. Dynamic repositioning of genes in the nucleus of lymphocytes preparing for cell division. *Mol Cell.* 3:207-17.
- Brown, K.E., S.S. Guest, S.T. Smale, K. Hahm, M. Merkenschlager, and A.G. Fisher. 1997. Association of transcriptionally silent genes with Ikaros complexes at centromeric heterochromatin. *Cell.* 91:845-54.
- Burke, B., and J. Ellenberg. 2002. Remodelling the walls of the nucleus. *Nat Rev Mol Cell Biol.* 3:487-97.
- Cai, M., Y. Huang, R. Ghirlando, K.L. Wilson, R. Craigie, and G.M. Clore. 2001. Solution structure of the constant region of nuclear envelope protein LAP2 reveals two LEM-domain structures: one binds BAF and the other binds DNA. *Embo J.* 20:4399-407.
- Caron, H., B. van Schaik, M. van der Mee, F. Baas, G. Riggins, P. van Sluis, M.C. Hermus, R. van Asperen, K. Boon, P.A. Voute, S. Heisterkamp, A. van Kampen, and R. Versteeg. 2001. The human transcriptome map: clustering of highly expressed genes in chromosomal domains. *Science.* 291:1289-92.
- Chalfie, M., Y. Tu, G. Euskirchen, W.W. Ward, and D.C. Prasher. 1994. Green fluorescent protein as a marker for gene expression. *Science.* 263:802-5.
- Cheutin, T., A.J. McNairn, T. Jenuwein, D.M. Gilbert, P.B. Singh, and T. Misteli. 2003. Maintenance of stable heterochromatin domains by dynamic HP1 binding. *Science.* 299:721-5.
- Chubb, J.R., S. Boyle, P. Perry, and W.A. Bickmore. 2002. Chromatin motion is constrained by association with nuclear compartments in human cells. *Curr Biol.* 12:439-45.
- Cook, P.R. 2002. Predicting three-dimensional genome structure from transcriptional activity. *Nat Genet.* 32:347-52.
- Cornforth, M.N., K.M. Greulich-Bode, B.D. Loucas, J. Arsuaga, M. Vazquez, R.K. Sachs, M. Bruckner, M. Molls, P. Hahnfeldt, L. Hlatky, and D.J. Brenner. 2002. Chromosomes are predominantly located randomly with respect to each other in interphase human cells. *J Cell Biol.* 159:237-44.
- Craig, J.M., and W.A. Bickmore. 1993. Chromosome bands--flavours to savour. *Bioessays.* 15:349-54.
- Cremer, M., K. Küpper, B. Wagler, L. Wizelman, J. von Hase, Y. Weiland, L. Kreja, J. Diebold, M.R. Speicher, and T. Cremer. 2003. Inheritance of gene-density related higher order chromatin arrangements in normal and tumor cell nuclei. (*submitted*).

- Cremer, M., L. Schermelleh, I. Solovei, and T. Cremer. 2003 (in press). Chromosomal arrangement during different phases of cell cycle. In Encyclopedia of the human genome. Macmillan Publishers Ltd, Nature Publishing Group.
- Cremer, M., J. von Hase, T. Volm, A. Brero, G. Kreth, J. Walter, C. Fischer, I. Solovei, C. Cremer, and T. Cremer. 2001. Non-random radial higher-order chromatin arrangements in nuclei of diploid human cells. *Chromosome Res.* 9:541-67.
- Cremer, T., and C. Cremer. 2001. Chromosome territories, nuclear architecture and gene regulation in mammalian cells. *Nat Rev Genet.* 2:292-301.
- Cremer, T., C. Cremer, H. Baumann, E.K. Luedtke, K. Sperling, V. Teuber, and C. Zorn. 1982. Rabl's model of the interphase chromosome arrangement tested in Chinese hamster cells by premature chromosome condensation and laser-UV- microbeam experiments. *Hum Genet.* 60:46-56.
- Cremer, T., G. Kreth, H. Koester, R.H. Fink, R. Heintzmann, M. Cremer, I. Solovei, D. Zink, and C. Cremer. 2000. Chromosome territories, interchromatin domain compartment, and nuclear matrix: an integrated view of the functional nuclear architecture. *Crit Rev Eukaryot Gene Expr.* 10:179-212.
- Cremer, T., A. Kurz, R. Zirbel, S. Dietzel, B. Rinke, E. Schrock, M.R. Speicher, U. Mathieu, A. Jauch, P. Emmerich, et al. 1993. Role of chromosome territories in the functional compartmentalization of the cell nucleus. *Cold Spring Harb Symp Quant Biol.* 58:777-92.
- Croft, J.A., J.M. Bridger, S. Boyle, P. Perry, P. Teague, and W.A. Bickmore. 1999. Differences in the localization and morphology of chromosomes in the human nucleus. *J Cell Biol.* 145:1119-31.
- Csink, A.K., and S. Henikoff. 1996. Genetic modification of heterochromatic association and nuclear organization in Drosophila. *Nature.* 381:529-31.
- Csink, A.K., and S. Henikoff. 1998. Large-scale chromosomal movements during interphase progression in Drosophila. *J Cell Biol.* 143:13-22.
- Daigle, N., J. Beaudouin, L. Hartnell, G. Imreh, E. Hallberg, J. Lippincott-Schwartz, and J. Ellenberg. 2001. Nuclear pore complexes form immobile networks and have a very low turnover in live mammalian cells. *J Cell Biol.* 154:71-84.
- Deng, W., S.W. Tsao, J.N. Lucas, C.S. Leung, and A.L. Cheung. 2003. A new method for improving metaphase chromosome spreading. *Cytometry.* 51A:46-51.
- Dernburg, A.F., K.W. Broman, J.C. Fung, W.F. Marshall, J. Philips, D.A. Agard, and J.W. Sedat. 1996. Perturbation of nuclear architecture by long-distance chromosome interactions. *Cell.* 85:745-59.
- Dernburg, A.F., and G.H. Karpen. 2002. A chromosome RNAissance. *Cell.* 111:159-62.
- Dietzel, S., A. Jauch, D. Kienle, G. Qu, H. Holtgreve-Grez, R. Eils, C. Munkel, M. Bittner, P.S. Meltzer, J.M. Trent, and T. Cremer. 1998. Separate and variably shaped chromosome arm domains are disclosed by chromosome arm painting in human cell nuclei. *Chromosome Res.* 6:25-33.
- Dietzel, S., K. Schiebel, G. Little, P. Edelmann, G.A. Rappold, R. Eils, C. Cremer, and T. Cremer. 1999. The 3D positioning of ANT2 and ANT3 genes within female X chromosome territories correlates with gene activity. *Exp Cell Res.* 252:363-75.
- Dillon, N., and R. Festenstein. 2002. Unravelling heterochromatin: competition between positive and negative factors regulates accessibility. *Trends Genet.* 18:252-8.
- Dimitrova, D.S., and R. Berezney. 2002. The spatio-temporal organization of DNA replication sites is identical in primary, immortalized and transformed mammalian cells. *J Cell Sci.* 115:4037-51.
- Dimitrova, D.S., and D.M. Gilbert. 1998. Regulation of mammalian replication origin usage in Xenopus egg extract. *J Cell Sci.* 111:2989-98.
- Dimitrova, D.S., and D.M. Gilbert. 1999. The spatial position and replication timing of chromosomal domains are both established in early G1 phase. *Mol Cell.* 4:983-93.

- Drouin, R., N. Lemieux, and C.L. Richer. 1990. Analysis of DNA replication during S-phase by means of dynamic chromosome banding at high resolution. *Chromosoma*. 99:273-80.
- Dundr, M., and T. Misteli. 2001. Functional architecture in the cell nucleus. *Biochem J*. 356:297-310.
- Edelmann, P., H. Bornfleth, D. Zink, T. Cremer, and C. Cremer. 2001. Morphology and dynamics of chromosome territories in living cells. *Biochim Biophys Acta*. 1551:M29-39.
- Ellenberg, J., E.D. Siggia, J.E. Moreira, C.L. Smith, J.F. Presley, H.J. Worman, and J. Lippincott-Schwartz. 1997. Nuclear membrane dynamics and reassembly in living cells: targeting of an inner nuclear membrane protein in interphase and mitosis. *J Cell Biol*. 138:1193-206.
- Endl, E., and J. Gerdes. 2000. The Ki-67 protein: fascinating forms and an unknown function. *Exp Cell Res*. 257:231-7.
- Fauth, C., and D. Zink. 2001. (Corrigendum 2003) Live-cell microscopy of single nuclear chromosomes and genome compartments: evaluation of labeling procedure and imaging conditions. *Cytometry*. 45:214-24.
- Federico, C., S. Saccone, and G. Bernardi. 1998. The gene-richest bands of human chromosomes replicate at the onset of the S-phase. *Cytogenet Cell Genet*. 80:83-8.
- Ferguson, M., and D.C. Ward. 1992. Cell cycle dependent chromosomal movement in pre-mitotic human T-lymphocyte nuclei. *Chromosoma*. 101:557-65.
- Ferreira, J., G. Paolella, C. Ramos, and A.I. Lamond. 1997. Spatial organization of large-scale chromatin domains in the nucleus: a magnified view of single chromosome territories. *J Cell Biol*. 139:1597-610.
- Festenstein, R., S.N. Pagakis, K. Hiragami, D. Lyon, A. Verreault, B. Sekkali, and D. Kioussis. 2003. Modulation of heterochromatin protein 1 dynamics in primary Mammalian cells. *Science*. 299:719-21.
- Fox, M.H., R.A. Read, and J.S. Bedford. 1987. Comparison of synchronized Chinese hamster ovary cells obtained by mitotic shake-off, hydroxyurea, aphidicolin, or methotrexate. *Cytometry*. 8:315-20.
- Francastel, C., D. Schubeler, D.I. Martin, and M. Groudine. 2000. Nuclear compartmentalization and gene activity. *Nat Rev Mol Cell Biol*. 1:137-43.
- Fricker, M., M. Hollinshead, N. White, and D. Vaux. 1997. Interphase nuclei of many mammalian cell types contain deep, dynamic, tubular membrane-bound invaginations of the nuclear envelope. *J Cell Biol*. 136:531-44.
- Furukawa, K. 1999. LAP2 binding protein 1 (L2BP1/BAF) is a candidate mediator of LAP2-chromatin interaction. *J Cell Sci*. 112:2485-92.
- Gasser, S.M. 2002. Visualizing chromatin dynamics in interphase nuclei. *Science*. 296:1412-6.
- Georgatos, S.D., A. Pyrpasopoulou, and P.A. Theodoropoulos. 1997. Nuclear envelope breakdown in mammalian cells involves stepwise lamina disassembly and microtubule-drive deformation of the nuclear membrane. *J Cell Sci*. 110:2129-40.
- Gerasimova, T.I., K. Byrd, and V.G. Corces. 2000. A chromatin insulator determines the nuclear localization of DNA. *Mol Cell*. 6:1025-35.
- Gerasimova, T.I., and V.G. Corces. 2001. Chromatin insulators and boundaries: effects on transcription and nuclear organization. *Annu Rev Genet*. 35:193-208.
- Gerlich, D., J. Beaudouin, B. Kalbfuss, N. Daigle, R. Eils, and J. Ellenberg. 2003. Global chromosome positions are transmitted through mitosis in mammalian cells. *Cell*. 112:751-64.
- Goldman, R.D., Y. Gruenbaum, R.D. Moir, D.K. Shumaker, and T.P. Spann. 2002. Nuclear lamins: building blocks of nuclear architecture. *Genes Dev*. 16:533-47.
- Goren, A., and H. Cedar. 2003. Replicating by the clock. *Nat Rev Mol Cell Biol*. 4:25-32.
- Gratzner, H.G. 1982. Monoclonal antibody to 5-bromo- and 5-iododeoxyuridine: A new reagent for detection of DNA replication. *Science*. 218:474-5.

- Habermann, F.A., M. Cremer, J. Walter, G. Kreth, J. von Hase, K. Bauer, J. Wienberg, C. Cremer, T. Cremer, and I. Solovei. 2001. Arrangements of macro- and microchromosomes in chicken cells. *Chromosome Res.* 9:569-84.
- Haukenes, G., A.M. Szilvay, K.A. Brokstad, A. Kanestrom, and K.H. Kalland. 1997. Labeling of RNA transcripts of eukaryotic cells in culture with BrUTP using a liposome transfection reagent (DOTAP). *Biotechniques*. 22:308-12.
- Heitz, E. 1932. Die Herkunft der Chromocentren. *Planta*. 18:371-635.
- Heun, P., T. Laroche, K. Shimada, P. Furrer, and S.M. Gasser. 2001. Chromosome Dynamics in the Yeast Interphase Nucleus. *Science*. 294:2181-2186.
- Horn, P.J., and C.L. Peterson. 2002. Molecular biology. Chromatin higher order folding--wrapping up transcription. *Science*. 297:1824-7.
- Hulspas, R., A.B. Houtsmuller, P.J. Krijtenburg, J.G. Bauman, and N. Nanninga. 1994. The nuclear position of pericentromeric DNA of chromosome 11 appears to be random in G0 and non-random in G1 human lymphocytes. *Chromosoma*. 103:286-92.
- Hutchison, C.J. 2002. Lamins: building blocks or regulators of gene expression? *Nat Rev Mol Cell Biol.* 3:848-58.
- Ikegami, S., T. Taguchi, M. Ohashi, M. Oguro, H. Nagano, and Y. Mano. 1978. Aphidicolin prevents mitotic cell division by interfering with the activity of DNA polymerase-alpha. *Nature*. 275:458-60.
- Jackson, D.A., and A. Pombo. 1998. Replicon clusters are stable units of chromosome structure: evidence that nuclear organization contributes to the efficient activation and propagation of S phase in human cells. *J Cell Biol.* 140:1285-95.
- Jackson, J.P., A.M. Lindroth, X. Cao, and S.E. Jacobsen. 2002. Control of CpNpG DNA methylation by the KRYPTONITE histone H3 methyltransferase. *Nature*. 416:556-60.
- Jaiswal, J.K., H. Mattoucci, J.M. Mauro, and S.M. Simon. 2003. Long-term multiple color imaging of live cells using quantum dot bioconjugates. *Nat Biotechnol.* 21:47-51.
- Jenuwein, T., and C.D. Allis. 2001. Translating the histone code. *Science*. 293:1074-80.
- Jones, P.A., and D. Takai. 2001. The role of DNA methylation in mammalian epigenetics. *Science*. 293:1068-70.
- Jones, P.L., G.J. Veenstra, P.A. Wade, D. Vermaak, S.U. Kass, N. Landsberger, J. Strouboulis, and A.P. Wolffe. 1998. Methylated DNA and MeCP2 recruit histone deacetylase to repress transcription. *Nat Genet*. 19:187-91.
- Kametaka, A., M. Takagi, T. Hayakawa, T. Haraguchi, Y. Hiraoka, and Y. Yoneda. 2002. Interaction of the chromatin compaction-inducing domain (LR domain) of Ki-67 antigen with HP1 proteins. *Genes Cells*. 7:1231-42.
- Kanda, T., K.F. Sullivan, and G.M. Wahl. 1998. Histone-GFP fusion protein enables sensitive analysis of chromosome dynamics in living mammalian cells. *Curr Biol*. 8:377-85.
- Kessel, D., and Y. Luo. 1996. Delayed oxidative photodamage induced by photodynamic therapy. *Photochem Photobiol*. 64:601-4.
- Kill, I.R. 1996. Localisation of the Ki-67 antigen within the nucleolus. Evidence for a fibrillarin-deficient region of the dense fibrillar component. *J Cell Sci.* 109:1253-63.
- Kimura, H., and P.R. Cook. 2001. Kinetics of core histones in living human cells: little exchange of H3 and H4 and some rapid exchange of H2B. *J Cell Biol.* 153:1341-53.
- Koberna, K., D. Stanek, J. Malinsky, M. Eltsov, A. Pliss, V. Ctrnacta, S. Cermanova, and I. Raska. 1999. Nuclear organization studied with the help of a hypotonic shift: its use permits hydrophilic molecules to enter into living cells. *Chromosoma*. 108:325-35.
- Koss, L.G. 1998. Characteristics of chromosomes in polarized normal human bronchial cells provide a blueprint for nuclear organization. *Cytogenet. Cell Genet.* 82:230-7.
- Kourmouli, N., P.A. Theodoropoulos, G. Dialynas, A. Bakou, A.S. Politou, I.G. Cowell, P.B. Singh, and S.D. Georgatos. 2000. Dynamic associations of heterochromatin protein 1 with the nuclear envelope. *Embo J.* 19:6558-68.

- Labrador, M., and V.G. Corces. 2002. Setting the boundaries of chromatin domains and nuclear organization. *Cell*. 111:151-4.
- Lachner, M., and T. Jenuwein. 2002. The many faces of histone lysine methylation. *Curr Opin Cell Biol*. 14:286-98.
- Lachner, M., D. O'Carroll, S. Rea, K. Mechtler, and T. Jenuwein. 2001. Methylation of histone H3 lysine 9 creates a binding site for HP1 proteins. *Nature*. 410:116-20.
- Lamond, A.I., and W.C. Earnshaw. 1998. Structure and function in the nucleus. *Science*. 280:547-53.
- Lee, M.Y., N.L. Toomey, and G.E. Wright. 1985. Differential inhibition of human placental DNA polymerases delta and alpha by BuPdGTP and BuAdATP. *Nucleic Acids Res*. 13:8623-30.
- Leitch, A.R. 2000. Higher levels of organization in the interphase nucleus of cycling and differentiated cells. *Microbiol. Mol. Biol. Rev*. 64:138-52.
- Lemke, J., J. Claussen, S. Michel, I. Chudoba, P. Muhlig, M. Westermann, K. Sperling, N. Rubtsov, U.W. Grummt, P. Ullmann, K. Kromeyer-Hauschild, T. Liehr, and U. Claussen. 2002. The DNA-Based Structure of Human Chromosome 5 in Interphase. *Am J Hum Genet*. 71:1051-9.
- Leonhardt, H., and M.C. Cardoso. 2000. DNA methylation, nuclear structure, gene expression and cancer. *J Cell Biochem Suppl*. Suppl:78-83.
- Leonhardt, H., H.P. Rahn, P. Weinzierl, A. Sporbert, T. Cremer, D. Zink, and M.C. Cardoso. 2000. Dynamics of DNA replication factories in living cells. *J Cell Biol*. 149:271-80.
- Lesko, S.A., D.E. Callahan, M.E. LaVilla, Z.P. Wang, and P.O. Ts'o. 1995. The experimental homologous and heterologous separation distance histograms for the centromeres of chromosomes 7, 11, and 17 in interphase human T-lymphocytes. *Exp Cell Res*. 219:499-506.
- Li, F., J. Chen, M. Izumi, M.C. Butler, S.M. Keezer, and D.M. Gilbert. 2001. The replication timing program of the Chinese hamster beta-globin locus is established coincident with its repositioning near peripheral heterochromatin in early G1 phase. *J Cell Biol*. 154:283-92.
- Lichter, P., T. Cremer, J. Borden, L. Manuelidis, and D.C. Ward. 1988. Delineation of individual human chromosomes in metaphase and interphase cells by *in situ* suppression hybridization using recombinant DNA libraries. *Hum Genet*. 80:224-34.
- Lucas, J.N., and E. Cervantes. 2002. Significant large-scale chromosome territory movement occurs as a result of mitosis, but not during interphase. *Int J Radiat Biol*. 78:449-55.
- Luderus, M.E., A. de Graaf, E. Mattia, J.L. den Blaauwen, M.A. Grande, L. de Jong, and R. van Driel. 1992. Binding of matrix attachment regions to lamin B1. *Cell*. 70:949-59.
- Luger, K., A.W. Mader, R.K. Richmond, D.F. Sargent, and T.J. Richmond. 1997. Crystal structure of the nucleosome core particle at 2.8 Å resolution. *Nature*. 389:251-60.
- Ma, H., J. Samarabandu, R.S. Devdhar, R. Acharya, P.C. Cheng, C. Meng, and R. Berezney. 1998. Spatial and temporal dynamics of DNA replication sites in mammalian cells. *J. Cell Biol*. 143:1415-25.
- Ma, H., A.J. Siegel, and R. Berezney. 1999. Association of chromosome territories with the nuclear matrix. Disruption of human chromosome territories correlates with the release of a subset of nuclear matrix proteins. *J Cell Biol*. 146:531-42.
- Mahy, N.L., P.E. Perry, S. Gilchrist, R.A. Baldock, and W.A. Bickmore. 2002. Spatial organization of active and inactive genes and noncoding DNA within chromosome territories. *J Cell Biol*. 157:579-89.
- Manders, E.M., H. Kimura, and P.R. Cook. 1999. Direct imaging of DNA in living cells reveals the dynamics of chromosome formation. *J Cell Biol*. 144:813-21.
- Manuelidis, L. 1985. Individual interphase chromosome domains revealed by *in situ* hybridization. *Hum Genet*. 71:288-93.
- Marshall, W.F. 2002. Order and disorder in the nucleus. *Curr Biol*. 12:R185-92.

- Marshall, W.F., A.F. Dernburg, B. Harmon, D.A. Agard, and J.W. Sedat. 1996. Specific interactions of chromatin with the nuclear envelope: positional determination within the nucleus in *Drosophila melanogaster*. *Mol Biol Cell*. 7:825-42.
- Marshall, W.F., A. Straight, J.F. Marko, J. Swedlow, A. Dernburg, A. Belmont, A.W. Murray, D.A. Agard, and J.W. Sedat. 1997. Interphase chromosomes undergo constrained diffusional motion in living cells. *Curr Biol*. 7:930-9.
- Martin, J.P., and N. Logsdon. 1987. The role of oxygen radicals in dye-mediated photodynamic effects in *Escherichia coli* B. *J Biol Chem*. 262:7213-9.
- Martou, G., and U. De Boni. 2000. Nuclear topology of murine, cerebellar Purkinje neurons: changes as a function of development. *Exp Cell Res*. 256:131-9.
- McNeil, P.L. 1989. Incorporation of macromolecules into living cells. *Methods Cell Biol*. 29:153-73.
- McNeil, P.L., R.F. Murphy, F. Lanni, and D.L. Taylor. 1984. A method for incorporating macromolecules into adherent cells. *J Cell Biol*. 98:1556-64.
- McNeil, P.L., and E. Warder. 1987. Glass beads load macromolecules into living cells. *J Cell Sci*. 88:669-78.
- Merrill, G.F. 1998. Cell synchronization. *Methods Cell Biol*. 57:229-49.
- Misteli, T. 2001. Protein dynamics: implications for nuclear architecture and gene expression. *Science*. 291:843-7.
- Moir, R.D., M. Montag-Lowy, and R.D. Goldman. 1994. Dynamic properties of nuclear lamins: lamin B is associated with sites of DNA replication. *J Cell Biol*. 125:1201-12.
- Moir, R.D., T.P. Spann, H. Herrmann, and R.D. Goldman. 2000a. Disruption of nuclear lamin organization blocks the elongation phase of DNA replication. *J Cell Biol*. 149:1179-92.
- Moir, R.D., M. Yoon, S. Khuon, and R.D. Goldman. 2000b. Nuclear lamins A and B1: different pathways of assembly during nuclear envelope formation in living cells. *J Cell Biol*. 151:1155-68.
- Nagele, R., T. Freeman, L. McMorrow, and H.Y. Lee. 1995. Precise spatial positioning of chromosomes during prometaphase: evidence for chromosomal order. *Science*. 270:1831-5.
- Nagele, R.G., T. Freeman, L. McMorrow, Z. Thomson, K. Kitson-Wind, and H. Lee. 1999. Chromosomes exhibit preferential positioning in nuclei of quiescent human cells. *J Cell Sci*. 112:525-35.
- Nakamura, H., T. Morita, and C. Sato. 1986. Structural organizations of replicon domains during DNA synthetic phase in the mammalian nucleus. *Exp Cell Res*. 165:291-7.
- Nakayasu, H., and R. Berezney. 1989. Mapping replicational sites in the eucaryotic cell nucleus. *J Cell Biol*. 108:1-11.
- Nielsen, S.J., R. Schneider, U.M. Bauer, A.J. Bannister, A. Morrison, D. O'Carroll, R. Firestein, M. Cleary, T. Jenuwein, R.E. Herrera, and T. Kouzarides. 2001. Rb targets histone H3 methylation and HP1 to promoters. *Nature*. 412:561-5.
- Ochs, B.A., W.W. Franke, R. Moll, C. Grund, M. Cremer, and T. Cremer. 1983. Epithelial character and morphologic diversity of cell cultures from human amniotic fluids examined by immunofluorescence microscopy and gel electrophoresis of cytoskeletal proteins. *Differentiation*. 24:153-73.
- Okada, C.Y., and M. Rechsteiner. 1982. Introduction of macromolecules into cultured mammalian cells by osmotic lysis of pinocytic vesicles. *Cell*. 29:33-41.
- O'Keefe, R.T., S.C. Henderson, and D.L. Spector. 1992. Dynamic organization of DNA replication in mammalian cell nuclei: spatially and temporally defined replication of chromosome-specific alpha-satellite DNA sequences. *J Cell Biol*. 116:1095-110.
- Paddy, M.R., A.S. Belmont, H. Saumweber, D.A. Agard, and J.W. Sedat. 1990. Interphase nuclear envelope lamins form a discontinuous network that interacts with only a fraction of the chromatin in the nuclear periphery. *Cell*. 62:89-106.

- Parada, L., and T. Misteli. 2002. Chromosome positioning in the interphase nucleus. *Trends Cell Biol.* 12:425.
- Parada, L.A., P.G. McQueen, P.J. Munson, and T. Misteli. 2002. Conservation of relative chromosome positioning in normal and cancer cells. *Curr Biol.* 12:1692-7.
- Pederson, T. 2000. Half a century of "the nuclear matrix". *Mol Biol Cell.* 11:799-805.
- Pepperkok, R., and W. Ansorge. 1995. Direct visualization of DNA replication sites in living cells by microinjection of fluorescein-conjugated dUTPs. *Methods Mol Cell Biol.* 5:112-117.
- Peters, A.H., J.E. Mermoud, D. O'Carroll, M. Pagani, D. Schweizer, N. Brockdorff, and T. Jenuwein. 2002. Histone H3 lysine 9 methylation is an epigenetic imprint of facultative heterochromatin. *Nat Genet.* 30:77-80.
- Peters, A.H., D. O'Carroll, H. Scherthan, K. Mechtler, S. Sauer, C. Schofer, K. Weipoltshammer, M. Pagani, M. Lachner, A. Kohlmaier, S. Opravil, M. Doyle, M. Sibilia, and T. Jenuwein. 2001. Loss of the Suv39h histone methyltransferases impairs mammalian heterochromatin and genome stability. *Cell.* 107:323-37.
- Politz, J.C., R.A. Tuft, T. Pederson, and R.H. Singer. 1999. Movement of nuclear poly(A) RNA throughout the interchromatin space in living cells. *Curr Biol.* 9:285-91.
- Pyrpasopoulou, A., J. Meier, C. Maison, G. Simos, and S.D. Georgatos. 1996. The lamin B receptor (LBR) provides essential chromatin docking sites at the nuclear envelope. *Embo J.* 15:7108-19.
- Rabl, C. 1885. Über Zelltheilung. *Morphologisches Jahrbuch.* 10:214-330.
- Rasband, W. 2002. ImageJ. <http://rsb.info.nih.gov/ij/>.
- Reichenzeller, M., A. Burzlaff, P. Lichter, and H. Herrmann. 2000. In vivo observation of a nuclear channel-like system: evidence for a distinct interchromosomal domain compartment in interphase cells. *J Struct Biol.* 129:175-85.
- Richards, E.J., and S.C. Elgin. 2002. Epigenetic codes for heterochromatin formation and silencing: rounding up the usual suspects. *Cell.* 108:489-500.
- Ross, R.A., B.A. Spengler, and J.L. Biedler. 1983. Coordinate morphological and biochemical interconversion of human neuroblastoma cells. *J Natl Cancer Inst.* 71:741-7.
- Rountree, M.R., K.E. Bachman, and S.B. Baylin. 2000. DNMT1 binds HDAC2 and a new co-repressor, DMAP1, to form a complex at replication foci. *Nat Genet.* 25:269-77.
- Sadoni, N., S. Langer, C. Fauth, G. Bernardi, T. Cremer, B.M. Turner, and D. Zink. 1999. Nuclear organization of mammalian genomes. Polar chromosome territories build up functionally distinct higher order compartments. *J. Cell Biol.* 146:1211-26.
- Saetzler, R.K., J. Jallo, H.A. Lehr, C.M. Philips, U. Vasthare, K.E. Arfors, and R.F. Tuma. 1997. Intravital fluorescence microscopy: impact of light-induced phototoxicity on adhesion of fluorescently labeled leukocytes. *J Histochem Cytochem.* 45:505-13.
- Schermelleh, L., I. Solovei, D. Zink, and T. Cremer. 2001. Two-color fluorescence labeling of early and mid-to-late replicating chromatin in living cells. *Chromosome Res.* 9:77-80.
- Scholzen, T., E. Endl, C. Wohlenberg, S. van der Sar, I.G. Cowell, J. Gerdes, and P.B. Singh. 2002. The Ki-67 protein interacts with members of the heterochromatin protein 1 (HP1) family: a potential role in the regulation of higher-order chromatin structure. *J Pathol.* 196:135-44.
- Shea, C.R., N. Chen, J. Wimberly, and T. Hasan. 1989. Rhodamine dyes as potential agents for photochemotherapy of cancer in human bladder carcinoma cells. *Cancer Res.* 49:3961-5.
- Shelby, R.D., K.M. Hahn, and K.F. Sullivan. 1996. Dynamic elastic behavior of alpha-satellite DNA domains visualized in situ in living human cells. *J Cell Biol.* 135:545-57.
- Simon, I., T. Tenzen, B.E. Reubinoff, D. Hillman, J.R. McCarey, and H. Cedar. 1999. Asynchronous replication of imprinted genes is established in the gametes and maintained during development. *Nature.* 401:929-32.

- Solovei, I., L. Schermelleh, K. Düring, A. Engelhardt, S. Stein, J. von Hase, C. Cremer, and T. Cremer. 2003. Differences in centromere positioning during cell cycle and at G0 in four types of human cells. *(in prep)*.
- Solovei, I., J. Walter, M. Cremer, F. Habermann, L. Schermelleh, and T. Cremer. 2002. FISH on three-dimensionally preserved nuclei. In *FISH: a practical approach*. J. Squire, B. Beatty, and S. Mai, editors. Oxford University Press, Oxford. 119-157.
- Spann, T.P., A.E. Goldman, C. Wang, S. Huang, and R.D. Goldman. 2002. Alteration of nuclear lamin organization inhibits RNA polymerase II-dependent transcription. *J Cell Biol.* 156:603-8.
- Spann, T.P., R.D. Moir, A.E. Goldman, R. Stick, and R.D. Goldman. 1997. Disruption of nuclear lamin organization alters the distribution of replication factors and inhibits DNA synthesis. *J Cell Biol.* 136:1201-12.
- Sporbert, A., A. Gahl, R. Ankerhold, H. Leonhardt, and M.C. Cardoso. 2002. DNA polymerase clamp shows little turnover at established replication sites but sequential de novo assembly at adjacent origin clusters. *Mol Cell.* 10:1355-65.
- Strahl, B.D., and C.D. Allis. 2000. The language of covalent histone modifications. *Nature.* 403:41-5.
- Struhl, K. 1998. Histone acetylation and transcriptional regulatory mechanisms. *Genes Dev.* 12:599-606.
- Sullivan, K.F., M. Hechenberger, and K. Masri. 1994. Human CENP-A contains a histone H3 related histone fold domain that is required for targeting to the centromere. *J Cell Biol.* 127:581-92.
- Sun, H.B., J. Shen, and H. Yokota. 2000. Size-dependent positioning of human chromosomes in interphase nuclei. *Biophys J.* 79:184-90.
- Sun, H.B., and H. Yokota. 1999. Correlated positioning of homologous chromosomes in daughter fibroblast cells. *Chromosome Res.* 7:603-10.
- Swanson, J.A., and P.L. McNeil. 1987. Nuclear reassembly excludes large macromolecules. *Science.* 238:548-50.
- Tamaru, H., and E.U. Selker. 2001. A histone H3 methyltransferase controls DNA methylation in *Neurospora crassa*. *Nature.* 414:277-83.
- Tanabe, H., S. Muller, M. Neusser, J. von Hase, E. Calcagno, M. Cremer, I. Solovei, C. Cremer, and T. Cremer. 2002. Evolutionary conservation of chromosome territory arrangements in cell nuclei from higher primates. *Proc Natl Acad Sci U S A.* 99:4424-4429.
- Taniura, H., C. Glass, and L. Gerace. 1995. A chromatin binding site in the tail domain of nuclear lamins that interacts with core histones. *J Cell Biol.* 131:33-44.
- Tashiro, S., N. Kotomura, A. Shinohara, K. Tanaka, K. Ueda, and N. Kamada. 1996. S phase specific formation of the human Rad51 protein nuclear foci in lymphocytes. *Oncogene.* 12:2165-70.
- Tsukamoto, T., N. Hashiguchi, S.M. Janicki, T. Tumbar, A.S. Belmont, and D.L. Spector. 2000. Visualization of gene activity in living cells. *Nat Cell Biol.* 2:871-8.
- Tucker, J.D., M.L. Christensen, C.L. Strout, and A.V. Carrano. 1986. Determination of the baseline sister chromatid exchange frequency in human and mouse peripheral lymphocytes using monoclonal antibodies and very low doses of bromodeoxyuridine. *Cytogenet Cell Genet.* 43:38-42.
- Tumbar, T., G. Sudlow, and A.S. Belmont. 1999. Large-scale chromatin unfolding and remodeling induced by VP16 acidic activation domain. *J Cell Biol.* 145:1341-54.
- Tumbar, T., and A.S. Belmont. 2001. Interphase movements of a DNA chromosome region modulated by VP16 transcriptional activator. *Nat Cell Biol.* 3:134-9.
- Vazquez, J., A.S. Belmont, and J.W. Sedat. 2001. Multiple regimes of constrained chromosome motion are regulated in the interphase Drosophila nucleus. *Curr Biol.* 11:1227-39.

- Visser, A.E., and J.A. Aten. 1999. Chromosomes as well as chromosomal subdomains constitute distinct units in interphase nuclei. *J Cell Sci.* 112:3353-60.
- Visser, A.E., R. Eils, A. Jauch, G. Little, P.J. Bakker, T. Cremer, and J.A. Aten. 1998. Spatial distributions of early and late replicating chromatin in interphase chromosome territories. *Exp Cell Res.* 243:398-407.
- Volpi, E.V., E. Chevret, T. Jones, R. Vatcheva, J. Williamson, S. Beck, R.D. Campbell, M. Goldsworthy, S.H. Powis, J. Ragoussis, J. Trowsdale, and D. Sheer. 2000. Large-scale chromatin organization of the major histocompatibility complex and other regions of human chromosome 6 and its response to interferon in interphase nuclei. *J Cell Sci.* 113:1565-76.
- Vourc'h, C., D. Taruscio, A.L. Boyle, and D.C. Ward. 1993. Cell cycle-dependent distribution of telomeres, centromeres, and chromosome-specific subsatellite domains in the interphase nucleus of mouse lymphocytes. *Exp Cell Res.* 205:142-51.
- Walter, J., L. Schermelleh, M. Cremer, S. Tashiro, and T. Cremer. 2003. Chromosome order in HeLa cells changes during mitosis and early G1, but is stably maintained during subsequent interphase stages. *J Cell Biol.* 160:685-97.
- Wansink, D.G., W. Schul, I. van der Kraan, B. van Steensel, R. van Driel, and L. de Jong. 1993. Fluorescent labeling of nascent RNA reveals transcription by RNA polymerase II in domains scattered throughout the nucleus. *J Cell Biol.* 122:283-93.
- Wei, X., J. Samarabandu, R.S. Devdhar, A.J. Siegel, R. Acharya, and R. Berezney. 1998. Segregation of transcription and replication sites into higher order domains. *Science.* 281:1502-6.
- Weimer, R., T. Haaf, J. Kruger, M. Poot, and M. Schmid. 1992. Characterization of centromere arrangements and test for random distribution in G0, G1, S, G2, G1, and early S' phase in human lymphocytes. *Hum Genet.* 88:673-82.
- Wenzel, A., C. Cziepluch, U. Hamann, J. Schurmann, and M. Schwab. 1991. The N-Myc oncogene is associated in vivo with the phosphoprotein Max(p20/22) in human neuroblastoma cells. *Embo J.* 10:3703-12.
- Williams, R.R., S. Broad, D. Sheer, and J. Ragoussis. 2002. Subchromosomal positioning of the epidermal differentiation complex (EDC) in keratinocyte and lymphoblast interphase nuclei. *Exp Cell Res.* 272:163-75.
- Wilson, K.L. 2000. The nuclear envelope, muscular dystrophy and gene expression. *Trends Cell Biol.* 10:125-9.
- Wu, T.W., N. Hashimoto, J. Wu, D. Carey, R.K. Li, D.A. Mickle, and R.D. Weisel. 1990. The cytoprotective effect of Trolox demonstrated with three types of human cells. *Biochem Cell Biol.* 68:1189-94.
- Ye, Q., and H.J. Worman. 1996. Interaction between an integral protein of the nuclear envelope inner membrane and human chromodomain proteins homologous to Drosophila HP1. *J Biol Chem.* 271:14653-6.
- Zink, D., H. Bornfleth, A. Visser, C. Cremer, and T. Cremer. 1999. Organization of early and late replicating DNA in human chromosome territories. *Exp Cell Res.* 247:176-88.
- Zink, D., and T. Cremer. 1998. Cell nucleus: chromosome dynamics in nuclei of living cells. *Curr Biol.* 8:R321-4.
- Zink, D., T. Cremer, R. Saffrich, R. Fischer, M.F. Trendelenburg, W. Ansorge, and E.H. Stelzer. 1998. Structure and dynamics of human interphase chromosome territories in vivo. *Hum Genet.* 102:241-51.

7. Appendix

7.1 Supplementary material

Video 1. Long-term live cell microscopy of HeLa H2B-GFP cells

HeLa histone H2B-GFP expressing cells were mounted on the stage of a Zeiss LSM 410 employing the long-term observation set-up described in 3.12.2 (corresponding to Figure 10). Cells were imaged automatically at low resolution for three days until they reach confluence demonstrating that cell viability is not impaired by the imaging conditions.

Video 2. 4D confocal time series after single-color SRL

4D time series of HeLa cells expressing histone H2B-GFP (displayed green or gray) showing individual chromosome territories labeled with Cy3-dUTP (displayed red) by scratch replication labeling 4.5 days prior to observation (see also Figure 17). Part I shows an overview of the observation area during 10 hours total observation time. Light optical serial sections were recorded with an interval of 6 min (total data set contains 100 time points with 30 nuclear sections each). In part II, two cells from the observation area (part I) are shown at higher magnification and after correction for translational and rotational nuclear movements. Movements of the labeled chromatin are locally constrained in interphase nuclei. Confocal live cell imaging was performed with an LSM 410 (Zeiss); 3D-volume rendering was performed with Amira™ 2.3 (TGS; <http://www.amiravis.com>).

Video 3. Projected time series after sequential two-color SRL

Live cell imaging of a HeLa H2B-GFP nucleus that was replication labeled in two consecutive S-phases with Cy3-dUTP (displayed red) and Cy5-dUTP (displayed green) respectively (corresponding to Figure 18). Observation started 4.5 days after the second labeling event. The GFP signal is indicated by a gray outline. The inset shows the GFP-signal of the corresponding confocal midsection at a lower magnification. In contrast to Cy3, Cy5 signals showed notable fading due to photobleaching; hence signal contrast was digitally enhanced for compensation. Differentially labeled chromosome territories are displayed as maximum intensity projections from light optical serial sections recorded at 10 min intervals. For observation of intranuclear chromatin movements, images were corrected for translational and rotational nuclear movements. Movements of labeled chromatin are locally constrained and red and green colored chromatin domains remain separated. The large-scale topography of labeled chromatin is maintained when the cell enters prophase 3 h 50 min after the start of the observation period (compare Figure 18 D).

Video 4. Live cell imaging after partial photobleaching of H2B

Live cell imaging of HeLa cells with H2B-GFP tagged chromatin after partial photobleaching leaving an unbleached chromatin region at the upper nuclear rim (corresponding to Figure 19). Movie shows maximum intensity projections from confocal serial sections recorded with at 20 min intervals (nucleus 1) and 30 min intervals (nucleus 2 and 3). In both daughter nuclei generated from mother nucleus 1 (corresponding to Figure 19 A) the unbleached chromatin patches form a single cluster. Unbleached chromatin patches in the daughters of mother nucleus 2 (compare Figure 19 B) are also clustered with the exception of two remote patches. Each of the two daughter cells was observed throughout the cell cycle and passed through another mitosis indicating the proliferative integrity of these cells. In the two daughter nuclei generated from mother nucleus 3 (compare Figure 19 C) the unbleached chromatin patches are widely distributed over the whole nucleus.

Videos 5 to 8. 3D reconstructions of nuclei of HeLa 4-cell clone after two-color FISH

Interactive 3D renderings of the two pairs of daughter cell nuclei from a four-cell clone displayed in Figure 21. For detailed comparisons of the topography of the painted chromosome territories #7 and #10 the nuclei can be rotated, moved and zoomed in Apple QuickTime.

Video 9. 4D confocal time series of nuclear lamina and chromatin movements

4D-imaging of CHO cells expressing lamin C-GFP (displayed turquoise) with mid-to-late replicating chromatin domains labeled with Cy3-dUTP (displayed red). Scratch replication labeling was performed 8 days prior to observation (corresponding to Figure 27). Light optical serial sections were recorded at 6 min intervals (total data set contains 75 time points with 28 nuclear sections each). In the first part of the movie (top view) the nucleus was corrected for translational and rotational (xy-direction) nuclear movements. During the first 2 hours of the observation the nucleus rotates 180° in z-axis, which was not corrected. Cy3-stained subchromosomal foci are mostly associated with the nuclear lamina. Note that one chromatin domain is closely associated with the prominent transnuclear invagination, both performing considerable concomitant movements.

Supplementary table. Detailed list of all $\Delta(\text{Max-Min})$ values

nucleus	# of evaluated time points	# of CTs (signal clusters)		$\Delta(\text{Max-Min}) \text{CT-CN}$ [μm]			$\Delta(\text{Max-Min}) \text{CT-CT}$ [μm]	
			absolute	corrected	absolute		corrected	
fixed	14	3	0.09 ± 0.10	0.11 ± 0.14	0.15 ± 0.22	0.16 ± 0.15	0.17 ± 0.03	0.16 (0.15 - 0.20)
		mean ± SD median (range)	0.09 ± 0.01 0.09 (0.07 - 0.10)	0.11 ± 0.03 0.11 (0.07 - 0.14)	0.15 ± 0.06 0.15 (0.09 - 0.22)	0.17 ± 0.03 0.16 (0.15 - 0.20)		
telophase - early G1								
1 <i>df</i>	9	2	0.88 ± 0.81	1.58 ± 1.22	<u>2.41</u>	-	-	-
2 <i>df</i>	8	1	0.87	1.93	0.87	1.33 ± 1.14	1.17 ± 0.61	1.17 ± 0.61
3 <i>df</i>	10	3	2.36 ± 1.53	2.26 ± 1.58	2.38 ± 1.49	3.15 ± 1.76	<u>2.06</u>	2.23 ± 1.53
4	14	3	1.73 ± 1.25	2.31 ± 1.65	2.37 ± 1.73	2.75 ± 2.37	2.40 ± 2.39	4.44 ± 2.23
5	9	4	2.08 ± 2.46	2.36 ± 2.05	1.73 ± 1.73	2.75 ± 1.53	2.40 ± 2.39	3.58 ± 3.58
6 <i>df</i>	8	1	1.48	0.78	-	0.70 ± 0.70	1.10 ± 1.87	3.08 ± 1.56
7	11	2	1.23 ± 1.88	1.67 ± 1.61	<u>3.17</u>	-	-	-
8	7	3	0.48 ± 0.30	1.34 ± 0.42	0.43 ± 0.43	0.92 ± 0.48	0.94 ± 1.30	<u>3.34</u>
1 <i>d2</i>	8	1	1.57	1.14	-	-	-	-
9	7	2	0.81 ± 0.62	1.09 ± 0.73	1.14 ± 1.09	1.24 ± 0.73	1.14 ± 0.52	-
10	8	2	0.79 ± 1.25	0.81 ± 1.24	-	-	-	-
11	9	1	0.60	0.54	-	-	-	-
		mean ± SD median (range)	1.38 ± 0.65 1.34 (0.30 - 2.46)	1.35 ± 0.61 1.26 (0.42 - 2.75)	1.86 ± 1.07 1.76 (0.48 - 4.10)	1.91 ± 1.17 1.53 (0.47 - 4.44)		
mid G1 - late G2								
9	5	2	0.80 ± 0.43	0.72 ± 0.36	0.40	-	-	-
2 <i>df</i>	4	1	0.32	0.28	-	-	-	-
6 <i>df</i>	4	1	1.25	1.09	-	-	-	-
12	11	4	1.12 ± 0.35	1.31 ± 1.07	1.12 ± 0.34	1.11 ± 0.96	1.52 ± 1.51	1.77 ± 1.20
4	12	3	0.90 ± 0.69	0.74 ± 0.69	0.96 ± 0.52	0.83 ± 0.83	1.95 ± 1.21	1.06 ± 0.96
5	7	4	0.82 ± 0.93	1.19 ± 1.61	1.02 ± 0.91	1.36 ± 1.48	1.07 ± 1.30	1.37 ± 1.12
13	7	2	0.47 ± 1.17	1.17 ± 1.17	0.52 ± 1.17	1.17 ± 1.17	0.80 ± 0.80	1.48 ± 1.28
8	18	3	1.68 ± 1.31	0.93 ± 0.93	1.15 ± 1.12	0.77 ± 0.77	1.24 ± 1.24	1.51 ± 1.12
10	16	2	1.71 ± 0.51	1.71 ± 0.90	1.14 ± 0.90	1.64 ± 1.64	-	-
11	19	1	1.33	0.96	-	-	-	-
14	16	2	1.33 ± 1.01	0.89 ± 0.63	<u>2.18</u>	-	-	-
3 <i>m</i>	27	4	1.18 ± 1.00	1.45 ± 0.85	0.91 ± 1.19	0.73 ± 0.57	1.61 ± 1.80	1.38 ± 1.36
15	11	2	0.56 ± 0.33	0.79 ± 0.79	0.78 ± 0.78	1.26 ± 1.26	1.86 ± 1.82	2.58 ± 2.58
16	11	4	1.05 ± 1.37	0.99 ± 1.19	0.46 ± 0.83	0.60 ± 0.76	1.75 ± 0.79	0.95 ± 0.95
1 <i>m</i>	14	3	1.70 ± 1.76	1.59 ± 1.59	1.32 ± 1.29	1.53 ± 1.53	1.86 ± 1.82	1.01 ± 1.01
2 <i>m</i>	7	2	1.62 ± 1.61	-	1.29 ± 1.43	-	1.70 ± 1.70	-
6 <i>m</i>	6	1	0.51	-	0.62 ± 0.62	-	-	-
17	6	1	1.34	-	1.32 ± 1.32	-	-	-
18	10	3	0.44 ± 0.63	0.99 ± 0.99	0.24 ± 0.73	0.81 ± 0.81	0.69 ± 0.69	0.93 ± 0.93
19	11	3	1.28 ± 0.58	0.59 ± 0.59	1.17 ± 0.59	0.66 ± 0.66	1.25 ± 1.25	2.09 ± 2.09
		mean ± SD median (range)	1.05 ± 0.41 1.06 (0.32 - 1.76)	0.89 ± 0.33 0.90 (0.24 - 1.53)	1.36 ± 0.51 1.26 (0.40 - 2.59)	1.11 ± 0.40 1.04 (0.25 - 2.11)		

Supplementary information to Table 6 and 7. The number of evaluated time points and of CTs as well as all determined $\Delta(\text{Max-Min})$ values from the measured CT-CN and CT-CT distances are listed for each evaluated cell. Values above 2 μm are underlined. Mean values (\pm SD) are indicated in addition to the median values. Mean values > median values of D(Max-Min) CT-CT in G1 are attributed to a higher motility of few CTs.

7.2 Materials and technical equipment

7.2.1 Cells

Cell type	Culture Medium	Source	Reference
BHK (baby hamster kidney)	DMEM	kindly provided by Dr. R.D. Goldman, Northwestern University, Chicago, IL	
CHO lamin C-GFP (Chinese hamster ovary stably expressing lamin C-GFP)	DMEM	kindly provided by Dr. Jos Broers, University of Maastricht, The Netherlands	(Broers <i>et al.</i> , 1999)
Primary human fibroblasts, XX	DMEM	Embryonic female cells provided by Abteilung medizinische Genetik, Kinderpolyklinik, München	
HeLa H2B-GFP HeLa cells stably expressing histone H2B-GFP	RPMI 1640	kindly provided by Dr. Kevin Sullivan, The Scripps Research Institute, La Jolla, California, USA	(Kanda <i>et al.</i> , 1998)
HeLa (subclone 6)	RPMI 1640	kindly provided by Prof. Dr. W.W. Franke, DKFZ, Heidelberg	
SH-EP N14 neuroblastoma cells, stably transfected with a CMV <i>N-myc</i> expression vector	RPMI 1640	kindly provided by Dr. J. Schürmann, DKFZ, Heidelberg	(Ross <i>et al.</i> , 1983; Wenzel <i>et al.</i> , 1991)

7.2.2 Chemicals, enzymes and reagents

Chemicals	
Acetic acid 100%	Merck, Darmstadt
Antifade-Medium Vectashield	Vector, Burlingame CA, USA
Aphidicolin	Calbiochem, Schwalbach
BSA (Fraction V)	Roche, Mannheim
Colcemide (10 µg/ml)	Seromed Biochrom, Berlin
DAPI	Serva
Digitonin	Sigma-Aldrich, Taufkirchen
Dimethyl-Sulfoxid (DMSO)	Merck, Darmstadt
Dulbecco's Modified Eagle Medium (DMEM) (with 25 mM HEPES and stable glutamine)	Gibco Invitrogen, Karlsruhe
Ethanol absolute p.a.	Merck, Darmstadt
Fetal bovine serum (FBS)	Seromed Biochrom, Berlin
Gentamycin (10 mg/ml)	Seromed Biochrom, Berlin
Glyzerin	Sigma-Aldrich, Taufkirchen
HCl 1N	Merck, Darmstadt
Magnesiumchloride	Merck, Darmstadt
Methanol	Merck, Darmstadt
PBS-Dulbecco w/o Ca ²⁺ ,Mg ²⁺ (PBS)	Seromed Biochrom, Berlin
Penicillin/Streptomycin (10000 I.E./10000 µg/ml)	Seromed Biochrom, Berlin
Potassiumchloride	Merck, Darmstadt
Potassiumdihydrogenphosphate	Merck, Darmstadt
Propidiumiodid	Sigma-Aldrich, Taufkirchen
RPMI 1640 medium (with 25 mM HEPES and stable glutamine)	Seromed Biochrom, Berlin
Sodium azide	Merck, Darmstadt
Sodiumchloride	Merck, Darmstadt
Sodium hydrogenphosphate dihydrat	Merck, Darmstadt
TOTO-3	Molecular Probes, Leiden, NL
TO-PRO-3	Molecular Probes, Leiden, NL
Tris Base	Sigma-Aldrich, Taufkirchen
Triton X-100	Merck, Darmstadt
Trolox™	Fluka / Sigma-Aldrich, Taufkirchen
Tween 20	Merck, Darmstadt
Enzymes	
DNase I (grade II)	Roche, Mannheim
Pepsin (10% in H ₂ O)	Sigma-Aldrich, Taufkirchen
RNase A	Roche, Mannheim

Nucleotides	
5-Bromo-2'-deoxyuridin	Sigma-Aldrich, Taufkirchen
Cy3-dUTP	Amersham-Pharmacia, Braunschweig
Cy5-dUTP	Amersham-Pharmacia, Braunschweig
Fluorescein-12-dUTP	Roche, Mannheim

Antibodies	
primary:	
<i>mouse</i> anti-BrdU	Roche Mannheim
<i>mouse</i> anti-BrdU (B44)	Becton Dickinson, UK
<i>rat</i> anti-BrdU (MAS 250c)	Harlan Sera-Lab, UK
<i>human</i> anti-CREST serum	gift from R. Goldman (NWU, Chicago)
<i>goat</i> anti-Lamin B (M-20)	Santa Cruz Biotechnology, USA
<i>rabbit</i> anti-Lamin B	gift from R. Goldman (NWU, Chicago)
<i>mouse</i> anti-Lamin A/C	Santa Cruz Biotechnology, USA
<i>rabbit</i> anti-LaminA/C (#266)	gift from R. Goldman (NWU, Chicago)
<i>rat</i> anti-LaminA/C (#270).	gift from R. Goldman (NWU, Chicago)
<i>mouse</i> anti-414 (NPC)	gift from R. Goldman (NWU, Chicago)
<i>mouse</i> anti-Digoxigenin	Sigma-Aldrich, Taufkirchen
<i>sheep</i> anti-Digoxigenin-FITC	Diananova, Hamburg
<i>rabbit</i> anti-Ki-67	DAKO, Denmark
secondary:	
<i>goat</i> anti- <i>mouse</i> -Alexa™ 488 (highly cross adsorbed)	Molecular Probes, Leiden, NL
<i>goat</i> anti- <i>mouse</i> -Cy™ 5	Diananova, Hamburg
<i>sheep</i> anti- <i>mouse</i> -Cy™ 3	Diananova, Hamburg
<i>sheep</i> anti- <i>mouse</i> -FITC	Sigma-Aldrich, Taufkirchen
<i>goat</i> anti- <i>rat</i> -Cy™ 3	Amersham-Pharmacia, Braunschweig
<i>goat</i> anti- <i>rat</i> -Cy™ 5	Amersham-Pharmacia, Braunschweig
<i>rabbit</i> anti- <i>goat</i> -FITC	Sigma-Aldrich, Taufkirchen
<i>donkey</i> anti- <i>goat</i> -Cy™ 5	Diananova, Hamburg

7.2.3 Media, buffers and solutions

Buffer / Solutions	Constituents	Notes
Aphidicolin stock solution	5µg/µl Aphidicolin	dissolve 1 mg aphidicolin in 200 µl EtOH absolute; store at -20°C.
Blocking solution	2 % BSA in PBS	5x: 20% BSA in PBS + 0,04% Na-Azid store at 4°C
DAPI stock solution	2 mg/ml dd H ₂ O	steril filtered
DAPI working solution	0,02µg/ml in PBST	dilute stock solution 1:4000 in PBST
Digitonin stock solution	10 mg/ml dd H ₂ O.	add 10 ml dd H ₂ O to 100 mg digitonin; store at RT; mix well before use!
DNase I stock solution	2 U/µl DNasel 0,3 M NaCl 50% Glycerin	1 mg/ml DNase I (2000 U/mg)
Fixative (for chromosomes)	3:1 Methanol/acetic acid	prepare fresh and cool to -20°C before use
Fixative (for 3D preserved cells)	3,7% Formaldehyde in PBS	Formalin (37%) 1:10 verdünnen or add 1,85 g paraformaldehyde and 3,5 ml dd H ₂ O in a 50 ml FALCON tube, cap and heat 30-60 s in boiling water. Add 90 µl of 1N NaOH. Heat 1 min in boiling water while gently shaking until the solution becomes clear. Cool down by placing the tube under cold water; steril filter. Dilute 1:10 in PBS.
KCl solution, hypotone	75 mM KCl	0,56g / 100 ml dd H ₂ O
NaCl solution (4 M)	4 M NaCl in PBST	23,4 g / 100 ml PBST
PBS (pH 7.4)	137 mM NaCl 2,7 mM KCl 8,0 mM Na ₂ HPO ₄ 1,5 mM KH ₂ PO ₄	10×PBS: 80 g NaCl 2 g KCl 11,5 g Na ₂ HPO ₄ 2,0 g KH ₂ PO ₄ ad 1 l dd H ₂ O 1×PBS-Aliquots autoklavieren
PBST	0,02% Tween 20 in 1×PBS	200 µl Tween 20 in 1l PBS
Propidium-Iodid (PI)	0,5 µg/ml in 1×PBS	1:20000 from 10 µg/µl stock solution
RNAse stock solution (20 µg/µl)	2% RNAse A 10 mM Tris-HCl pH 7.5 15 mM NaCl	200 mg RNAse A 100 µl 1 M Tris-HCl 30 µl 5 M NaCl 10 ml dd H ₂ O 15 min 90°C. aliquot and store at -20°C.
RPMI 1640 full medium	500 ml RPMI 1640 50 ml FBS (10%) 5 ml Penicillin/Streptomycin (100 I.E./100 µg/ml)	Bestandteile RPMI 1640: 25 mM HEPES 5,5 g/l NaCl 2,0 g NaHCO ₃ 5 mg/l Phenolrot 0,532 g/l N-Acetyl-L-alanyl-L-glutamin prewarm to 37° before use

Freezing medium	20% FBS 10% DMSO in appropriate medium	
Tris-HCl	1M Tris Base	Add 12,11 g to 100 ml dd H ₂ O Adjust desired pH by adding HCl.
Tris high salt washing buffer (pH 8,0)	0,5 M NaCl 40 mM Tris-HCl 0,5% Tween 20	29,2 g/l NaCl 1:25 1M Tris-HCl (pH 8.0)
Triton 0,2%	0,2% Triton X-100 in 1×PBS	
Trolox stock solution	100 mM Trolox ((±)6-Hydroxy-2,5,7,8-tetramethylchroman-2-carbonic acid)	add 0.25 g to 9.8 ml dd H ₂ O, add 100µl 1N NaOH and mix well until all Trolox is dissolved (clear yellow color!). Then neutralize with 100µl 1N HCl. The solution will become a white suspension. Aliquot and store at 4°C.
Trypsin-EDTA	0.05% Trypsin 0.02% EDTA	Prepare from 10x concentrated solution (Biochrom)

7.2.4 Equipment and Instrumentation

Microscopes		
Cell culture phase contrast microscope	Axiovert 25 C	Zeiss, Jena
Objectives	CP Achromat $\times 5 / 0,12$ CP Achromat $\times 10 / 0,25$ Ph1 LD Achrostigmat $\times 20 / 0,3$ Ph1 LD Achrostigmat $\times 40 / 0,55$ Ph2	
Epifluorescence-microscope	Axiophot 2	Zeiss, Jena
Objektives	Plan-Neofluar $16\times / 0,5$ (N.A.) Plan-Neofluar $40\times / 1,3$ oil Plan-APOCHROMAT $63\times / 1,4$ oil Plan-Neofluar $100\times / 1,3$ oil	
Fluorescence filters	DAPI (BP 365; FT 395; LP 450-490 nm) FITC (BP 450-490; FT 510; LP 515-565 nm) Cy3 (BP: 546; FT 580; LP: 590 nm) Cy5 (BP: 575-625; FT 645; BP: 660-710 nm)	
CCD-Camera	Coolview CCD Camera System	Applied Imaging, UK
Software	CytoVision™	Applied Imaging, UK
Confocal laser scanning mikroskop	LSM 410	Zeiss, Jena
Objectives	Plan-APOCHROMAT $63\times / 1,4$ oil	
Laser	Ar+-laser 488 nm, 15 mW HeNe-laser 543 nm, 0.5 mW HeNe-laser 633 nm, 5 mW	
Dichroic mirror	FT 488 / 543	
Emission filters	FITC (BP 502 - 542) Cy3 (LP 570 or BP 575 - 640) Cy5 (LP 650)	
Software	LSM 410 software version 3.95	
Confocal laser scanning mikroskop	Leica TCS SP	Leica, Heidelberg
Objectives	Plan-APOCHROMAT $100\times / 1,4$ oil	
Laser	Ar ⁺ -laser 457 / 488/ 514 nm HeNe-laser 633 nm	
Dichroic mirror	RSP 525 TD 488 / 568 / 647	
Emission filters	Spectrally adjustable detection system. Adjustment: GFP (490-540 nm), PI (590-680 nm), Cy5 (650-750 nm)	
Software	TCS-SP software	

Microinjection

Phase contrast microscope	Axiovert S 100	Zeiss, Jena
Objectives	A-Plan 5× / 0,12 Ph1 LD Achromat 20× / 0,30 Ph1 LD Achromat 32× / 0,40 Ph1 LD Achromat 40× / 0,60 Ph2	
Injection system	AIS 2 Transjektor 5246	Lugis & Neumann Eppendorf, Hamburg
Capillary puller	P-97 Micropipette Puller	Sutter Instruments, USA
Glass capillaries	GC120TF 10 (Øi 0.94 mm, Øe 1.2 mm)	Clark, U.K.

Live cell observation setup

Live cell microscopy chamber system	FCS2 living cell chamber / objective heater	Bioptechs, Butler, USA
Flexible-tube pump and silicone fittings	flow rate 0.03-8.2 ml/min	neoLab, Heidelberg
Solid state relay, accessory	(SSR)	Conrad Elektronik, München
Tygon tubing	2275 (Øi 1.6 mm, Øe 4.8 mm, Ep. 1.6 mm)	neoLab, Heidelberg
Tygon tubing	3350 (Øi 1.6 mm, Øe 3.2 mm, Ep. 0.8 mm)	neoLab, Heidelberg
Tube connectors	Luer Lock Øi 1.6mm, female	neoLab, Heidelberg
Tube connectors	Luer Lock Øi 1.6mm, male	neoLab, Heidelberg
2-way plastic valve	Luer Lock Øi, male and female	neoLab, Heidelberg
Sterile filter	0.45 µm yellow or 0.20 µm blue	Sartorius / Schubert & Weiss, München
Plastic syringe	20ml with Luer lock (not cone)	Braun Melsungen / Schubert & Weiss

Instrumentations

CO₂-Incubator	B 5060 and BB 6220	Heraeus, Hanau
Laminar flow cabinet	Antares 48	Biohit, Köln
Autoclave	Varioklav 400	H+P Labortechnik GmbH, Oberschleißheim
Centrifuge	Biofuge pico	Heraeus, Hanau
	Rotana / S	Hettich, Tuttlingenbat
Pipette aid	accu-jet® BRAND	Schubert & Weiss, München

Office and image processing software

Office 2000	Microsoft, Redmond, USA
Photoshop® 6.0	Adobe Systems, Inc., San Jose, USA
Illustrator® 9.0	Adobe Systems, Inc., San Jose, USA
Amira™ 2.3	TGS, Mérignac, France (http://www.amiravis.com)
LSM 410 dummy software (v 3.98)	Carl Zeiss, Jena
LSM 5 Image Browser (v 3.1)	Carl Zeiss, Jena
ImageJ (v 1.28)	Wayne Rasband, NIH, Bethesda, USA (http://rsb.info.nih.gov/ij/)
SPSS 11.0	SPSS Inc. Chicago, Illinois, USA

Glass and plasticware

CELLocate® coverslips 175µm square size	Eppendorf Hamburg
Photoetched coverslips (23×23 mm)	Bellco Glass Inc., USA
Round glass coverslips, Ø40mm (No. 1001)	Assistant
PP-tubes FALCON®, 50 ml / 15ml	Becton Dickinson, Heidelberg
Reaction tubes 1,5 ml / 0,5 ml	Eppendorf, Hamburg
Microloader tips	Eppendorf, Hamburg
Tissue culture flasks 25 cm ² / 75 cm ² / 182 cm ²	Greiner bio-one, Frickenhausen
Tissue culture dishes 35/10 mm	Becton Dickinson, Heidelberg.
FALCON® Easy Grip	Becton Dickinson, Heidelberg.
Tissue culture dishes 60/15 mm	Becton Dickinson, Heidelberg.
FALCON® Easy Grip	
Tissue culture dishes 94/16 mm	Greiner bio-one, Frickenhausen
Serological pipettes 5 ml / 10 ml / 25 ml	Nunc, Wiesbaden
Sterile filters (20 µm / 45 µm pore size)	Satorius, Göttingen
Disposable hypodermic needles (Ø 0.45×25 mm)	Braun, Melsungen
Vacuum grease: Bayer silicone (medium viscous)	Neolab, Heidelberg

Miscellaneous

- Coverslips 15×15 / 20×20 mm
- Microscopic slides 76×26 mm
- PARAFILM® "M" laboratory film
- Diamond pen
- Fine forceps
- Glasscribe® Tungsten marker
- Metal box with cover
- Nail Polish (transparent)
- Water bath 37°C
- Cool/heat pack
- Immersion oil
- Pipettes and tips

Publikationen

Schermelleh, L., S. Thalhammer, W. Heckl, H. Posl, T. Cremer, K. Schutze, and M. Cremer (1999). Laser microdissection and laser pressure catapulting for the generation of chromosome-specific paint probes. *Biotechniques*. 27:362-367.

Schermelleh, L., I. Solovei, D. Zink, and T. Cremer (2001). Two-color fluorescence labeling of early and mid-to-late replicating chromatin in living cells. *Chromosome Res.* 9:77-80.

Solovei, I., A. Cavallo, L. Schermelleh, F. Jaunin, C. Scasselati, D. Cmarko, C. Cremer, S. Fakan, and T. Cremer (2002). Spatial Preservation of Nuclear Chromatin Architecture during Three- Dimensional Fluorescence in Situ Hybridization (3D-FISH). *Exp Cell Res.* 276:10-23.

Solovei, I., J. Walter, M. Cremer, F. Habermann, L. Schermelleh, and T. Cremer. 2002. FISH on three-dimensionally preserved nuclei. In *FISH: a practical approach*. J. Squire, B. Beatty, and S. Mai, editors. Oxford University Press, Oxford. 119-157.

Schermelleh, L., and J. Walter (2002). Long term live cell confocal microscopy. *G.I.T. Imaging & Microscopy*. 4:47-50 and (2003) *BIOforum International*. 7: 48-50.

Walter, J., L. Schermelleh, M. Cremer, S. Tashiro, and T. Cremer (2003). Chromosome order in HeLa cells changes during mitosis and early G1, but is stably maintained during subsequent interphase stages. *J Cell Biol.* 160: 685-697. (J. Walter and L. Schermelleh contributed equally.)

Cremer, M., L. Schermelleh, I. Solovei, and T. Cremer (2003). Chromosomal arrangement during different phases of cell cycle. In *Encyclopedia of the human genome*. Macmillan Publishers Ltd, Nature Publishing Group. (in press)

Cremer, C., Cavallo, A., Kepper, N., Edelmann, P., Kreth, G., Solovei, I., Schermelleh, L., Cremer, T. (2003). The dynamics of the cell nucleus: 3D-image sequencing of large-scale genome structure. In *Image sequence analysis to investigate dynamic processes*. Springer-Verlag, Berlin. (in press)

Solovei, I., L. Schermelleh, K. Düring, A. Engelhardt, S. Stein, J. von Hase, C. Cremer, and T. Cremer (2003). Differences in centromere positioning during cell cycle and at G0 in four types of human cells. (in prep)

Lebenslauf

Name: Lothar Joachim Oswald Schermelleh
Geburtsdatum: 16.07.1971
Geburtsort: München

Schulausbildung: 09/77 - 07/81 Grundschule in der Wilhelmstrasse München
09/81 - 07/90 Willi-Graf-Gymnasium München

Zivildienst: 09/92 - 12/93 Städt. Krankenhaus München Schwabing

Hochschulausbildung: 11/91 - 07/92
und
11/93 - 11/98 Diplom-Studium Biologie an der LMU
München
seit 01/ 99 Promotion am Department Biologie II
der LMU München

Praktische Tätigkeiten: 08/90 - 01/98 Mitarbeit im elterlichen Einzelhandelsbetrieb
02/98 - 11/98 Diplomarbeit in der Arbeitsgruppe von
Prof. T. Cremer
02/00 - 03/00 Forschungsaufenthalt an der Northwestern
University Medical School, Chicago (IL)
in der Arbeitsgruppe von Robert D. Goldman